Potential for Saltwater Intrusion into the Lower Tamiami Aquifer near Bonita Springs, Southwestern Florida

By W. Barclay Shoemaker and K. Michelle Edwards

U.S. GEOLOGICAL SURVEY

Water-Resources Investigations Report 03-4262

Prepared in cooperation with the

South Florida Water Management District

Tallahassee, Florida
2003

U.S. DEPARTMENT OF THE INTERIOR
GALE A. NORTON, Secretary

U.S. GEOLOGICAL SURVEY
CHARLES G. GROAT, Director

Any use of trade, product, or firm names in this publication is for descriptive purposes only and does not imply endorsement by the U.S. Geological Survey.

For additional information write to:

U.S. Geological Survey
2010 Levy Avenue
Tallahassee, FL 32310

Copies of this report can be purchased from:

U.S. Geological Survey
Branch of Information Services
Box 25286
Federal Center
Denver, CO 80225
888-ASK-USGS

Additional information about water resources in Florida is available on the Internet at http://fl.water.usgs.gov

CONTENTS

Abstract 1
Introduction 2
Purpose and Scope 2
Description of Study Area 2
Previous Studies 5
Acknowledgments 5
Hydrogeology of Southwestern Florida 6
Lithology and Stratigraphy 6
Hydrogeologic Units and Hydraulic Characteristics 7
Water Budget 15
Water Quality and Geochemistry 20
Ground-Water Flow and Mechanisms of Saltwater Intrusion 20
Lateral Encroachment 22
Upward Leakage 22
Downward Leakage 24
Relict Seawater 25
Simulation of Saltwater Intrusion near Bonita Springs 25
Modeling Approach 26
Code Selection 29
Constant-Density Ground-Water Flow Simulator 29
Variable-Density Ground-Water Flow Simulator 29
Spatial Discretization and Assignment of Aquifer Properties 30
Simulation of Predevelopment Conditions 34
Boundary Conditions 34
Recharge 34
Rivers 35
No Flow 35
Constant Heads and Concentrations 37
Simulation Results 37
Model Calibration to Typical, Modern, and Seasonal Stresses 38
Boundary Conditions 38
No Flow 40
Constant Heads 40
Rivers 40
General Heads 41
Recharge 41
Wells 42
Parameter Estimation 42
Confidence Intervals 49
Potential Movement of Saltwater to Equilibrium with Typical, Modern, and Seasonal Stresses 52
Baseline Scenario 52
Mechanisms of Saltwater Intrusion 53
Extent of Saltwater Intrusion 54
Sensitivity Analyses 55
Mechanisms of Saltwater Intrusion 56
Extent of Saltwater Intrusion 57
Model Limitations 60

Summary 63
Selected References 64
Appendix: Monitoring Stations Used for this Study 69

PLATES

1. Maps showing boundary conditions for simulating the predevelopment distribution of saltwater ..... pocket
2. Maps showing boundary conditions for calibrating the model to March and September 1996 conditions and moving the predevelopment distribution of saltwater to equilibrium ..... pocket

FIGURES

1. Map showing location of the study area in southwestern Florida 3
2. Maps showing major watersheds and physiographic features in the study area 4
3. Column showing generalized geologic and hydrogeologic units in the study area 6
4. Histograms of the log of estimated horizontal hydraulic conductivity values of the water-table, lower Tamiami, and sandstone aquifers 8
5. Map showing lines of equal thickness of the rock units that comprise the water-table aquifer 9
6. Map showing spatial distribution of horizontal hydraulic conductivity in the water-table aquifer estimated from analyses of aquifer performance tests 10
7. Map showing lines of equal thickness of the rock units that comprise the lower Tamiami aquifer 11
8. Map showing spatial distribution of horizontal hydraulic conductivity in the lower Tamiami aquifer estimated from analyses of aquifer performance tests 12
9. Map showing lines of equal thickness of the rock units that comprise the sandstone aquifer 13
10. Map showing spatial distribution of estimated horizontal hydraulic conductivity in the sandstone aquifer 14
11. General hydrogeologic section showing hypothetical control volume and selected water-budget components within the study area 15
12. Map showing average annual head difference between the lower Tamiami and sandstone aquifers in 1996 18
13. Bar graph showing average annual ground-water withdrawals from municipal supply facilities in Lee and Collier Counties, 1985-98 19
14. Bar graph showing average monthly ground-water withdrawals from municipal supply facilities in Lee and Collier Counties, 1995 19
15. Scatter plot of historical trends in chloride concentration for selected monitoring wells near Bonita Springs, 1968-98 21
16. Maps showing lines of equal chloride concentration in the lower Tamiami aquifer near Bonita Springs over time 22
17. Generalized cross section showing potential mechanisms of saltwater intrusion in the lower Tamiami aquifer near Bonita Springs 23
18. Bar graphs showing historical record of annual rainfall at Bonita Springs Utility rainfall monitoring station, 1943-54 and 1993-99 27
19. Graph of average monthly water levels from selected monitoring wells in the water-table and lower Tamiami aquifers near Bonita Springs 28
20. Three-dimensional diagram showing the distribution of bulk horizontal hydraulic conductivity in selected model cells 32
21. Schematic of approach used to compute bulk hydraulic conductivities for each model cell using weighted arithmetic and harmonic averaging 33
22. Map showing average monthly water levels in the water-table and lower Tamiami aquifers during March and September 1996 36
23. Diagram showing three-dimensional view of the simulated predevelopment distribution of saltwater 38
24. Map showing the approximate position of the simulated predevelopment saltwater interface at the base of the lower Tamiami aquifer 39
25. Bar graph showing total monthly pan evaporation from several monitoring stations near Bonita Springs 42
26. Map showing areas with potentially large quantities of unmonitored ground-water pumpage 43
27. Bar graph showing composite-scaled sensitivities computed while calibrating the model to March and September 1996 conditions 46

28. Scatter plot showing comparison of observed and simulated water levels 48
29. Scatter plot showing comparison of weighted residuals and weighted simulated values 49
30. Map showing simulated net recharge to the water-table aquifer during March 1996 50
31. Map showing simulated net recharge to the water-table aquifer during September 1996 51
32. Graph showing total salt mass in the model while moving the simulated predevelopment distribution of saltwater to equilibrium with calibrated March and September 1996 conditions 52
33. Map showing simulated potential extent of saltwater intrusion in the lower Tamiami aquifer from the baseline scenario near Bonita Springs 53
34. Three-dimensional diagram of the saltwater interface and upconing plumes near equilibrium with calibrated March and September 1996 conditions in the water-table and lower Tamiami aquifers near Bonita Springs. 54
35. Cross section A-A' along row 40 of the model grid showing a mound of ground water between the cones of depression in the lower Tamiami aquifer and the saltwater interface 55
36. Map showing distribution of saltwater at the base of the lower Tamiami aquifer at the end of the baseline scenario, and two sensitivity analysis scenarios 57
37. Bar graph showing sensitivity analysis of the extent of saltwater intrusion 59
38. Graph showing average monthly rainfall from selected rainfall stations in southwestern Florida, 1909-99 61

TABLES

1. Average 1996 water levels computed from selected monitoring wells in the lower Tamiami and sandstone aquifers 17
2. Description and primary use of modeling tasks 25
3. Hydraulic conductivities used in the conceptual permeability model 31
4. Observations used during model calibration to March and September 1996 conditions 44
5. Estimates of unmonitored ground-water pumpage and evapotranspiration multipliers with confidence intervals computed by UCODE 47
6. UCODE estimated parameter correlation coefficients 47
7. Changes made to baseline scenario parameters for a sensitivity analysis of the extent of saltwater intrusion in the lower Tamiami aquifer near Bonita Springs 58

CONVERSION FACTORS, ACRONYMS, ABBREVIATIONS, AND VERTICAL DATUM

Multiply	By	To obtain
millimeter per year (mm/yr)	0.03937	inch per year
meter (m)	3.281	foot
meter per day (m/d)	3.281	foot per day
meter per year (m/yr)	3.281	foot per year
square meter (m^2)	10.76	square foot
cubic meter per day (m^3/d)	35.31	cubic foot per day
cubic meter per second (m^3/s)	35.31	cubic foot per second
kilometer (km)	0.6214	mile
square kilometer (km^2)	0.3861	square mile
centimeter (cm)	0.3937	inch
centimeter (cm)	3.281×10^{-2}	foot
centimeter per day (cm/d)	3.281×10^{-2}	foot per day
centimeter per year (cm/yr)	3.281×10^{-2}	foot per year
kilogram per cubic meter (kg/m^3)	0.06243	pound per cubic foot

OTHER UNITS OF ABBREVIATION

MHz	megahertz
mg/L	milligram per liter

ACRONYMS

ADAPS	Automated Data Processing System
CSS	composite-scaled sensitivities
DBHYDRO	Hydrometeorologic Database (South Florida Water Management District)
DC	direct current
HMOC	hybrid method of characteristics
MAE	mean absolute error
MOC	method of characteristics
MMOC	modified method of characteristics
NGVD	National Geodetic Vertical Datum
NOAA	National Oceanic and Atmospheric Administration
NWIS	National Water Information System (U.S. Geological Survey database)
PSS	prediction-scaled sensitivities
QWDATA	Water Quality Database
SFWMD	South Florida Water Management District
USGS	U.S. Geological Survey
VCONT	vertical conductance

Vertical coordinate information is referenced to the National Geodetic Vertical Datum of 1929 (NGVD of 1929); horizontal coordinate information is referenced to the North American Datum of 1983 (NAD83).

Potential for Saltwater Intrusion into the Lower Tamiami Aquifer near Bonita Springs, Southwestern Florida

By W. Barclay Shoemaker *and* K. Michelle Edwards

Abstract

A study was conducted to examine the potential for saltwater intrusion into the lower Tamiami aquifer beneath Bonita Springs in southwestern Florida. Field data were collected, and constant- and variable-density ground-water flow simulations were performed that: (1) spatially quantified modern and seasonal stresses, (2) identified potential mechanisms of saltwater intrusion, and (3) estimated the potential extent of saltwater intrusion for the area of concern.

MODFLOW and the inverse modeling routine UCODE were used to spatially quantify modern and seasonal stresses by calibrating a constant-density ground-water flow model to field data collected in 1996. The model was calibrated by assuming hydraulic conductivity parameters were accurate and by estimating unmonitored ground-water pumpage and potential evapotranspiration with UCODE. Uncertainty in these estimated parameters was quantified with 95-percent confidence intervals. These confidence intervals indicate more uncertainty (or less reliability) in the estimates of unmonitored ground-water pumpage than estimates of pan-evaporation multipliers, because of the nature and distribution of observations used during calibration. Comparison of simulated water levels, streamflows, and net recharge with field data suggests the model is a good representation of field conditions.

Potential mechanisms of saltwater intrusion into the lower Tamiami aquifer include: (1) lateral inland movement of the freshwater-saltwater interface from the southwestern coast of Florida; (2) upward leakage from deeper saline water-bearing zones through natural upwelling and upconing, both of which could occur as diffuse upward flow through semiconfining layers, conduit flow through karst features, or pipe flow through leaky artesian wells; (3) downward leakage of saltwater from surface-water channels; and (4) movement of unflushed pockets of relict seawater. Of the many potential mechanisms of saltwater intrusion, field data and variable-density ground-water flow simulations suggest that upconing is of utmost concern, and lateral encroachment is of second-most concern. This interpretation is uncertain, however, because the predominance of saltwater intrusion through leaky artesian wells with connection to deeper, more saline, and higher pressure aquifers was difficult to establish.

Effective management of ground-water resources in southwestern Florida requires an understanding of the potential extent of saltwater intrusion in the lower Tamiami aquifer near Bonita Springs. Variable-density, ground-water flow simulations suggest that when saltwater is at dynamic equilibrium with 1996 seasonal stresses, the extent of saltwater intrusion is about 100 square kilometers areally and 70,000 hectare-meters volumetrically. The volumetric extent of saltwater intrusion was most sensitive to changes in recharge, ground-water pumpage, sea level, salinity of the Gulf of Mexico, and the potentiometric surface of the sandstone aquifer, respectively.

INTRODUCTION

Urbanization is proceeding rapidly along the coast of southwestern Florida, with cities and communities springing up from Fort Myers to Naples. In fact, the coast around Bonita Springs is one of the Nation's fastest growing areas. The expanded population has resulted in increased public-supply withdrawals from the lower Tamiami aquifer that have lowered ground-water levels and reversed hydraulic gradients in the aquifer between Bonita Springs and the coastline. Long-term movement of saltwater into coastal aquifers is often attributed to declines in ground-water levels, thus limiting the future availability of potable-water supplies.

Saltwater intrusion is defined by Stewart (1999) as the mass transport of saline waters into zones previously occupied by fresher waters. This definition is broad because natural processes (such as sea level rise and drought) and anthropogenic processes (such as ground-water pumpage and construction of canals) can cause saltwater intrusion. Thus, the investigator is faced with a "classic" inverse problem because an observed distribution of saltwater could be explained equally well by one or more mechanisms of saltwater intrusion. Under these circumstances, multiple sources of information are useful to help identify the predominant mechanisms of saltwater intrusion, including ground-water levels and pumpage, geochemical data (such as chloride concentrations and strontium isotope analysis), surface and borehole geophysical data, research from previous studies, and numerical modeling tools.

Water managers need a clear understanding of the saltwater intrusion process to ensure protection of the fresh ground-water resources in southwestern Florida. In 1999, the U.S. Geological Survey (USGS), in cooperation with the South Florida Water Management District (SFWMD), initiated a study to: (1) quantify modern (stresses with the desired characteristics) and seasonal stresses; (2) help identify potential mechanisms of saltwater intrusion; and (3) estimate the potential extent of saltwater intrusion in the lower Tamiami aquifer near Bonita Springs. Field data and numerical methods were used in this effort.

Purpose and Scope

The purpose of this report is to describe the results of numerical simulation procedures that represent the movement of saltwater in the lower Tamiami aquifer beneath Bonita Springs in southwestern Florida. Water-budget components were characterized and mathematically represented to help simulate ground-water flow and saltwater intrusion in the surficial aquifer system, which includes the lower Tamiami aquifer. A modular, three-dimensional, finite-difference, ground-water flow model was used to represent modern and seasonal stresses during March and September 1996 when ground-water levels are generally at their lowest and highest, respectively. Field data were collected and variable-density, ground-water flow simulations were performed to help identify mechanisms of saltwater intrusion of utmost concern and estimate the potential extent of saltwater intrusion in the lower Tamiami aquifer beneath Bonita Springs. The extent of saltwater intrusion was simulated from predevelopment distribution to dynamic equilibrium with calibrated March and September 1996 conditions.

Description of Study Area

The study area encompasses about 860 km^2 in Lee and western Collier Counties (fig. 1), and is characterized by low topographic relief and a high water table. The physiographic provinces that comprise the study area (fig. 2) are the Gulf Coastal Lowlands, Caloosahatchee Incline, Desoto Plain, Southwestern Slope, Immokalee Rise, Everglades, Okeechobee Plain, Big Cypress Spur, and the Reticulate Coastal Swamps (Fernald and Purdum, 1998). The Immokalee Rise, a sandy ridge formed during high sea-level stands, occupies the highest part of the study area to the northeast (at an elevation of about 12 m) and borders the Caloosahatchee River and Big Cypress watersheds.

The Caloosahatchee River, Estero Bay, and Big Cypress watersheds are located in the study area (fig. 2). The Caloosahatchee River watershed extends from Lake Okeechobee to San Carlos Bay and passes through parts of Charlotte, Glades, Hendry, and Lee Counties and dips slightly into Collier County. The lower reaches of the watershed are characterized by a shallow bay, extensive seagrass beds, and sand flats.

The Estero Bay watershed (fig. 2) occupies central and southern Lee County and parts of northern Collier and western Hendry Counties. The principal surface-water features are Estero River, Spring Creek, Kehl Canal, Imperial River, and Cocohatchee River. The low gradients in these channels result in sluggish and tidally induced flow that is probably much greater than freshwater flow. Channel stages fluctuate

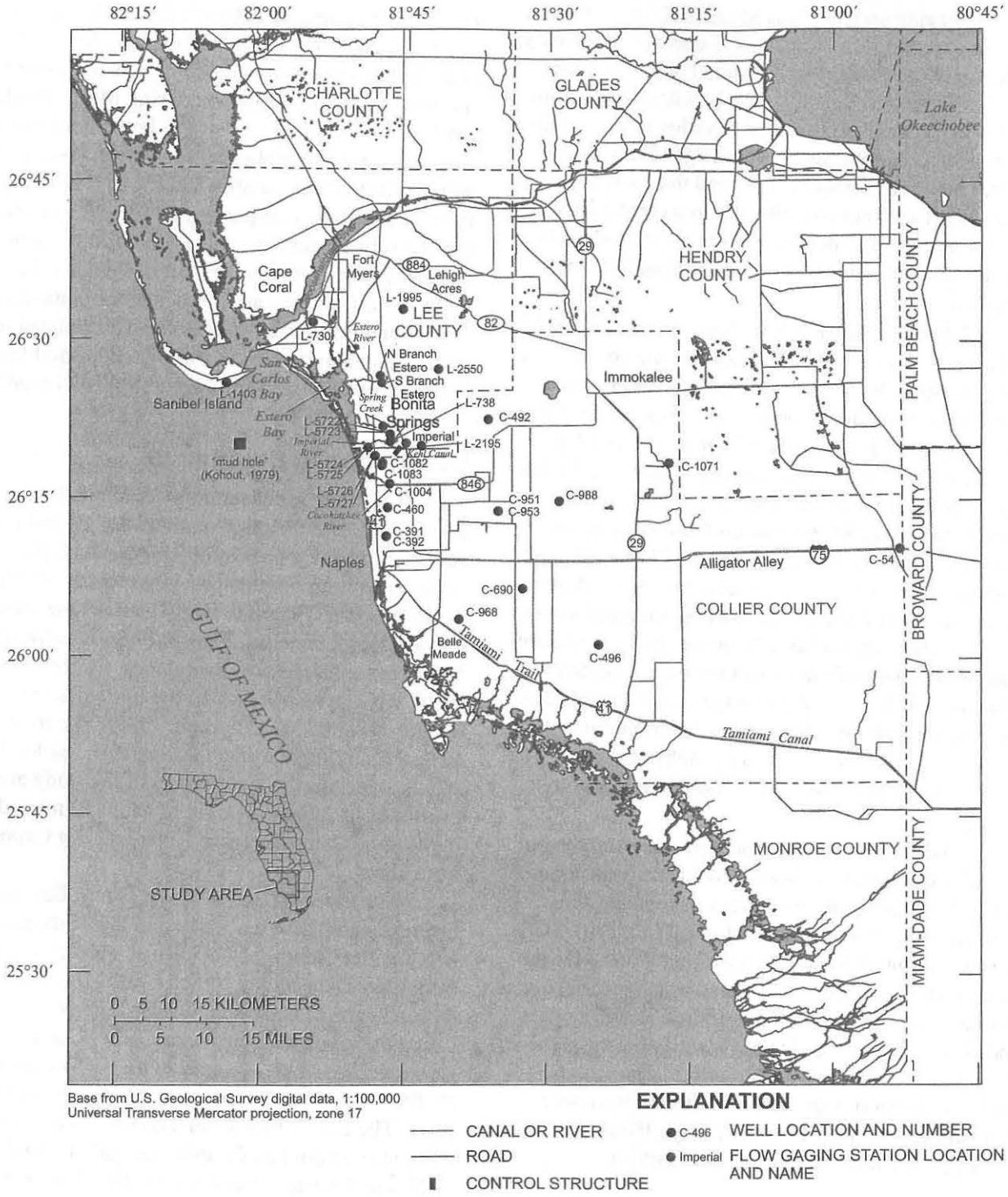


Figure 1. Location of the study area in southwestern Florida.

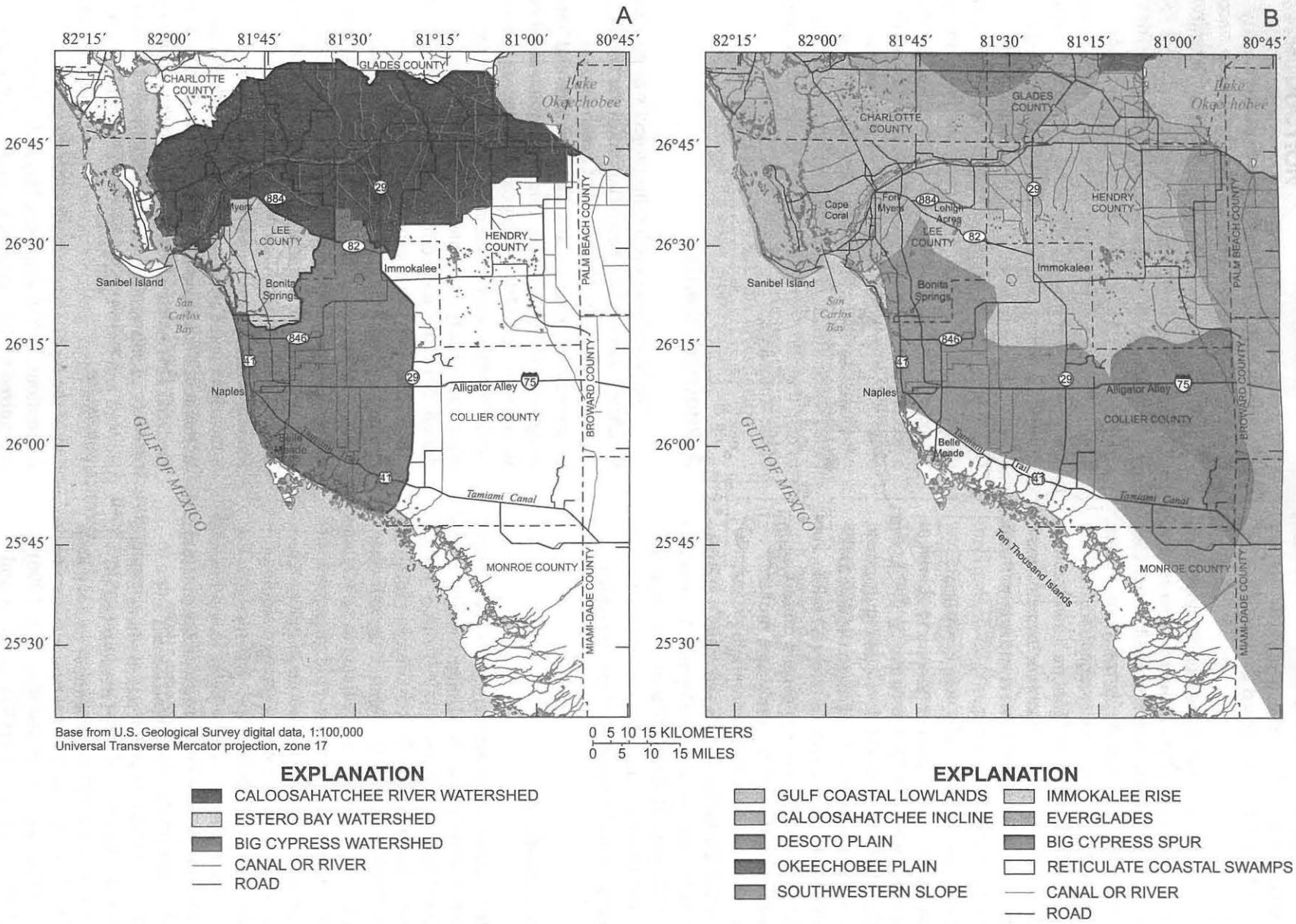


Figure 2. (A) Major watersheds (South Florida Water Management District, 1989), and (B) physiographic features (modified from Fernald and Purdum, 1998) in the study area. The Big Cypress watershed includes the Corkscrew Swamp Sanctuary northeast of Naples, Florida.

seasonally with the highest and lowest levels occurring during summer and winter, respectively. The flora and fauna of the Estero Bay watershed are varied and abundant.

The Big Cypress watershed (fig. 2) drains a wide area through a large network of man-made canals and natural sloughs in southern Lee and Hendry Counties and western Collier County. A variety of grasses, shrubs, and small cypress trees dominate the Big Cypress watershed, which includes the Corkscrew Swamp Sanctuary located northeast of Naples. South of Naples, freshwater sloughs and rivers mix with Gulf of Mexico bays and tidal creeks.

Development in the study area is primarily urban and agricultural. Urban development is greatest along the coast west of I-75 (Interstate 75) in Lee and Collier Counties. Agricultural development, located between wetland systems, increases to the east and south in the study area. The undeveloped regions consist of flatwoods, sloughs, swamps, and estuaries. Predevelopment sheetflow in the study area probably was slow due to the vegetation, geomorphology, and low land-elevation gradients. Canals and roads resulting from urban and agricultural development have nearly eliminated the natural sheetflow across the land surface and altered the natural drainage patterns by concentrating stormwater runoff in canals and ditches.

Previous Studies

Many studies of saltwater intrusion have been conducted over the years, and a comprehensive record can be found in Bear and others (1999). Two "classic" studies were completed by Badon-Ghyben (1888) and Herzberg (1901) in which the depth of the saltwater interface below sea level was predicted to be 40 times the freshwater head above sea level in the aquifer of interest, given hydrostatic conditions in a homogeneous unconfined aquifer with a seaward sloping water-table surface. Kohout (1964) recorded that the saltwater front in the Biscayne aquifer in southeastern Florida is as much as 13 km seaward of the position predicted by the Ghyben-Herzberg equation due to ground-water circulation patterns near the saltwater interface. Later research of saltwater intrusion in southeastern Florida was accomplished by Hull and Meyer (1973), Klein and Waller (1985), Klein and Ratzlaff (1989), Sonenshein and Koszalka (1996), Merritt (1996), Sonenshein (1997), Konikow and Reilly (1999), and Langevin (2001). Merritt (1996) used a sensitivity analysis of numerical simulations to address the importance of properties and processes affecting the saltwater interface in Broward County along the southeastern coast of Florida.

On the southwestern coast of Florida, Klein (1954) studied saltwater intrusion in coastal areas near Naples. In the 1960's, field studies by McCoy (1962), Cooper (1964), Henry (1964), and Glover (1964) advanced the knowledge and understanding of ground-water movement near the saltwater interface in southern Florida. Sherwood and Klein (1963) mapped a salinity plume beneath the Caloosahatchee River, whose source was a leaky well with connection to the deeper, more saline, and higher pressure Floridan aquifer system. Kohout (1979) used remote sensing to map a geothermal submarine ground-water spring off the coast of Bonita Springs, informally known as the "mudhole" by local fisherman. Stewart and others (1982) used direct-current (DC) resistivity soundings to map the saltwater interface near Belle Meade south of the study area.

Acknowledgments

Technical support for this project was provided by Chris Langevin and Keith Halford of the USGS, Mark Stewart of the University of South Florida Department of Geology, and Akin Owosina and Terry Bengtsson of the SFWMD. Terry Bengtsson and Lee Worst from the SFWMD helped delineate areas near Bonita Springs where unmonitored ground-water pumpage is likely occurring. Pamela Telis helped design, distribute, and compile results from a survey designed to estimate unmonitored ground-water pumpage. Several colleagues reviewed the initial drafts of this report, including Terry Bengtsson and Rama Rani, and the following USGS employees: Barbara Howie, Eric Swain, Chris Langevin, Melinda Wolfert, Richard Krulikas, Ward Sanford, Gary Mahon, Eve Kuniansky, Michael Deacon, Roy Sonenshein and David Schmerge. Fernando Miralles-Wilhelm of the University of Miami and Eric Swain of the USGS provided useful insight into the sensitivity behavior of saltwater intrusion simulations. Rhonda Howard and Barbara Howie provided many suggestions that significantly improved the clarity and content of the report. Kimberly Swidarski prepared the illustrations. USGS employee Haymeli Castillo, is recognized for her constant support, patience, and guidance.

HYDROGEOLOGY OF SOUTHWESTERN FLORIDA

Southern Florida is underlain by rocks of Cenozoic age to a depth of about 1,525 m. These rocks principally are carbonates (limestone and dolostone), with minor amounts of evaporites (gypsum and anhydrite) in the lower part of the section and clastics (sand and clay) in the upper part. The movement of ground water from inland areas to the ocean (and the reverse) occurs primarily through the carbonate rocks (Meyer, 1989, p. G5). This section of the report describes the hydrogeologic framework of the study area including the lithology, stratigraphy, hydrogeologic units, and hydraulic characteristics. Also discussed are the water-budget components, which used in conjunction with the hydrogeologic framework, are necessary to understand the processes that affect ground-water flow. Finally, water-quality and geochemical data collected from the lower Tamiami aquifer near Bonita Springs are used to examine salinity. The locations of monitoring stations for data used in the study are presented in the appendix.

Lithology and Stratigraphy

Geologic units in southwestern Florida consist, in ascending order, of the Suwannee Limestone of Oligocene age, Hawthorn Group of Oligocene to Pliocene age, Tamiami Formation of Pliocene age, and undifferentiated sediments of Holocene to Pleistocene age (fig. 3). The Suwannee Limestone is composed of fossiliferous, calcarenitic limestone with minor amounts of quartz sand. The thickness of the limestone varies widely, but commonly is greater than 100 m in Lee and Collier Counties. The basal Suwannee Limestone generally contains fine-grained, phosphatic, clastic material with interbeds of micrite and clay (Reese, 2000).

The Hawthorn Group is divided into the Arcadia Formation and the Peace River Formation (fig. 3). The Arcadia Formation, which unconformably overlies the Suwannee Limestone, consists of fine-grained carbonate sediments as well as sandy limestone, shell beds, dolomite, phosphatic sand and carbonate, sand, silt, and clay. The predominantly clastic Peace River Formation has a highly irregular erosional, and karstic surface. The contact with the overlying Tamiami Formation appears to be unconformable in some areas,

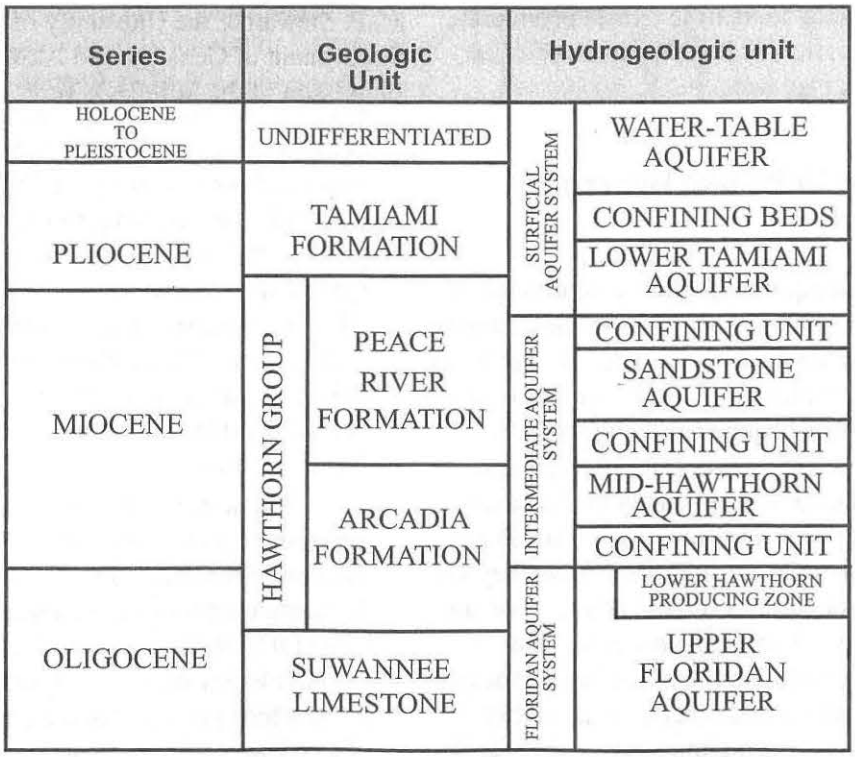


Figure 3. Generalized geologic and hydrogeologic units in the study area. Modified from Reese (2000).

but indistinct in other areas. The siliciclastic sediments of the Peace River Formation consist of interbedded, fine- to coarse-grained quartz sand, quartz silt, gravel, clay, carbonate, and phosphatic sand (Reese, 2000).

The Tamiami Formation overlies the Peace River Formation and consists of varying amounts of silt, sandy clay, micritic limestone, sandy and shelly limestone, calcareous sandstone, and quartz sand. The lithology of the Tamiami Formation varies greatly because of the complex nature of the depositional environment. The limestone is well indurated to unindurated, slightly phosphatic, variably sandy, and fossiliferous. The sand facies varies from well sorted, clean sand with abundant shells and traces of silt-size phosphate, to clayey sand with sand-size phosphate, clay-size carbonate in the matrix, and abundant well-preserved mollusk shells (Knapp and others, 1986; Reese, 2000).

The undifferentiated sediments of Holocene to Pleistocene age overlie the Tamiami Formation at land surface (Reese, 2000). These deposits mainly consist of quartz sand with minor amounts of shell and clay, and contain interfingering limestones, sandstones, and shell beds. With increasing elevation inland, the sand becomes thicker and less calcareous. The sand facies varies from fine to coarse grained, nonindurated to poorly indurated, and nonclayey to slightly clayey. Included in this group are marine terrace sediments, aeolian sand dunes, fluvial deposits, freshwater carbonates, peats, and clay beds.

Hydrogeologic Units and Hydraulic Characteristics

The principal aquifer systems in southwestern Florida are, in descending order, the surficial, intermediate, and Floridan aquifer systems (fig. 3). The focus of this report is the water-table and lower Tamiami aquifers of the surficial aquifer system and the sandstone aquifer of the upper part of the intermediate aquifer system. The confining beds of the Tamiami Formation and the upper confining unit of the Peace River Formation also are considered because they vertically "straddle" the lower Tamiami aquifer. For simplicity, these semiconfining units are called the Tamiami confining beds and the upper Hawthorn confining unit (Wedderburn and others, 1982) in this report. More detailed information on the water-bearing and confining units in southwestern Florida is presented in Reese (2000).

Maps are used in this section to show estimated hydraulic conductivities and depict the lines of equal thickness of the rock units that comprise the water-table, lower Tamiami, and sandstone aquifers. Maps showing lines of equal thicknesses were constructed by the South Florida Water Management District (1994). Histograms (fig. 4) and maps showing estimated hydraulic conductivities were developed using well construction reports and previous aquifer performance test data (Knapp and others, 1986; Montgomery, 1988). Many previously conducted aquifer performance tests were reanalyzed to assess reliability and to "fill in data gaps" (K.M. Edwards, U.S. Geological Survey, written commun., 2000). Horizontal hydraulic conductivity values (in meters per day) were computed by dividing transmissivity estimates by the thickness of the aquifer at the location of the aquifer performance test. Numerous estimates of hydraulic characteristics were compiled from various sources. Hydraulic conductivity was assumed to be log-normally distributed when computing permeability averages and standard deviations (fig. 4).

In southwestern Florida, the water-table aquifer is present in the undifferentiated deposits of Holocene to Pleistocene age and the upper part of the Tamiami Formation (fig. 3). The lines of equal thickness of the rock units that comprise the water-table aquifer range from 6 m (about 20 ft) in Hendry County south of the Caloosahatchee River to 30 m (about 100 ft) in northern Collier County along the border with Lee and Hendry Counties (fig. 5). The spatial distribution of estimated horizontal hydraulic conductivity in the water-table aquifer (fig. 6) reflects the complex heterogeneity of this characteristic in the study area. In log space (fig. 4A), the mean and standard deviation of 244 log estimates of horizontal hydraulic conductivity in the water-table aquifer were 2.16 and 0.6, respectively. In parameter space, this translates to a range of about 40 to 600 m/d, which is one standard deviation from the mean.

The water-table aquifer is underlain by rocks and sediments that form the confining beds of the Tamiami Formation (fig. 3). The thickness of these Tamiami confining beds ranges from 0 to about 15 m (about 0 to 50 ft) in Lee, Collier, and Hendry Counties (South Florida Water Management District, 1994). The beds, which pinch out in the central and northern parts of Lee County and northwestern Hendry County, are thickest in localized areas near Bonita Springs in northern and eastern Collier County, and in central and

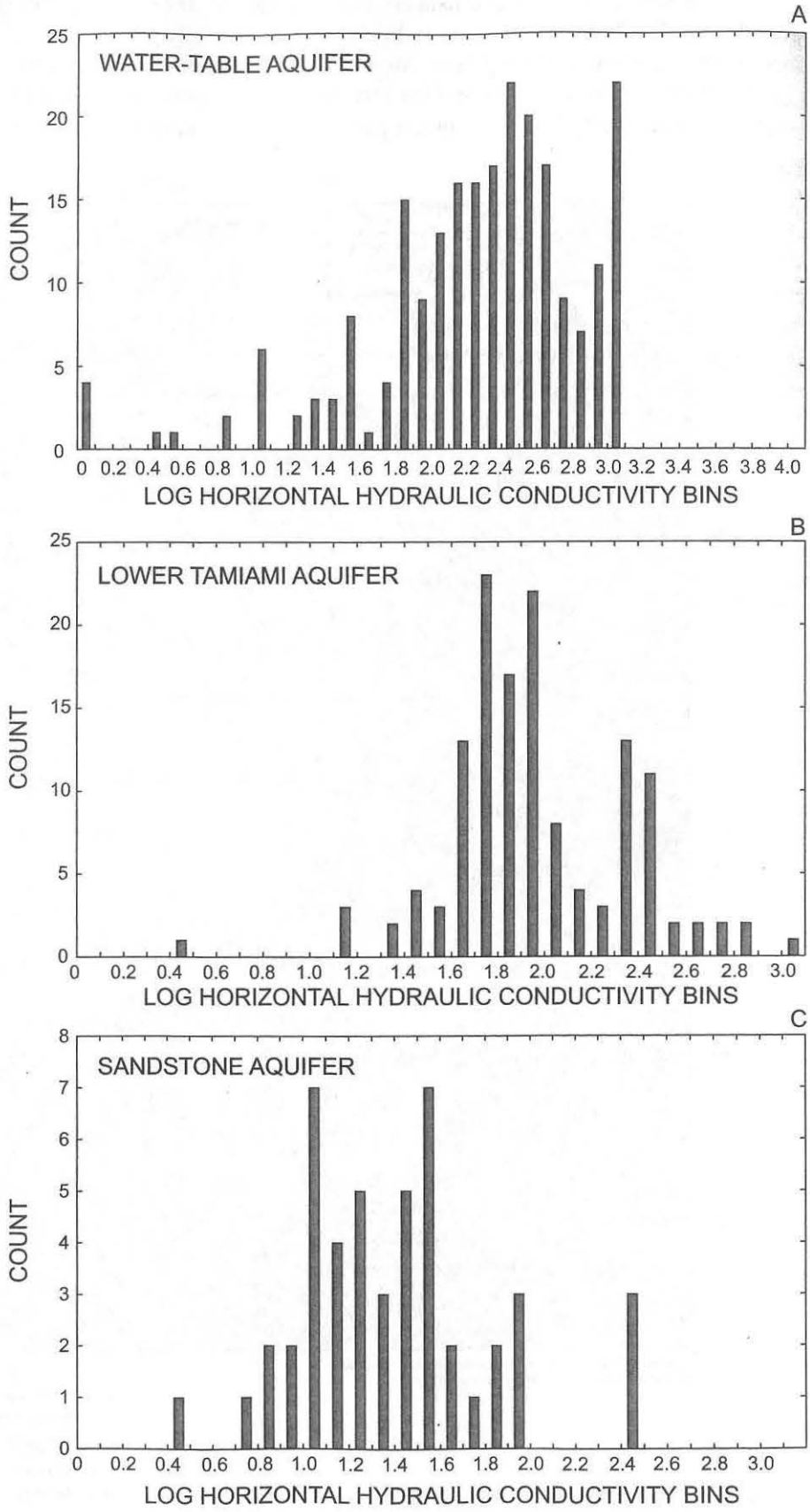


Figure 4. Estimated horizontal hydraulic conductivity values of the (A) water-table, (B) lower Tamiami, and (C) sandstone aquifers. The values of hydraulic conductivity are in meters per day.

southern Hendry County. Sparse data are available to describe the distribution of vertical hydraulic conductivity in the Tamiami confining beds. Montgomery (1988) reports a value of 0.004 m/d for vertical hydraulic conductivity based on aquifer performance tests. In a reanalysis of aquifer performance tests (K.M. Edwards, U.S. Geological Survey, written commun., 2000), four reliable values of the vertical hydraulic conductivity of the Tamiami confining beds each equaled about 0.004 m/d.

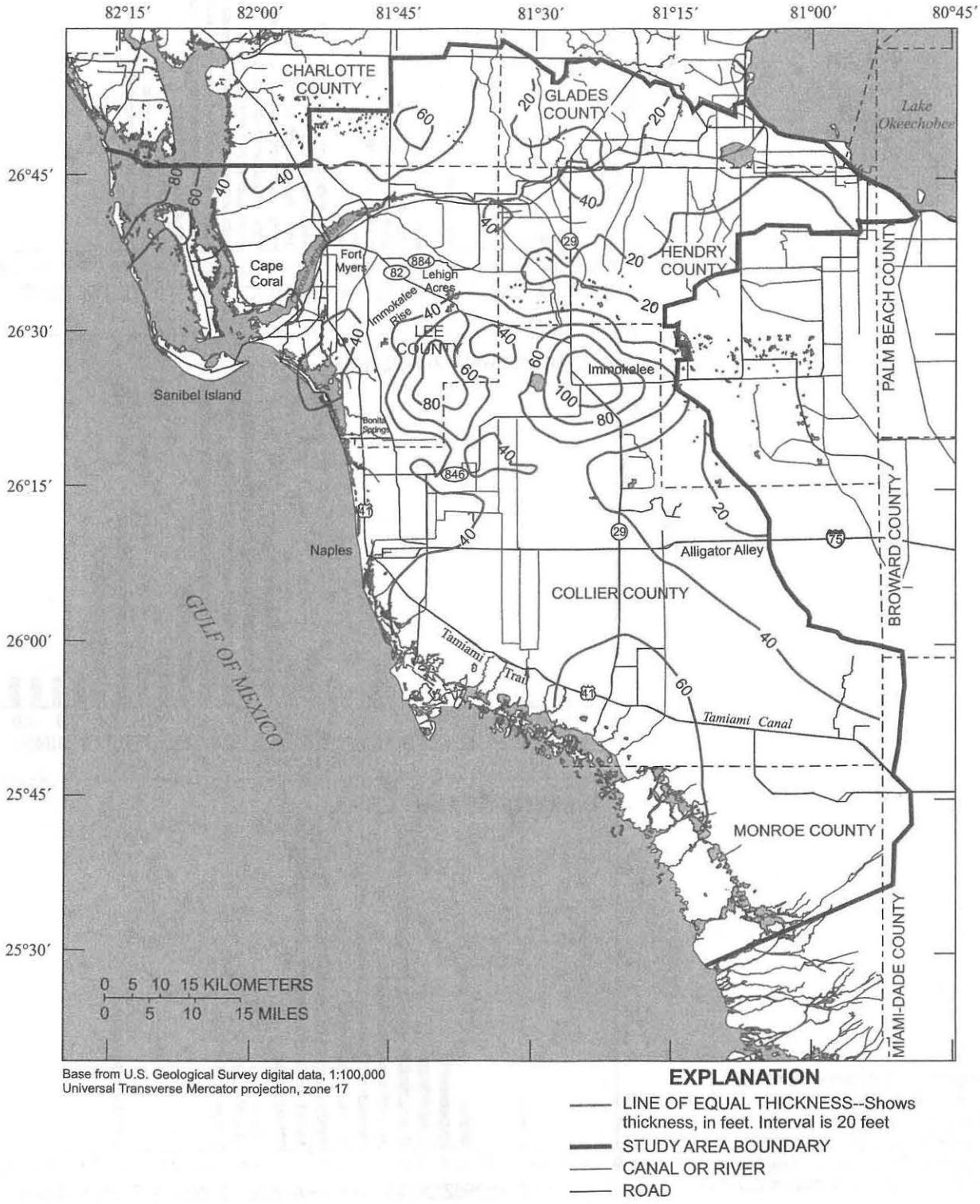


Figure 5. Lines of equal thickness of the rock units that comprise the water-table aquifer. From the South Florida Water Management District (1994).

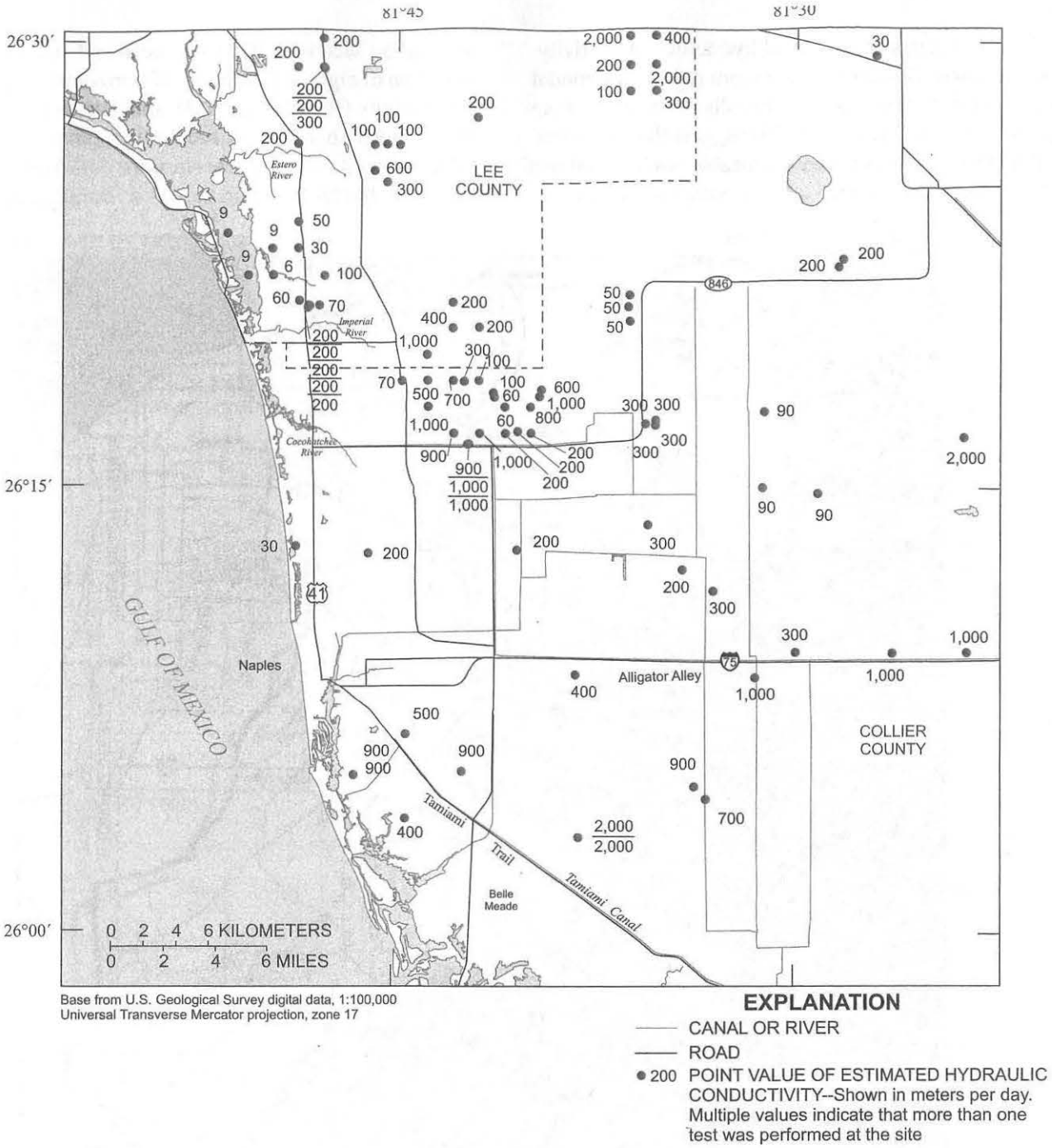


Figure 6. Spatial distribution of horizontal hydraulic conductivity in the water-table aquifer estimated from analyses of aquifer performance tests.

Underlying the confining beds, the lower Tamiami aquifer, a major water-producing unit within much of the study area, generally lies within the lower part of the Tamiami Formation of Pliocene age (fig. 3). In some places, the lower Tamiami aquifer includes unconsolidated quartz sand of late Miocene age (Knapp and others, 1986; Weedman and others, 1997; Edwards and others, 1998). The lines of equal thickness of the rock units that comprise the lower Tamiami aquifer ranges from 0 to 55 m (about 0 to 180 ft) in Lee, Henry, and Collier Counties (fig. 7). The aquifer, which is not present in the central and northern parts of Lee County and in northwestern Hendry County, is thickest in localized areas southeast of Bonita Springs (fig. 7).

Estimates of horizontal hydraulic conductivity in the lower Tamiami aquifer seem to have a bimodal log K distribution (fig. 4B). Results from this and previous research (Meeder, 1979) suggest that the lower Tamiami aquifer is highly permeable where coral reef facies are present (fig. 8). In the coral reef facies mapped by Meeder (1979), the mean and standard deviation of eight log estimates of horizontal hydraulic conductivity (fig 4B) were 2.11 and 0.4, respectively. In parameter space, this translates to a range of about 50 to 300 m/d, which is one standard deviation from the mean. In places within the lower Tamiami aquifer

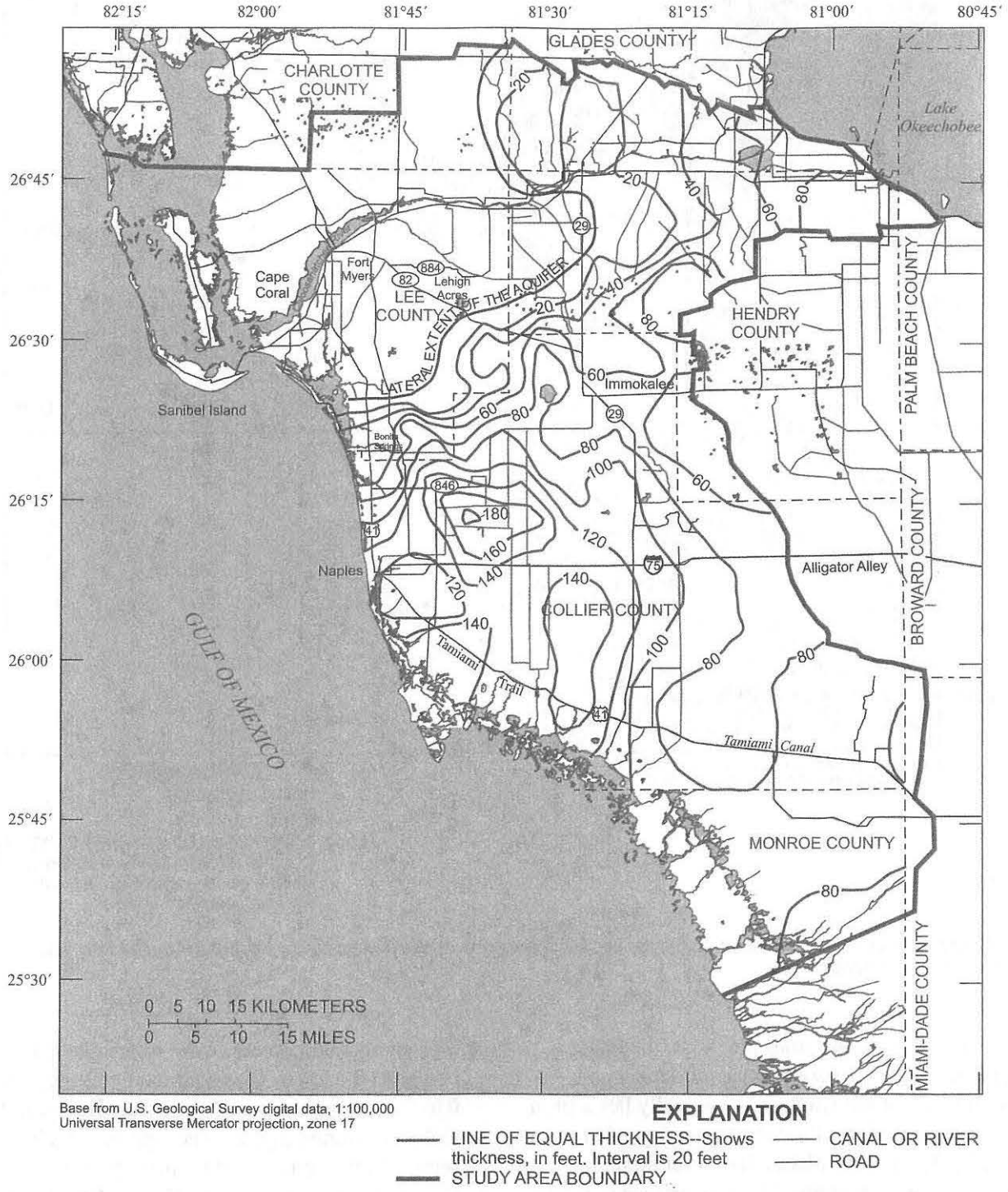


Figure 7. Lines of equal thickness of the rock units that comprise the lower Tamiami aquifer. From the South Florida Water Management District (1994).

where coral reef facies are not present, the mean and standard deviation of 136 log estimates of horizontal hydraulic conductivity (fig. 4B) were 1.8 and 0.4, respectively. In parameter space, this translates to a range of about 30 to 200 m/d, which is one standard deviation from the mean.

The lower Tamiami aquifer is underlain by rocks and sediments that form the upper confining unit of the Hawthorn Group (fig. 3). This unit, called the upper Hawthorn confining unit in this report, thins and may be absent near Bonita Springs (Wedderburn and others, 1982). Limited data are available to describe the

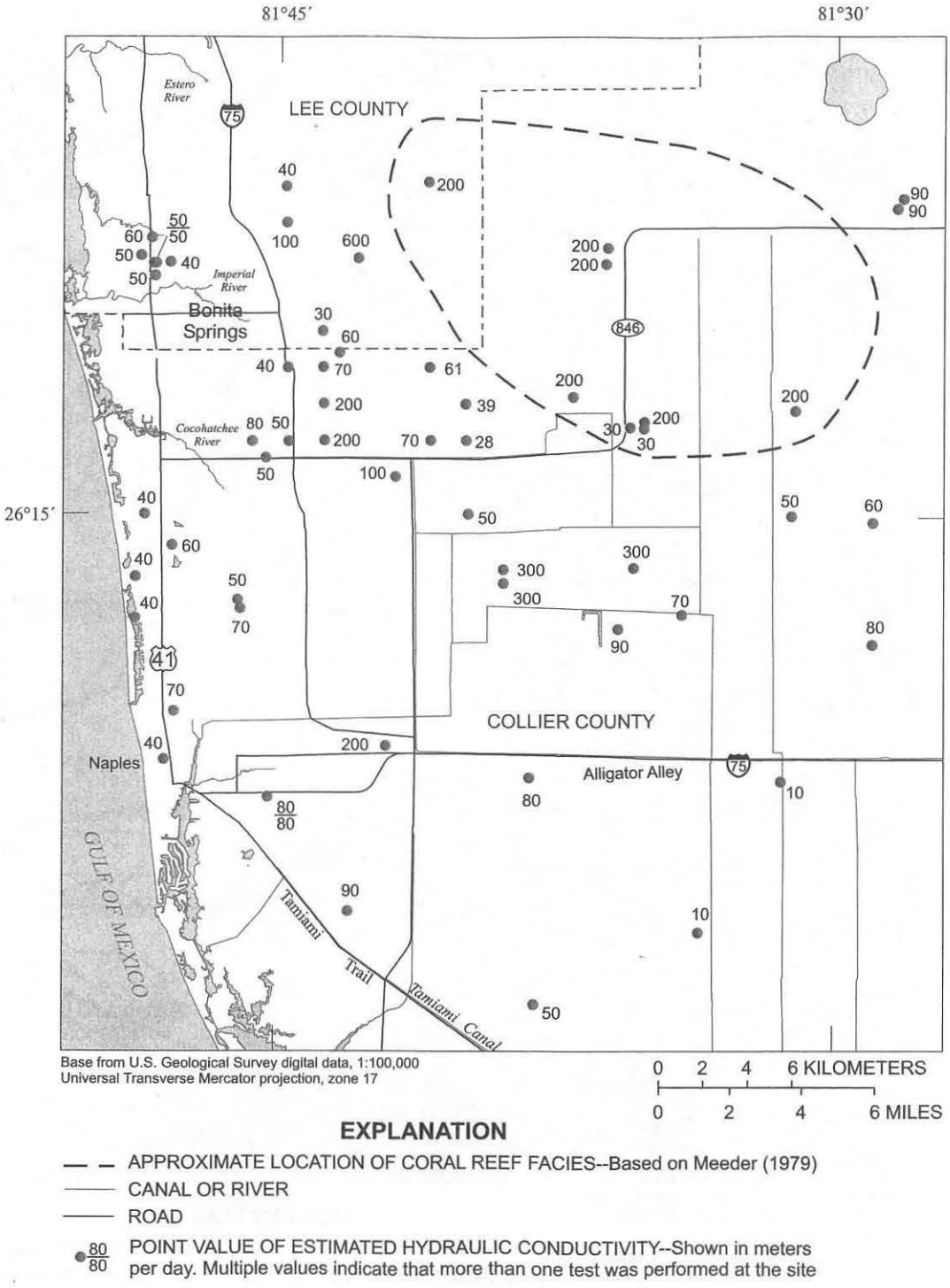


Figure 8. Spatial distribution of horizontal hydraulic conductivity in the lower Tamiami aquifer estimated from analyses of aquifer performance tests.

distribution of vertical hydraulic conductivity in the upper Hawthorn confining unit. Montgomery (1988) reports a value of 0.003 m/d for vertical hydraulic conductivity based on aquifer performance tests. This value was used by Bower and others (1990) and Bennett (1992) in numerical models for parts of the study area.

The sandstone aquifer underlies the upper Hawthorn confining unit in the intermediate aquifer system (fig. 3). The lines of equal thickness of the rock units that comprise the sandstone aquifer range from 0 to 33 m (0 to about 110 ft) in Lee, Henry, and Collier Counties (fig. 9). The sandstone aquifer seems to be

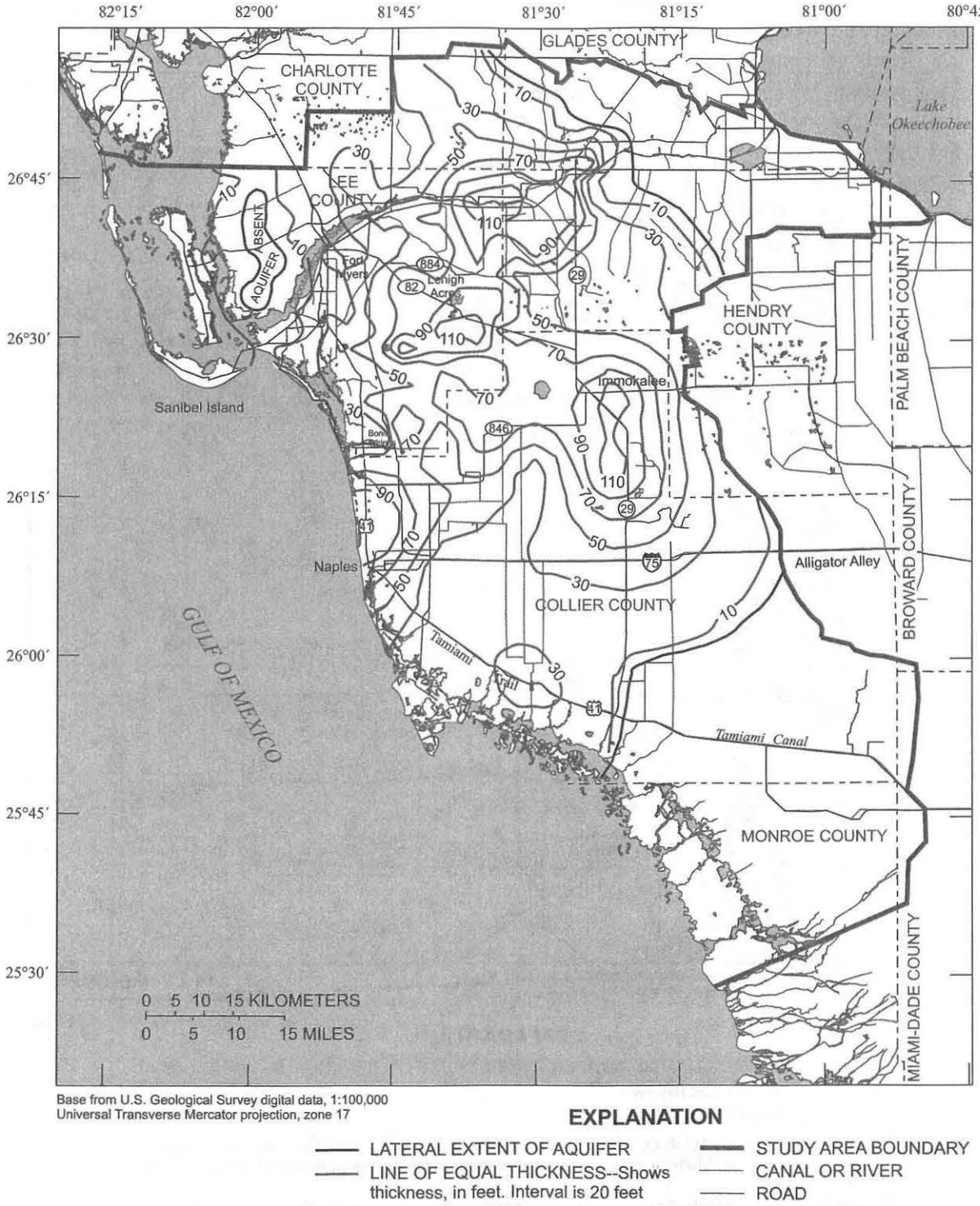


Figure 9. Lines of equal thickness of the rock units that comprise the sandstone aquifer. From the South Florida Water Management District (1994).

thickest in localized areas in northern Collier County, southeastern Lee County, and northeastern Lee County and is absent in southeastern Collier County, northeastern Hendry County, and in parts of northwestern Lee County (fig. 9). The spatial distribution of estimated horizontal hydraulic conductivity in the sandstone aquifer (fig. 10) reflects the complex heterogeneity of this characteristic in the study area. In log space (fig. 4C), the mean and standard deviation of 25 log estimates of horizontal hydraulic conductivity in the sandstone aquifer were 1.26 and 0.4, respectively. In parameter space, this translates to a range of about 10 to 50 m/d, which is one standard deviation from the mean.

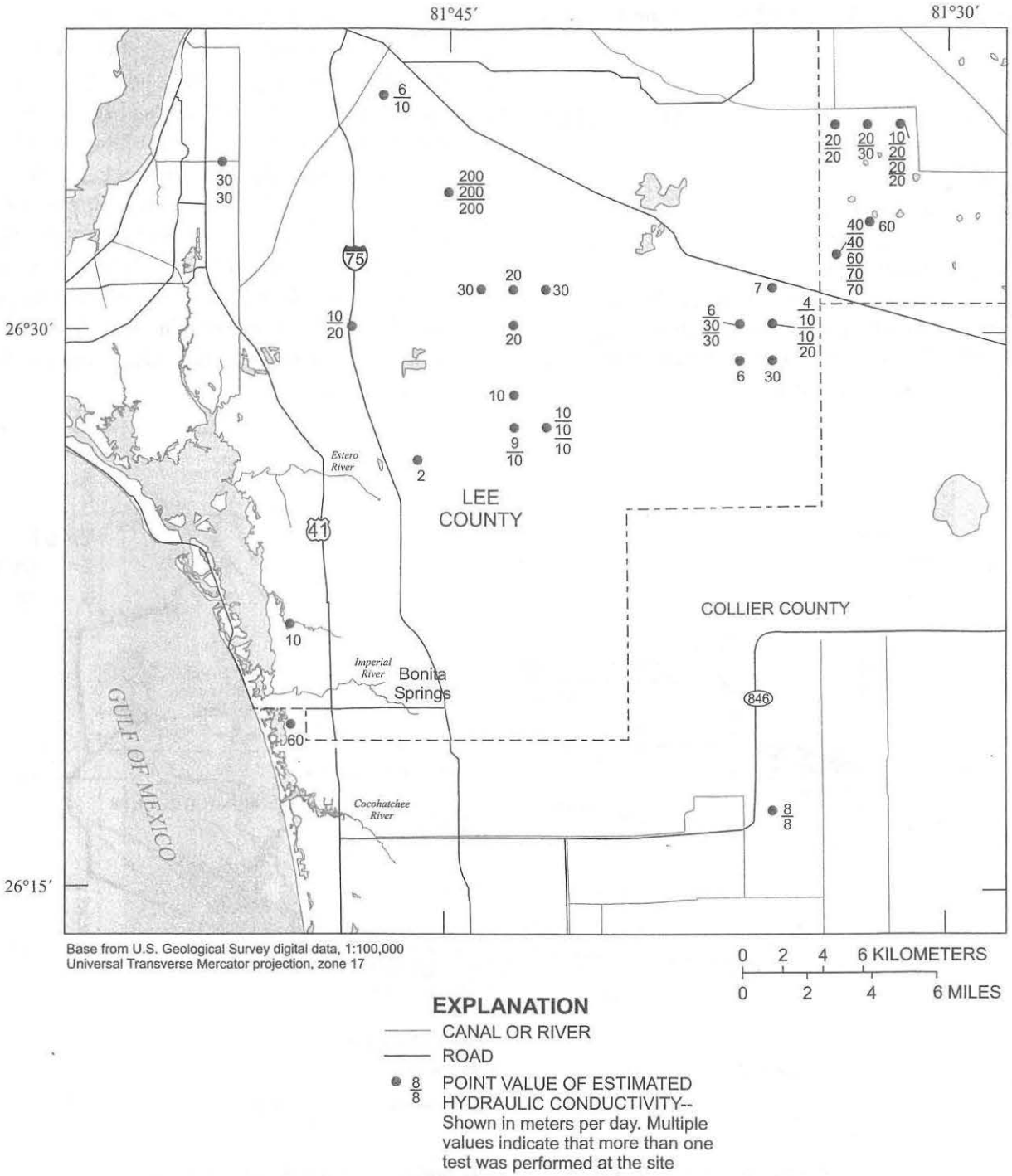


Figure 10. Spatial distribution of estimated horizontal hydraulic conductivity in the sandstone aquifer.

Water Budget

This section describes components of the water budget that may be affecting saltwater movement in the water-table and lower Tamiami aquifers near Bonita Springs (fig. 11). Equation 1 provides a qualitative understanding of how these components interact. The terms are not summed together in this analysis; therefore, the units of each component are sometimes reported differently depending upon the source of information.

$$P + I - ET - D - Q_S - Q_P - Q - Q_{uk} = \Delta S \cong 0, \quad (1)$$

where

P is precipitation;
I is irrigation;
ET is evapotranspiration;
D is net deep leakage between the sandstone aquifer and the lower Tamiami aquifer;
Q_S is submarine ground-water discharge to the Gulf of Mexico,
Q_P is pumpage from the water-table and lower Tamiami aquifers;
Q is stream discharge, which is composed of surface runoff, Q_{ro}, and baseflow, Q_B;
Q_{uk} is other or unknown components of the water budget that may be affecting saltwater movement; and
ΔS is change in storage, which is assumed to be negligible over the long term.

Precipitation (P) and irrigation (I) that exceed evapotranspiration (ET) and runoff (Q_{ro}) can recharge the water table if it infiltrates land surface and overcomes capillary forces in the unsaturated zone. This recharge is generally called net recharge. Krulikas and Giese (1995) estimate net recharge in the study area to range from 1.5 to 22.9 cm/yr, using chloride concentration ratios and flow-tube analysis methods. They further indicate that net recharge rates greater than 22.9 cm/yr could be induced by lowering the water table through ground-water withdrawals or seepage to canals.

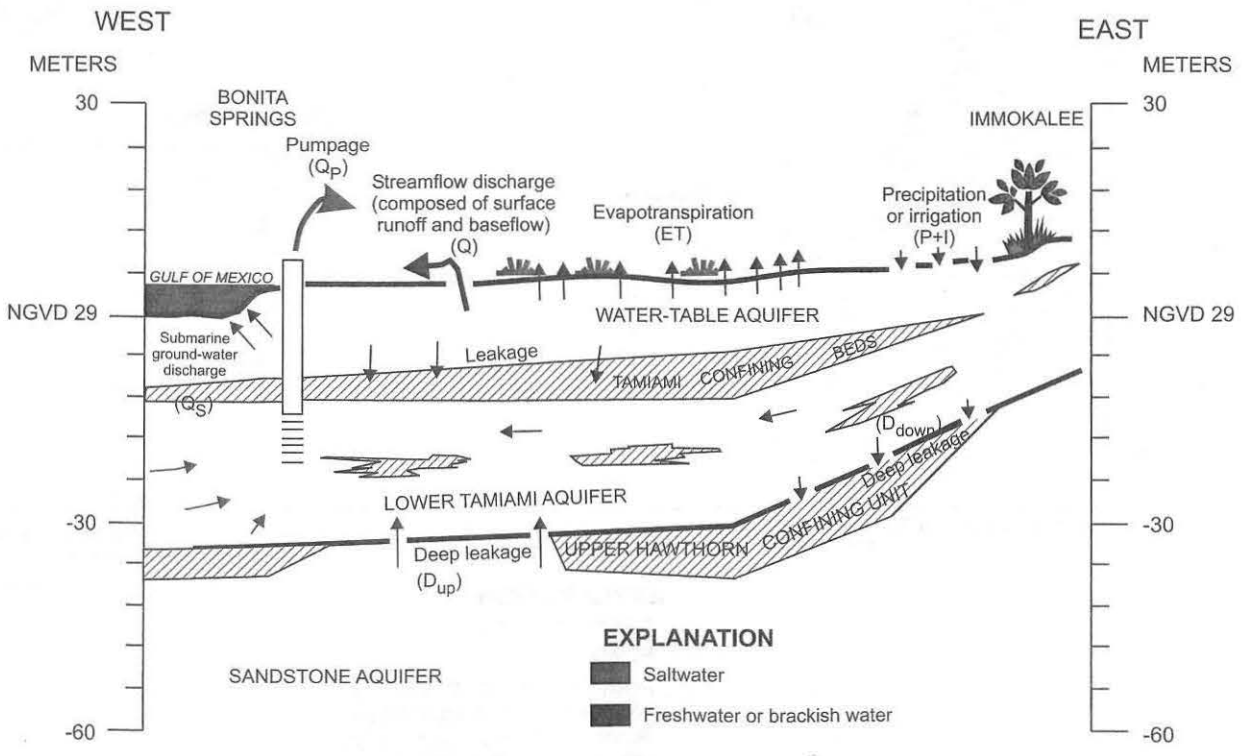


Figure 11. Hypothetical control volume and selected water-budget components within the study area. D_{up} is deep upward leakage and D_{down} is deep downward leakage. NGVD 29 is National Geodetic Vertical Datum of 1929.

Net deep leakage, D, represents the difference between upward, D_{up}, and downward leakage, D_{down}, that occurs naturally between the lower Tamiami and sandstone aquifers. This leakage results from the semiconfining nature of the upper Hawthorn confining unit and the difference in head between the aquifers (fig. 11). Deep leakage was inferred between the lower Tamiami and sandstone aquifers using a map of the head difference between these two units. Average 1996 water levels were computed from water levels measured in 45 USGS monitoring wells in the lower Tamiami aquifer, and from 30 USGS monitoring wells in the sandstone aquifer (table 1). Average water levels were plotted and contoured and spatially interpolated to a common grid. The difference in interpolated head between the lower Tamiami and sandstone aquifers was then computed. This approach has many assumptions including: (1) water-level contours in the lower Tamiami aquifer are vertical; (2) water-level contours in the sandstone aquifer are vertical; and (3) the head difference, as calculated from the water-level contours, occurs directly within the upper Hawthorn confining unit.

In 1996, head differences between the lower Tamiami and sandstone aquifers ranged from -2.0 to 2.6 m (fig. 12). A negative sign suggests leakage is upward into the lower Tamiami aquifer, whereas a positive sign suggests leakage is downward into the sandstone aquifer. Areas where relatively large amounts of deep leakage occur are indicated by large positive or negative head-difference values. For example, Bonita Springs may have the largest amount of deep leakage occurring into the lower Tamiami aquifer because this area has the largest negative head-difference values (about -2.0 to -0.5 m). The assumption is that the upper Hawthorn confining unit is continuous with a constant vertical hydraulic conductivity.

Submarine ground-water discharge to the Gulf of Mexico, Q_S, occurs as ground water flowing toward the Gulf of Mexico moves upward and over more saline ground water. Fresher ground water discharges to the bottom of the Gulf of Mexico or Estero Bay. Estimates of submarine ground-water discharge are difficult to find in the study area. However, a recent study of submarine ground-water discharge from the Biscayne aquifer to Biscayne Bay in coastal southeastern Florida was completed by Langevin (2001). The average rate of submarine ground-water discharge to Biscayne Bay over a 10-year period was 200,000 m^3/d along 100 km of coastline. The Biscayne aquifer is more permeable and receives more recharge than the water-table aquifer near Bonita Springs, which suggests submarine ground-water discharge near this area would be less than that in Biscayne Bay.

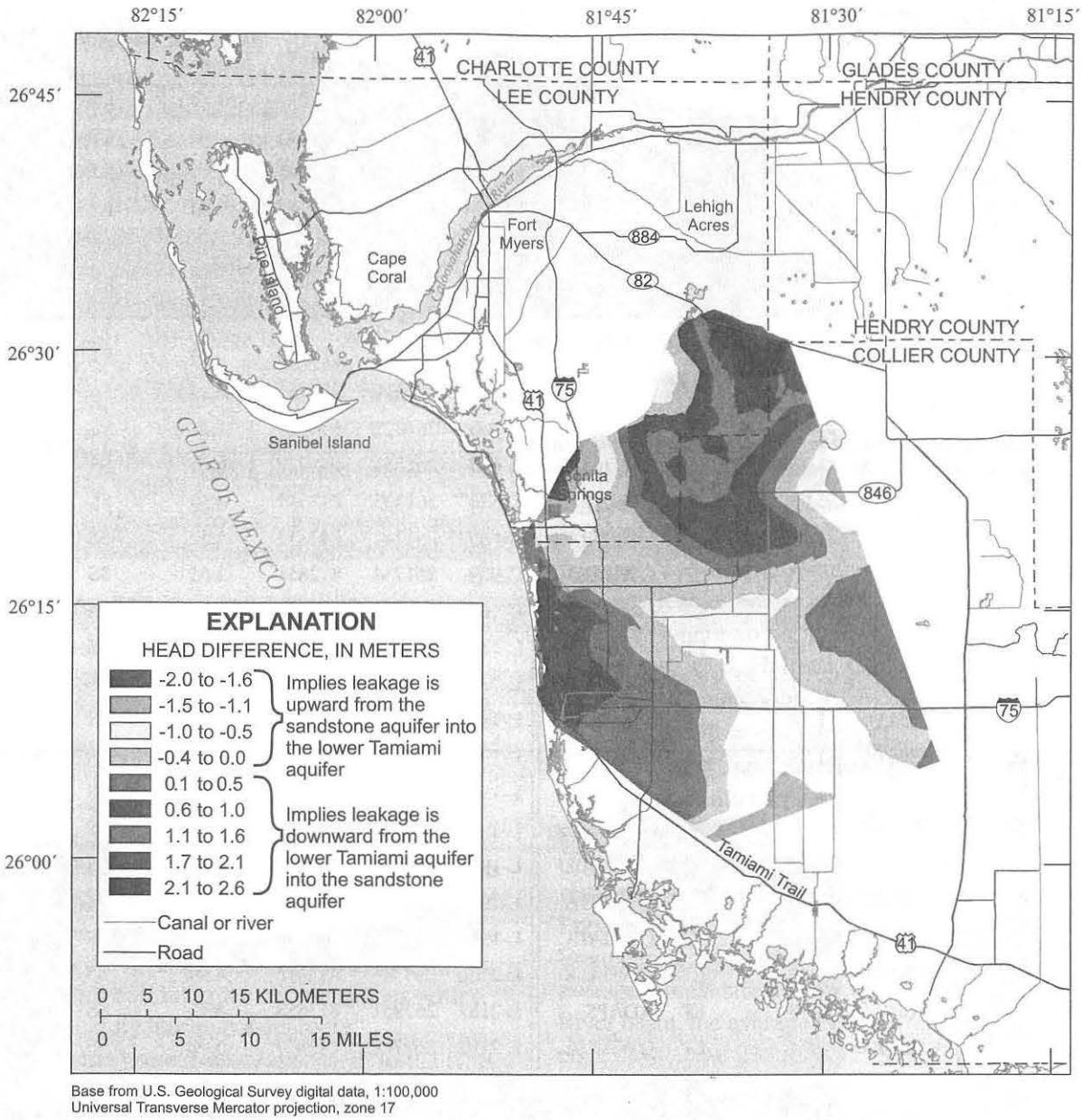
Ground-water pumpage, Q_P, from the water-table and lower Tamiami aquifers in the study area (fig. 11) is monitored by the SFWMD. According to R.L. Marella (U.S. Geological Survey, written commun., 1999), ground-water withdrawals by municipal supply facilities in Lee and Collier Counties nearly doubled from 1985 to 1998 (fig. 13). Withdrawals generally are greater during the dry season (October to May) when rainfall is scarce than during the wet season (June to September) when rainfall is abundant (fig. 14). A water-use survey suggests a large volume of unmonitored ground-water pumpage from the lower Tamiami aquifer occurred for irrigation and agricultural uses (P.A. Telis, U.S. Geological Survey, written communication, 2000). This survey, however, was restricted to a small sample size with an even smaller number of responses. Unmonitored ground-water pumpage could exceed monitored ground-water pumpage in the lower Tamiami aquifer because the deepest areas of potentiometric drawdown exist at locations where no monitored ground-water pumpage is occurring (K.J. Halford, U.S. Geological Survey, written communication, 1999).

Streamflow discharge, Q, is composed of surface runoff, Q_{ro}, and baseflow, Q_B (fig. 11). In 1996, the average annual streamflow (including runoff and baseflow) at four gaging stations was about 2 m^3/s (fig. 1, Spring Creek, Imperial River, and northern and southern branches of Estero River). The area of the Imperial River basin is about 2.2×10^8 m^2 (Johnson Engineering, Inc., and others, 1999). By dividing the average annual streamflow by the area of the Imperial River basin, the average rate of streamflow in the basin equates to about 29 cm/yr in 1996. The rainfall rate in the Imperial River basin was about 1.3 m/yr in 1996, as estimated from a rainfall monitoring station near Bonita Springs. Land use in the Imperial River basin is predominantly nonurban where runoff coefficients averaged from Bennett (1992) are about 0.1. Using this runoff coefficient to assume a 13-cm/yr average runoff rate from the 1.3-m/yr rainfall rate, the average rate of baseflow, B_f, in the basin equates to about 16 cm/yr. Higher (wet season) water levels from the water-table aquifer can force more baseflow to surface-water features, creating rates greater than 16 cm/yr. Conversely, lower (dry season) water levels can induce baseflow rates less than 16 cm/yr.

Table 1. Average 1996 water levels computed from selected monitoring wells in the lower Tamiami and sandstone aquifers

[USGS, U.S. Geological Survey; Aquifer: SS, sandstone; LT, lower Tamiami; QWDATA, Water-Quality Database; ADAPS, Automated Data Processing System]

Site identification	Latitude	Longitude	Average 1996 head (meters)	Aquifer	USGS data source	Site identification	Latitude	Longitude	Average 1996 head (meters)	Aquifer	USGS data source
C-130	260903	814803	0.76	LT	QWDATA	C-1083	261856	814719	0.77	LT	ADAPS
C-304	261636	813612	2.19	LT	QWDATA	L-738	262023	814640	.40	LT	ADAPS
C-363	262556	812424	7.89	LT	QWDATA	L-1625	263330	813942	5.17	LT	QWDATA
C-391	261124	814730	1.24	LT	ADAPS	L-1691	262043	814549	.80	LT	QWDATA
C-458	261402	814613	1.52	LT	QWDATA	L-5723	262103	814643	-.03	LT	QWDATA
C-460	261406	814654	1.33	LT	QWDATA	L-5725	261947	814902	.47	LT	QWDATA
C-460	261408	814706	1.78	LT	ADAPS	L-5745	261925	814536	.52	LT	QWDATA
C-462	262725	812606	8.73	LT	QWDATA	L-5747	262259	814716	-.20	LT	QWDATA
C-472A	260926	814751	1.05	LT	QWDATA	C-298	262508	812351	6.25	SS	QWDATA
C-474A	261115	814822	.47	LT	QWDATA	C-303	261622	814122	1.71	SS	QWDATA
C-490	261244	814802	1.25	LT	QWDATA	C-687	262555	812837	6.66	SS	QWDATA
C-492	262228	813619	5.09	LT	ADAPS	C-688	261803	813547	3.30	SS	QWDATA
C-516	261157	814757	1.54	LT	QWDATA	C-689	261741	812353	3.52	SS	QWDATA
C-525	261003	814836	.83	LT	QWDATA	C-989	261734	812854	2.61	SS	QWDATA
C-526	261019	814840	.80	LT	QWDATA	C-1077	262823	812131	7.88	SS	QWDATA
C-528	261201	814829	.68	LT	QWDATA	L-727	263851	813653	4.10	SS	QWDATA
C-600	260550	814418	.91	LT	QWDATA	L-741	262553	814585	2.61	SS	QWDATA
C-951	261349	813513	1.54	LT	ADAPS	L-1853	262707	814353	2.30	SS	QWDATA
C-956	261344	813847	1.24	LT	QWDATA	L-1907	264309	814059	2.71	SS	QWDATA
C-973	260844	813241	1.72	LT	QWDATA	L-1963	263345	813616	4.47	SS	QWDATA
C-975	260305	813913	2.08	LT	QWDATA	L-1965	263354	813357	4.83	SS	QWDATA
C-977	260916	813858	1.92	LT	QWDATA	L-1974	263719	814849	4.91	SS	QWDATA
C-979	262122	813554	4.46	LT	QWDATA	L-1975	264400	814246	4.83	SS	QWDATA
C-982	262159	812833	2.77	LT	QWDATA	L-1977	264321	813656	2.80	SS	QWDATA
C-985	261734	812854	3.02	LT	QWDATA	L-2186	263345	813616	4.99	SS	QWDATA
C-988	261447	812849	3.73	LT	ADAPS	L-2187	263951	813553	4.15	SS	QWDATA
C-998	261621	814501	.71	LT	QWDATA	L-2192	262700	813824	5.08	SS	QWDATA
C-1003	261437	814802	1.78	LT	QWDATA	L-2194	262022	814321	1.93	SS	ADAPS
C-1004	261622	814644	.92	LT	ADAPS	L-2200	264330	813403	2.91	SS	QWDATA
C-1058	261538	814611	.22	LT	QWDATA	L-2215	263128	813515	5.63	SS	QWDATA
C-1064	260138	813758	.58	LT	QWDATA	L-2216	264609	814540	5.46	SS	QWDATA
C-1066	255638	812813	-.04	LT	QWDATA	L-5648	263250	814743	4.61	SS	QWDATA
C-1068	260315	813230	1.02	LT	QWDATA	L-5649	262935	814957	3.73	SS	QWDATA
C-1070	260814	812142	3.85	LT	QWDATA	L-5664	262515	81933	2.81	SS	QWDATA
C-1073	261741	812353	4.22	LT	QWDATA	L-5666	262514	814328	1.63	SS	QWDATA
C-1074	262520	811620	7.16	LT	QWDATA	L-5668	262514	814717	2.57	SS	QWDATA
C-1076	262823	812131	8.40	LT	QWDATA	L-5672	262332	813831	4.25	SS	QWDATA
						L-5673	262332	813831	1.90	SS	QWDATA



Base from U.S. Geological Survey digital data, 1:100,000
Universal Transverse Mercator projection, zone 17

Figure 12. Average annual head difference between the lower Tamiami and sandstone aquifers in 1996.

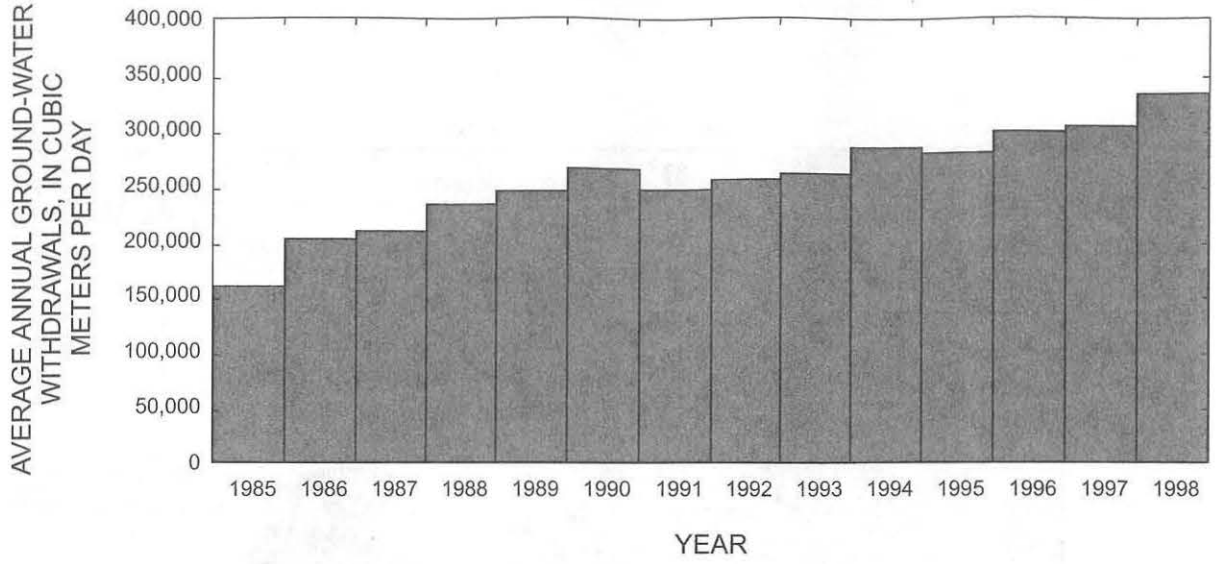


Figure 13. Average annual ground-water withdrawals from municipal supply facilities in Lee and Collier Counties, 1985-98. From R.L Marella (U.S. Geological Survey, written commun. 1999).

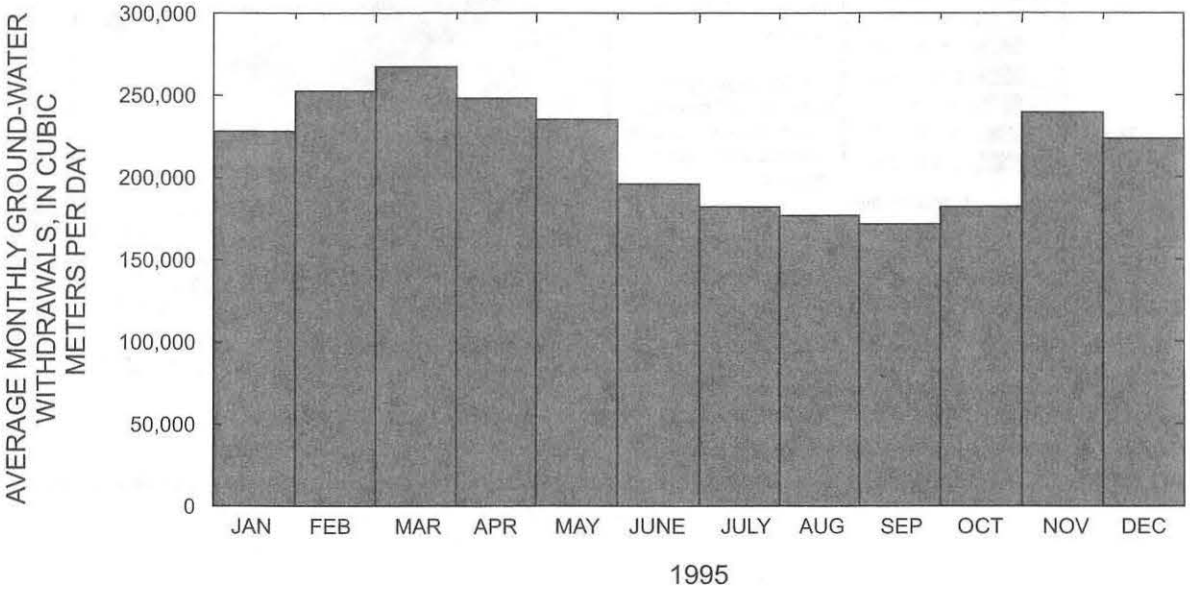


Figure 14. Average monthly ground-water withdrawals from municipal supply facilities in Lee and Collier Counties, 1995.

Water Quality and Geochemistry

Water-quality and geochemical data collected from the lower Tamiami aquifer near Bonita Springs were used to examine historical trends in salinity and to identify potential sources of saltwater. Numerous water samples were collected and analyzed for chloride concentration and strontium isotopes (Schmerge, 2001). Chloride concentration is a common surrogate for salinity, and strontium isotopes have proven to be a useful tracer for determining ground-water movement and the origin of salinity (Clark and Fritz, 1997). Further explanation of methods and data analysis of strontium isotopes can be found in Schmerge (2001).

Historical trends in salinity were examined for nine USGS monitoring wells open to the lower Tamiami aquifer near Bonita Springs; chloride concentrations ranged from about 10 to 1,300 mg/L (fig. 15). Monitoring well L-738 is the only well examined with a record that pre-dates 1985. Chloride concentrations in well L-738 have increased steadily from about 100 mg/L in 1968 to about 350 mg/L in 1998. A statistical analysis conducted by Prinos and others (2002) detected a significant upward trend in chloride concentration at monitoring well L-738. Chloride concentrations in this well have increased at a rate of about 6.6 mg/L annually from 1974 through 1998 (Prinos and others, 2002). Several possible explanations for this increasing chloride concentration are presented later in the discussion of ground-water flow and mechanisms of saltwater intrusion. In the other eight wells, chloride concentrations remained relatively stable or decreased over time.

Salinity also was examined historically by comparing areal maps of chloride concentration in the lower Tamiami aquifer. In a study by Knapp and others (1986), lines of equal chloride concentration reached a maximum value of 500 mg/L near Bonita Springs (fig. 16A). In a study by Schmerge (2001), lines of equal chloride concentration reached a maximum value of 1,000 mg/L near Bonita Springs (fig. 16B). Additionally, the 300-mg/L line of equal chloride concentration extended farther inland in the latter study. This comparison suggests saltwater occurs farther eastward than in 1986 in the lower Tamiami aquifer near Bonita Springs. Differences in the locations of lines of equal chloride concentrations, however, could be explained by differences in the amount and location of data available for contouring in Knapp and others (1986) and Schmerge (2001). With this in mind, the historical comparison of lines of equal chloride concentration does not conclusively determine if saltwater has moved since 1986.

Water samples were collected from the lower Tamiami aquifer near Bonita Springs for strontium isotope analyses (Schmerge, 2001). Strontium isotope data can be used in conjunction with the hydrogeologic framework to provide evidence of the source of strontium in ground water (Sacks and Tihansky, 1996). Results suggest that the source of strontium in ground water sampled in the lower Tamiami aquifer near Bonita Springs is the underlying Floridan aquifer system (Schmerge, 2001).

GROUND-WATER FLOW AND MECHANISMS OF SALTWATER INTRUSION

Ground-water flow patterns and potential mechanisms of saltwater intrusion in the study area are described in this section. Lateral ground-water flow in the lower Tamiami aquifer occurs in a southwesterly direction and becomes radially convergent near Bonita Springs. Vertical ground-water flow can be inferred from a map of the head difference between the lower Tamiami and sandstone aquifers (fig. 12). This map suggests that the greatest rates of vertical ground-water flow from the sandstone aquifer to the lower Tamiami aquifer are occurring beneath Bonita Springs, assuming that the upper Hawthorn confining unit is continuous and uniform in thickness and hydraulic conductivity. Approaching the saltwater interface, fresher ground water flowing toward the Gulf of Mexico moves upward and over more saline ground water that is flowing toward inland areas in lower parts of the lower Tamiami aquifer. This circulation process in the saltwater interface was observed in the Biscayne aquifer by Kohout (1964) and can only be inferred from the current monitoring well network established near Bonita Springs.

The distribution of saltwater in the lower Tamiami aquifer is likely not at equilibrium with current hydrologic conditions near Bonita Springs because of rapidly increasing rates of ground-water pumpage, rising sea level, and the lag in response time for saltwater to move to equilibrium when hydrologic conditions change. In fact, four potential mechanisms could move saltwater into zones of the lower Tamiami aquifer previously occupied by fresher waters. These mechanisms are: (1) lateral movement of the

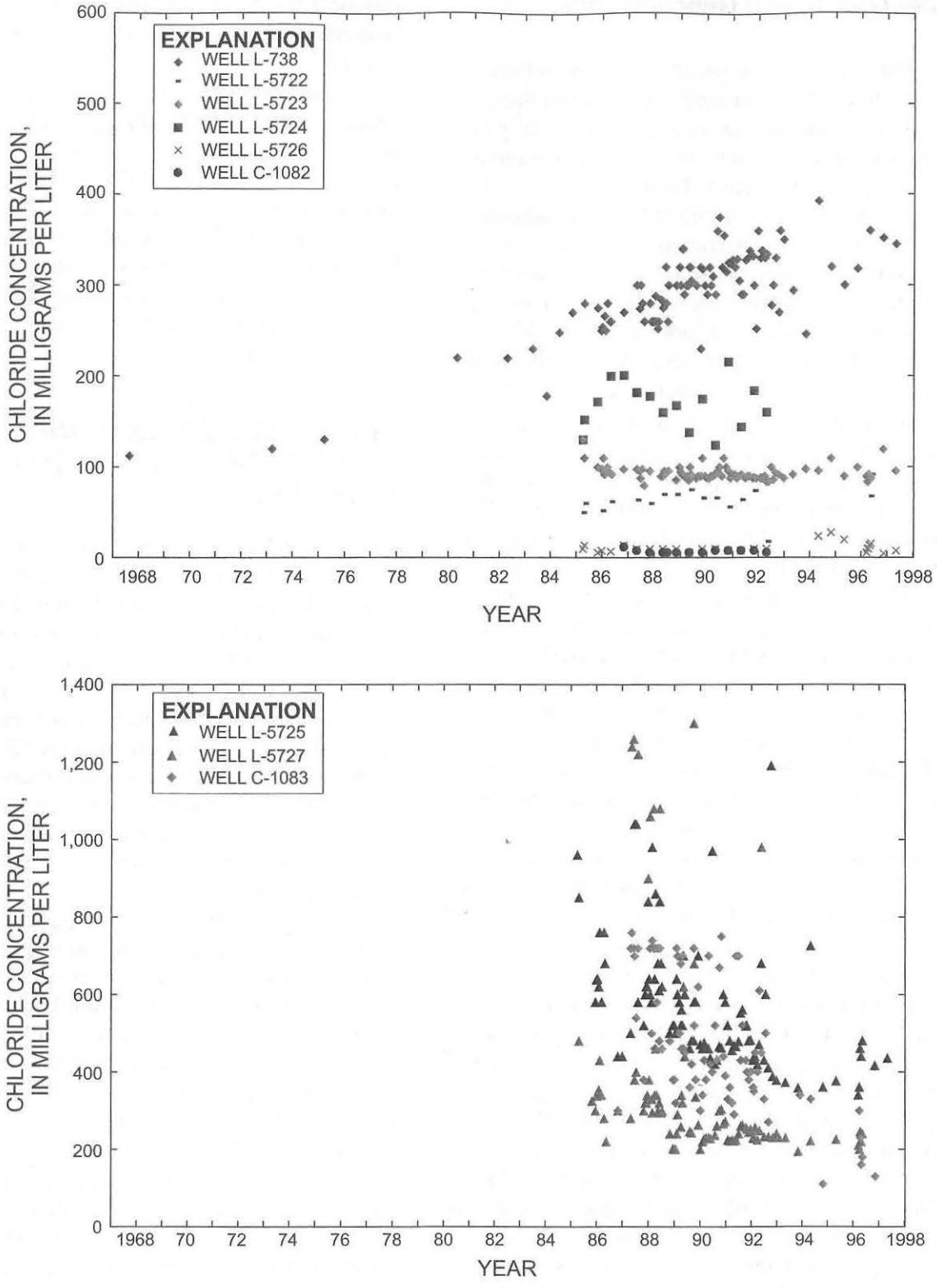


Figure 15. Historical trends in chloride concentration for selected monitoring wells near Bonita Springs, 1968-98. Well locations are shown in figure 1.

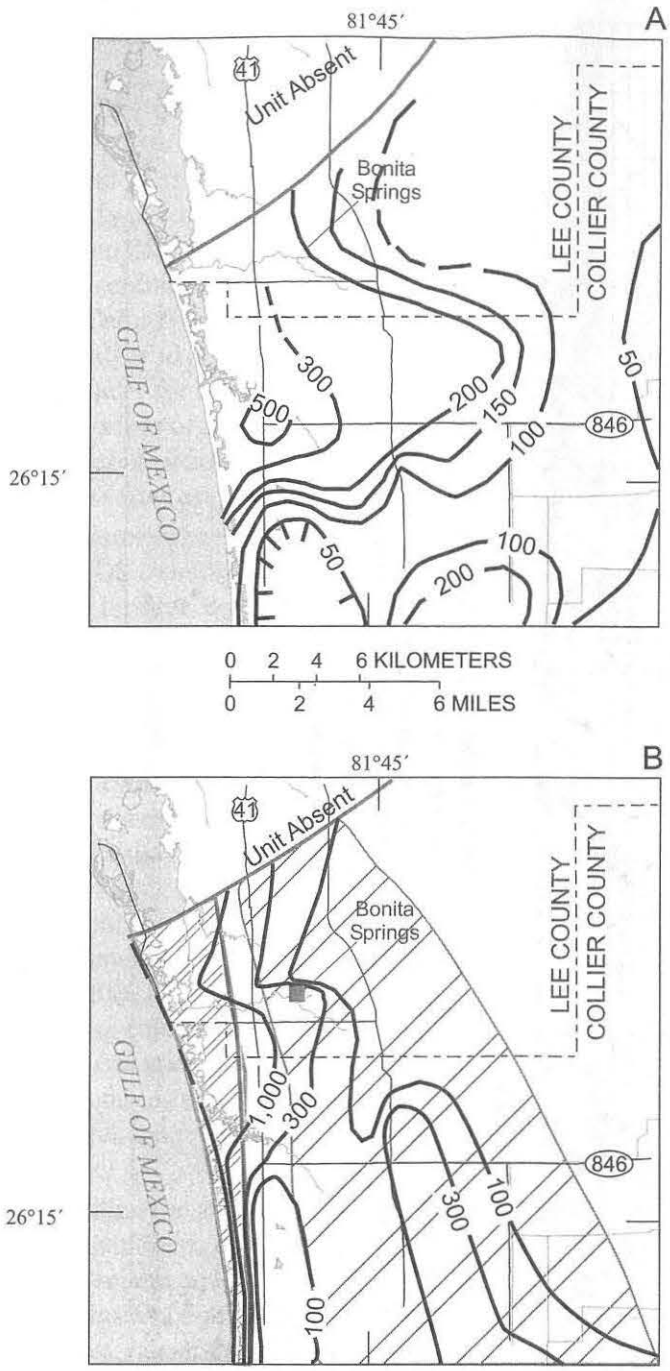


Figure 16. Lines of equal chloride concentration in the lower Tamiami aquifer near Bonita Springs over time. Map A modified from Knapp and others (1986), and map B modified from Schmerge (2001).

freshwater-saltwater interface inland from the southwestern coast of Florida; (2) upward leakage from deeper, saline water-bearing zones through natural upwelling and upconing; (3) downward leakage of saltwater from surface-water channels; and (4) movement of unflushed pockets of relict seawater in the lower Tamiami and water-table aquifers (fig. 17).

Lateral Encroachment

Lateral encroachment of recent seawater into the lower Tamiami aquifer may be possible in southwestern Florida. Saline ground water beneath the Gulf of Mexico could move through the permeable rock comprising the lower Tamiami aquifer to come into equilibrium with modern natural and anthropogenic stresses, such as withdrawals, sea level, and drought (fig. 17). Some evidence indirectly suggests the occurrence of lateral encroachment in the lower Tamiami aquifer near Bonita Springs. For instance, the average annual potentiometric surface of the lower Tamiami aquifer in 1996 is below sea level in some areas beneath Bonita Springs adjacent to the Gulf of Mexico; however, the predominance of lateral encroachment is uncertain.

Upward Leakage

A plausible mechanism for the movement of saline ground water into the freshwater zones of the lower Tamiami aquifer near Bonita Springs is upward leakage (fig. 17) either through natural upwelling or upconing. Natural upwelling is defined here as the upward movement of ground water within or into the lower Tamiami aquifer due to head differences caused by natural stress-producing processes. Natural upwelling can cause saltwater intrusion where salinity is higher in deeper locations of higher head. Upconing is defined here as the upward movement of saline ground water within or into the lower Tamiami aquifer due to head differences caused by anthropogenic stress. The primary difference between these two processes is the source of stress, either natural or anthropogenic.

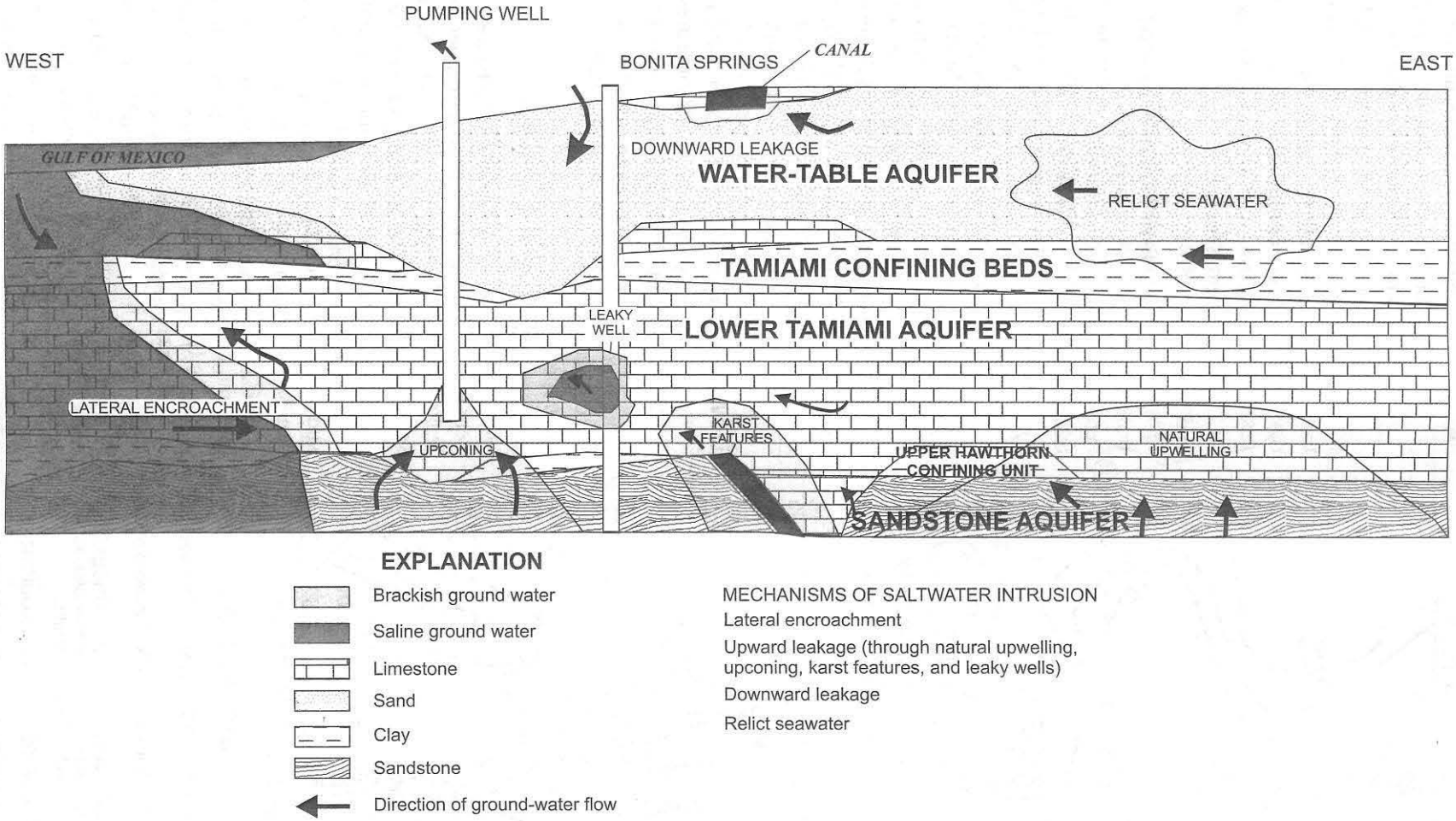


Figure 17. Potential mechanisms of saltwater intrusion in the lower Tamiami aquifer near Bonita Springs.

Diffuse natural upwelling of brackish ground water from the sandstone aquifer to the lower Tamiami aquifer probably is occurring in some parts of the study area. There is evidence of upward leakage to the base of the lower Tamiami aquifer in southwestern Collier County several kilometers north and south of I-75 and north of U.S. Highway 41 (fig. 12). These areas can be isolated as natural upwelling rather than upconing because they are characterized by sloughs, swamps, cypress domes, pine and/or oak islands, and mangrove estuaries where little anthropogenic stress, such as ground-water withdrawal, occurs. Upward leakage through natural upwelling is not apparent in the lower Tamiami aquifer beneath Bonita Springs because the potentiometric surface of the aquifer has been drawn down as a result of ground-water pumpage. This drawdown means natural upwelling probably is secondary to upconing.

Upconing of saltwater probably can be considered of utmost concern in the lower Tamiami aquifer beneath Bonita Springs. Upward leakage to the base of the lower Tamiami aquifer was inferred to be occurring at maximum rates beneath Bonita Springs in 1996 (fig. 12), assuming the upper Hawthorn confining unit is continuous and uniform. However, Wedderburn and others (1982) report that the upper confining unit thins and is absent in southernmost Lee County near Bonita Springs. Thus, saltwater upconing can occur more easily in this area because of less resistance to vertical flow. Other evidence shows that water in this area of the lower Tamiami aquifer was less saline in the past (Prinos and others, 2002) and originated from deeper discharging aquifers (Schmerge, 2001). This latter evidence also suggests that upconing may be occurring in the lower Tamiami aquifer beneath Bonita Springs.

As previously discussed, diffuse natural upwelling probably is not important in the lower Tamiami aquifer near Bonita Springs. Earlier studies had suggested that non-diffuse natural upwelling and upconing of saltwater through karst features could be occurring. Kohout (1979) identified the "mudhole" (fig. 1) discharging warm water to the Gulf of Mexico about 26 km northwest of Bonita Springs. Additionally, heads in the Floridan aquifer system are about 10 m higher than heads in the lower Tamiami aquifer near Bonita Springs. Thus, ground water would naturally tend to flow from deeper, more saline, and more pressurized aquifer systems to the lower Tamiami aquifer along preferential karstic flow paths. Although karst features exist in the study area, this mechanism of saltwater intrusion probably is not predominant in the lower Tamiami aquifer near Bonita Springs based on historical chloride concentration trends (Prinos and others, 2002). Water in the lower Tamiami aquifer would have chloride concentrations similar to the Floridan aquifer system (about 1,200 to 1,600 mg/L) if karst features were naturally transporting large quantities of saltwater from deeper aquifers for thousands of years.

According to previous investigators (Sherwood and Klein, 1963; Burns, 1983; Schmerge, 2001), natural upwelling and upconing of saltwater through leaky wells could be occurring in the lower Tamiami aquifer near Bonita Springs. Additionally, a poorly sealed annulus of well L-2310 (not shown) was hypothesized as the source of saltwater intrusion in well L-738 (fig. 15) by Schmerge (2001). Well L-2310 tapped the Upper Floridan aquifer and may have provided a pathway for upward leakage to the lower Tamiami aquifer near well L-738. The existence of other leaky wells (or potential leaky wells) is unknown; therefore, the predominance of leaky wells as a mechanism of saltwater intrusion in the lower Tamiami aquifer near Bonita Springs remains uncertain.

Downward Leakage

Downward leakage could occur as saline water from surface-water channels moves through the water-table aquifer and underlying Tamiami confining beds to come into equilibrium with modern natural and anthropogenic stresses. Downward leakage of saltwater from rivers and canals has been documented in the water-table aquifer near Naples (McCoy, 1962) and near boat basins in Naples (Klein, 1954). Downward leakage, however, seems an unlikely mechanism of saltwater intrusion in the lower Tamiami aquifer near Bonita Springs. Gaging stations on the northern and southern branches of the Estero River, Spring Creek, and the Imperial River record flow during the dry season, suggesting ground water flows from the water-table aquifer to these rivers and creeks even in times of drought. Additionally, flow from the water-table aquifer to the base of the Imperial River was observed during field reconnaissance in July 2000. Given these observations, it seems unlikely that saltwater moving upstream along Spring Creek and the Estero, Imperial, and Cocohatchee Rivers (fig. 1) would infiltrate through the water-table aquifer and underlying Tamiami confining beds and result in the distribution of saltwater mapped by Knapp and others (1986) and Schmerge (2001).

Relict Seawater

Relict seawater from former high sea-level stands could move through the permeable rock comprising the lower Tamiami aquifer to come into equilibrium with modern natural and anthropogenic stresses (fig. 17). The presence of unflushed relict seawater has been hypothesized as a source of brackish ground water in the shallow surficial aquifer system in parts of southwestern Florida (Sherwood and Klein, 1963; Schmerge, 2001). Evidence suggests, however, that relict seawater is not present in the lower Tamiami aquifer near Bonita Springs. For example, strontium isotope data indicate ground water in the area is from deeper discharging aquifers (Schmerge, 2001). Additionally, McCoy (1962) reports that flushing of most seawater in the shallow aquifers would have occurred since the Pleistocene based on ambient ground-water flow and recharge rates. According to Knapp and others (1986), the regional presence of unflushed water from sea inundations during Pleistocene interglacial stages is minimal.

SIMULATION OF SALTWATER INTRUSION NEAR BONITA SPRINGS

Numerical simulation is used to quantify modern and seasonal stresses, help identify mechanisms of saltwater intrusion, and estimate the potential extent of saltwater intrusion in the lower Tamiami aquifer near Bonita Springs. Numerical codes were selected to (1) solve the constant-density ground-water flow equation, (2) solve the variable-density ground-water flow and solute transport equations, and (3) facilitate model calibration and sensitivity analysis in three dimensions (table 2). Model discretization, assignment of aquifer properties, and assignment of boundary conditions provided the spatial and temporal framework necessary for solving the finite-difference equations. A predevelopment distribution of saltwater was simulated, and the model was calibrated to typical and modern stresses. The potential movement of saltwater from predevelopment distribution to dynamic equilibrium with calibrated typical, modern, and seasonal stresses was then simulated. Modern stresses are represented as stresses with the desired characteristics.

Table 2. Description and primary use of modeling tasks

Task	Spatial discretization	Temporal discretization	Code[1]	Initial conditions	Primary use
1	105 rows, 80 columns, 17 layers[2]	One steady-state flow stress period, representing predevelopment (1930) conditions. Transient transport time steps	SEAWAT	Freshwater equivalent heads equal to zero, a wall of saltwater at coast	Estimate predevelopment salinity conditions and establish initial head and salinity conditions for predictive simulations of saltwater movement
2	Same as above	Two steady-state flow stress periods, representing March and September 1996 conditions. Transient transport time steps	MODFLOW-88	Heads at land surface	Obtain an accurate representation of March and September 1996 head and flow conditions
3	Same as above	1,200 alternating steady-state flow stress periods, representing March and September 1996.[3] Transient transport time steps.	SEAWAT	Final predevelopment distribution of freshwater equivalent head and salinity	Help identify mechanisms of saltwater intrusion and estimate the extent of saltwater intrusion in the lower Tamiami aquifer beneath Bonita Springs

[1]SEAWAT (Guo and Langevin, 2002); MODFLOW-88 (McDonald and Harbaugh, 1988).
[2]Aquifer properties as described in this report.
[3]Ran for a total of 600 years.

Modeling Approach

The modeling approach for this study can be summarized by three tasks (table 2):

1. Variable-density simulation of predevelopment conditions,
2. Calibration of a constant-density flow model to typical, modern and seasonal stresses, and
3. Variable-density predictive simulations of saltwater movement to equilibrium with the typical, modern, and seasonal stresses.

The rationale and limitations for each modeling task, and solely simulating advective solute transport while neglecting the effects of dispersion, were considered.

The first task of simulating a predevelopment distribution of saltwater was performed so a comparison could be made between the distribution of saltwater under predevelopment conditions and the distribution of saltwater at equilibrium with typical, modern, and seasonal stresses. This comparison was made to determine the potential occurrence of saltwater intrusion. Additionally, the predevelopment simulation provided a no-flow boundary condition at the saltwater interface for model calibration in task 2. Another reason for simulating a predevelopment distribution of saltwater was to develop initial conditions of freshwater equivalent head and ground-water salinity that were internally self-consistent for predictive simulations of saltwater movement (task 3). While performing variable-density flow simulations, consistent initial conditions of equivalent freshwater head and salinity will result in a model that responds to the imposed hydrologic stresses rather than to disequilibrium of the initial conditions.

The second task in the modeling approach is model calibration. A constant-density ground-water flow simulator was chosen for this task for two reasons:

1. Matching observed heads and flows in the study area was not highly dependent upon simulating saltwater movement. Chloride concentrations in observation wells were about 100 to 1,300 mg/L (fig. 15), suggesting the bulk of the saltwater transition zone remains either offshore, between the monitoring wells and the coastline, or within deeper hydrogeologic units. Thus, the difference between hydraulic-head observations and their simulated equivalents (when modeling) was more likely attributable to uncertainties in aquifer properties and boundary conditions, rather than saltwater or saltwater movement.
2. Computer run times for constant-density ground-water flow simulations are much shorter than computer run times for variable-density flow simulations. Therefore, more time is available to test different conceptual models and parameter estimates while calibrating with a constant-density flow simulator. A limitation of this approach, however, was that the information contained in salinity observation could not be used to better estimate values of transport parameters, such as effective porosity and dispersivity. These parameters are important to solute transport, and thus saltwater movement.

The model was calibrated to typical, modern, and seasonal stresses with certain attributes. A year with "typical" stresses was selected to prevent approximations of saltwater movement from being biased toward wet or dry years. A year with "modern" stresses was selected to determine whether natural and anthropogenic stresses such as recharge, ground-water withdrawal, canal drainage, and sea level would move saltwater to areas previously occupied by fresher waters. "Seasonal" stresses were represented to test theories that alternating wet- and dry-season water levels move saltwater into and out of the lower Tamiami aquifer, respectively, but result in no net saltwater intrusion over a typical water year.

Typical, modern, and seasonal stresses were observed during 1996, so this year was chosen for model calibration. The year 1996 (which had about 1.3 m of rainfall) was selected as "typical" after plotting average annual rainfall values at Bonita Springs Utility rainfall monitoring station (fig. 18). The rainfall data indicate that 1995 represents a wet year (with about 2.1 m of rainfall) and 1950 represents a dry year (with about 1.1 m of rainfall). The average of annual rainfall values in figure 18 is about 1.4 m. The 1996 year also was selected because: (1) pumpage data obtained from the SFWMD began that year, and (2) numerous water-level and flow measurements were taken near Bonita Springs that year relative to other years. Perhaps the flooding of Bonita Springs during the heavy rains of 1995 (Johnson Engineering, Inc., and others, 1999) prompted increased awareness about the importance of data collection during 1996.

During model calibration, seasonal fluctuations in water levels were approximated by designing two steady-state flow stress periods, representing time periods in 1996 when water levels were high (wet

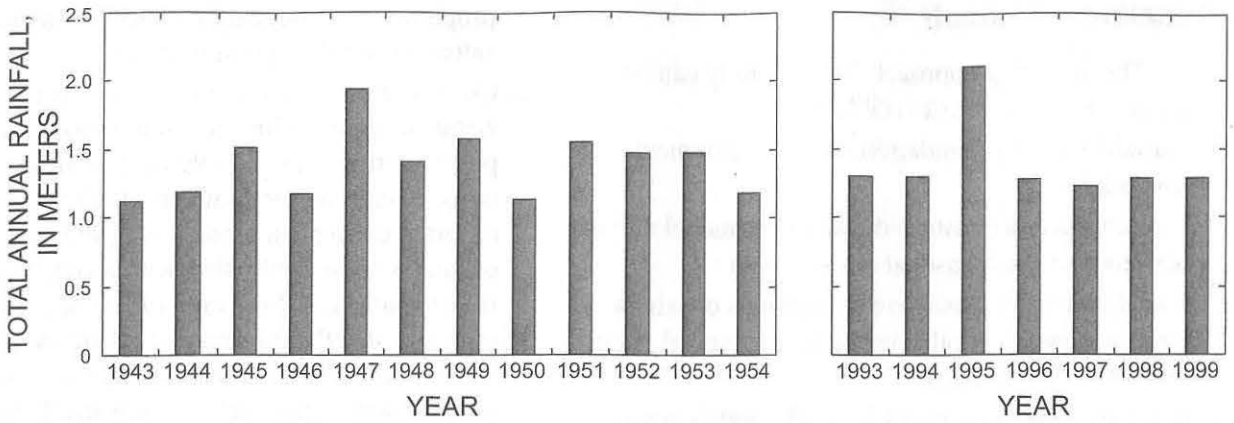


Figure 18. Historical record of annual rainfall at Bonita Springs Utility rainfall monitoring station, 1943-54 and 1993-99.

season) and low (dry season) (table 2). By simulating periods with high and low water levels, the seasonal movement of the saltwater interface can be approximated. Additionally, a steady-state approach can be employed when the selected time periods show relatively stable water levels, suggesting the ground-water flow system is as close to steady state as realistically possible. There are two advantages to using the steady-state approach. First, a steady-state model does not require aquifer storage values. This eliminates the need to specify an additional parameter, which may be highly uncertain. Second, steady-state models tend to run faster than transient models because there are fewer input requirements and fewer solutions to the flow equation. Shorter computer run times allow more time for calibration and sensitivity analysis. A disadvantage of the steady-state approach is the possibility of developing a model that may fail to represent transient particularities important to the true nature of ground-water flow and saltwater movement near Bonita Springs.

March and September 1996 were selected to represent typical, modern, and seasonal stresses because ground-water levels in the water table and lower Tamiami aquifers generally were at or near seasonal lows and highs and also were relatively stable (fig. 19), justifying the steady-state assumption. Given these data and the above considerations, developing a model with two steady-state stress periods calibrated to average March and September 1996 conditions seemed to be a reasonable representation of typical, modern, and seasonal stresses.

Most ground-water models are calibrated by adjusting hydraulic conductivity until simulation results match with observed field conditions. The model documented here was calibrated by assuming hydraulic conductivity parameters were accurate, and estimating unmonitored ground-water pumpage and pan evaporation multipliers using UCODE. Unmonitored ground-water pumpage was estimated because unknown pumpage parameters caused the largest discrepancies between observed and simulated heads near the coast in the lower Tamiami aquifer beneath Bonita Springs. Accurately simulated heads in this location are most important for accurately simulating saltwater movement in this location, which was a primary objective of this study. Pan evaporation multipliers were estimated simultaneously with unmonitored pumpage because pan evaporation parameters were the most sensitive model parameters that were not correlated with unknown pumpage. Correlated parameter values cannot be simultaneously estimated by parameter estimation codes, such as UCODE. This is because coordinated linear changes in correlated parameter values produce the same simulated heads and flows at observation locations (Poeter and Hill, 1997).

The third task in the modeling approach was to simulate the movement of saltwater to equilibrium with the typical, modern, and seasonal stresses. This task was accomplished using the predevelopment distribution of saltwater and calibrated March and September 1996 steady-state flow stress periods. The calibrated steady-state flow stress periods were run in continual succession with a variable density ground-water flow simulator until the total salt mass in the simulation approached "dynamic equilibrium." At dynamic equilibrium, the average annual total salt mass in the simulation is a constant value, even though some seasonal fluctuation in total salt mass may occur between stress periods.

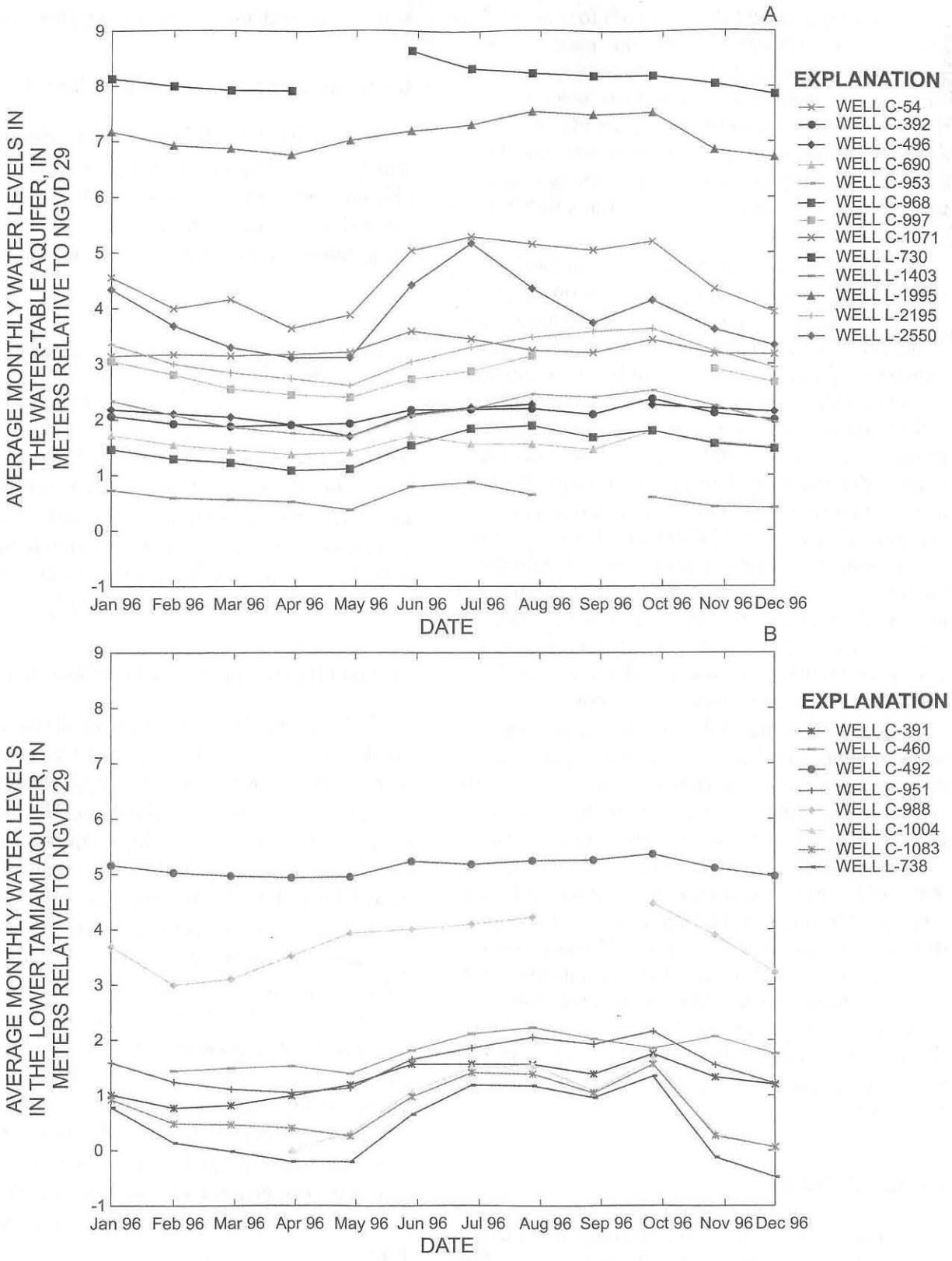


Figure 19. Average monthly water levels from selected monitoring wells in the (A) water-table and (B) lower Tamiami aquifers near Bonita Springs. Well locations are shown in figure 1. NGVD 29 is National Geodetic Vertical Datum of 1929.

Steady-state flow conditions were used for task 3 by assigning a small value (1×10^{-8}) for aquifer storage properties. This means that within each transport step, heads respond instantaneously (or nearly instantaneously) to changes in salinity. Thus, heads and flows for a particular transport step are always of steady state with salinity for that transport step. This approach is a simpler alternative than trying to determine appropriate storage values and run a fully transient model.

Advective solute transport was simulated while solving for the predevelopment distribution of saltwater and solving for the potential movement of saltwater from predevelopment distribution. Dispersive solute transport was not simulated. According to traditional advection-dispersion theory, hydrodynamic dispersion is the tendency for a solute to spread from the path it would be expected to follow according to advective hydraulics (Freeze and Cherry, 1979). Hydrodynamic dispersion results from molecular diffusion and mechanical dispersion. Molecular diffusion, the process by which a plume spreads due to concentration gradients, is small enough in magnitude to be ignored in ground-water flow systems with velocities as high as the system near Bonita Springs. Mechanical dispersion, another process by which a plume spreads, is caused by small-scale velocity variations.

Rather than assign dispersivity values, which would contain a high level of uncertainty, the numerical dispersion caused by the model was assumed to be similar in magnitude to the actual dispersion in the aquifer. Although there was no way to evaluate this assumption, it seemed justified by a lack of field data that could be used to calibrate dispersivity values and considerably long computer run times for simulations that directly represented dispersion. Neglecting dispersion may cause the potential extent of saltwater intrusion to be overestimated. This limitation is discussed in more detail in the model limitation section of the report. If field data are available, the effects of dispersion could be evaluated with future simulations of saltwater intrusion.

Code Selection

Two modular, three-dimensional, finite-difference models were used to simulate ground-water flow and salinity transport in this study (table 2). MODFLOW (McDonald and Harbaugh, 1988) was chosen as the constant-density ground-water flow simulator, and SEAWAT (Guo and Langevin, 2002) was chosen as the variable-density ground-water flow simulator.

Constant-Density Ground-Water Flow Simulator

MODFLOW (McDonald and Harbaugh, 1988), widely accepted by the modeling community as a reliable tool, was chosen as the constant-density ground-water flow simulator. This program was used to solve the following steady-state ground-water flow equation:

$$\frac{\partial}{\partial x}\left(K_{xx}\frac{\partial h}{\partial x}\right)+\frac{\partial}{\partial y}\left(K_{yy}\frac{\partial h}{\partial y}\right)+\frac{\partial}{\partial z}\left(K_{zz}\frac{\partial h}{\partial z}\right)-W=0 \quad (2)$$

where K_{xx}, K_{yy}, and K_{zz} are values of hydraulic conductivity along the x-, y-, and z-coordinate axes, which are assumed to be parallel to the major axes of hydraulic conductivity [LT^{-1}]; h is the potentiometric head [L], and W is a volumetric flux per unit volume and represents sources and/or sinks of water [T^{-1}].

Variable-Density Ground-Water Flow Simulator

SEAWAT (Guo and Langevin, 2002), capable of solving for variable-density ground-water flow patterns in three dimensions, was chosen as the variable-density ground-water flow simulator. The SEAWAT program explicitly or implicitly couples a variable-density form of the ground-water flow equation solved with MODFLOW-88 (McDonald and Harbaugh, 1988) to the solute transport equation solved with MT3Dms (Zheng and Wang, 1998). Because MT3Dms is used, solute concentrations or salinities are approximated with transient, three-dimensional, variable-density, ground-water flow patterns. Several methods are available to solve the advection and dispersion terms of the transport equation using MT3Dms (Zheng and Wang, 1998). Thus, the user can experiment to find a solution with acceptable levels of numerical dispersion and/or artificial oscillation while attempting to maintain a reasonable computer run time.

SEAWAT reformulates the ground-water flow equation to solve for freshwater equivalent head as follows:

$$\frac{\partial}{\partial x}\left(\rho K_{fx}\left[\frac{\partial h_f}{\partial x}+\frac{\rho-\rho_f}{\rho_f}\frac{\partial Z}{\partial x}\right]\right)+\frac{\partial}{\partial y}\left(\rho K_{fy}\left[\frac{\partial h_f}{\partial y}+\frac{\rho-\rho_f}{\rho_f}\frac{\partial Z}{\partial y}\right]\right)+\frac{\partial}{\partial z}\left(\rho K_{fz}\left[\frac{\partial h_f}{\partial z}+\frac{\rho-\rho_f}{\rho_f}\frac{\partial Z}{\partial z}\right]\right)=\rho S_f\frac{\partial h_f}{\partial t}+\theta\frac{\partial \rho}{\partial C}\frac{\partial C}{\partial t}-\bar{\rho}q_s \quad , \quad (3)$$

where x, y, and z are the principal directions of permeability,

ρ is fluid density [M/L^3],

K_f is the freshwater hydraulic conductivity [L/T],

h_f is the freshwater equivalent head [L],

ρ_f is the density of freshwater [M/L^3],

Z is the vertical direction or elevation of the center of the model cell [L],

S_f is the freshwater equivalent storage coefficient [L^{-1}],

t is time [T],

θ is effective porosity [dimensionless],

C is the solute concentration [M/L^3],

$\bar{\rho}$ is the density of water from the source or sink [M/L^3], and

q_s is the volumetric flux of water representing sources and sinks per unit volume of aquifer [T^{-1}].

The reformulated ground-water flow equation is coupled to the following solute-transport equation:

$$\nabla(D\nabla C)-\nabla\bullet(\vec{v}C)-\frac{q_s}{\theta}C_s+\sum_{k=1}^{n}R_k=\frac{\partial C}{\partial t}, \quad (4)$$

where

D is the hydrodynamic dispersion coefficient [L^2/T],

∇ is the spatial gradient operator,

$\vec{v}$ is the fluid velocity vector [L/T],

C_s is the solute concentration of the source or sink [M/L^3], and

R_k is the rate of solute production or decay in reaction k of n different reactions [M/L^{3}T].

Equations 3 and 4 are sequentially solved by first solving the variable-density ground-water flow equation and then solving the solute-transport equation. After new concentrations are calculated, a linear equation of state is used to relate solute concentrations to fluid density. The linear equation of state is:

$$\rho = \rho_f + EC \quad , \quad (5)$$

where E is an empirical, dimensionless constant with an approximate value of 0.7143 for salts commonly found in seawater.

Spatial Discretization and Assignment of Aquifer Properties

Finite-difference methods require the discretization of space into a grid consisting of rows, columns, and layers of model cells. Additionally, ground-water flow is proportional to the horizontal and vertical permeability properties of the aquifer matrix, and advective and dispersive solute transport is dependent upon the effective porosity of the aquifer matrix. Thus, in a three-dimensional, finite-difference SEAWAT model using the robust layer type 3 option (LAYCON 3), information describing the grid discretization, horizontal hydraulic conductivity, vertical conductance (VCONT) (McDonald and Harbaugh, 1988), and effective porosity must be written to model input files. The aquifer property information must be assigned to model cells in a way that reflects the bulk occurrence of these properties within the entire volume of the model cell.

The study area was spatially discretized into a grid with 105 rows, 80 columns, and 17 layers of square cells. Seventeen layers were used to obtain sufficient vertical resolution of the saltwater interface. Each model cell is 600 by 600 m and 5 m thick, except for layer 1 where the cell top varies to match land surface, and the cell bottom is 5 m below National Geodetic Vertical Datum (NGVD) of 1929. Uniform cell volumes were used, except for layer 1, to minimize mass-balance errors that could occur if a mixed Eulerian-Lagrangian method was needed to solve the advection term of the transport equation. Examples of such a method with MT3Dms are the method of characteristics (MOC), modified method of characteristics (MMOC), or hybrid method of characteristics (HMOC). Eulerian-Lagrangian methods do not guarantee local mass conservation at a particular time step because of the discrete nature of particle tracking used in these techniques (Zheng and Wang, 1998).

Mass-balance errors can be exacerbated by nonuniform cell volumes.

Bulk values of horizontal hydraulic conductivity and VCONT were assigned to model cells using a three-dimensional conceptual permeability model, the configuration of the model grid, and weighted arithmetic or harmonic averaging. The three-dimensional conceptual permeability model was developed by assigning the values of horizontal and vertical hydraulic conductivity, shown in table 3, to the framework of the water-table aquifer, Tamiami confining beds, lower Tamiami aquifer, upper Hawthorn confining unit, and sandstone aquifer. Because hydraulic conductivity typically is considered to be log-normally distributed, permeability values were assigned (as described below) using the log K histograms of aquifer horizontal hydraulic conductivity (fig. 4) compiled from: (1) previous literature (Bower and others, 1990), and (2) reanalysis of previous aquifer performance tests (K.M. Edwards, U.S. Geological Survey, written commun., 2000).

Table 3. Hydraulic conductivities used in the conceptual permeability model

Hydrogeologic unit	Hydraulic conductivity (meters per day)	
	Horizontal	Vertical
Water-table aquifer	300	15
Tamiami confining beds	.04	.004
Lower Tamiami aquifer	70	3.5
Lower Tamiami aquifer, coral reef facies	130	6.5
Upper Hawthorn confining unit	.03	.003
Sandstone aquifer	20	2

The water-table aquifer was assigned a horizontal hydraulic conductivity of 300 m/d (table 3). The horizontal hydraulic conductivity was based on the inverse log of the midpoint of the first mode in the distribution of 244 measurements (fig. 4A). A vertical hydraulic conductivity of 15 m/d was assigned to the water-table aquifer (table 3) because reanalysis of aquifer performance tests in the study area by K.M. Edwards (U.S. Geological Survey, written commun., 2000) suggests that the anisotropy ratio of horizontal to vertical hydraulic conductivity is about 20:1 in the water-table aquifer.

The Tamiami confining beds and the upper Hawthorn confining unit were assigned horizontal hydraulic conductivities of 0.04 and 0.03 m/d, respectively, and vertical hydraulic conductivities of 0.004 and 0.003 m/d, respectively (table 3). The same vertical hydraulic conductivities (0.004 and 0.003 m/d) were measured by Montgomery (1988). Little published information was available to constrain values of horizontal hydraulic conductivity for both confining units. In modeling applications, the ratio of horizontal hydraulic conductivity to vertical hydraulic conductivity is often assumed to range from 1 to 1,000 (Anderson and Woessner, 1992). Thus, the horizontal hydraulic conductivities of the Tamiami confining beds and the upper Hawthorn confining unit were set to 0.04 and 0.03 m/d, respectively, or 10 times the measured vertical hydraulic conductivity found by Montgomery (1988). This may seem somewhat arbitrary, but the results of ground-water flow models typically are insensitive to values of horizontal hydraulic conductivity in confining units. Because of the low permeability of these units, horizontal flow within them is essentially negligible.

In the lower Tamiami aquifer, horizontal hydraulic conductivity appears to have a bimodal log K distribution (fig. 4B). Results from aquifer performance tests compiled for this study (figs. 4B and 8) and for previous research (Meeder, 1979) suggest that permeabilities in the lower Tamiami aquifer are much greater in areas where coral reef facies are present. The lower Tamiami aquifer was assigned a horizontal hydraulic conductivity value of 130 m/d in areas where the coral reef facies are known to exist (table 3). This value was the inverse log of the arithmetic average log K value computed from eight aquifer performance tests completed in coral reef facies (fig. 8). Elsewhere, the lower Tamiami aquifer was assigned a horizontal hydraulic conductivity of 70 m/d (table 3) –the inverse log of the arithmetic average log K value computed from 136 measurements (fig. 4B). A vertical hydraulic conductivity value of 6.5 m/d was assigned in areas of the lower Tamiami aquifer where coral reef facies are present and 3.5 m/d elsewhere because reanalysis of aquifer performance tests suggests the anisotropy ratio of horizontal to vertical hydraulic conductivity is about 20:1 in the aquifer.

The sandstone aquifer was assigned a horizontal hydraulic conductivity of 20 m/d and a vertical hydraulic conductivity of 2 m/d (table 3). The horizontal hydraulic conductivity was based on the inverse log of the arithmetic average log K value computed from the distribution of 25 measurements (fig. 4C). Little published information was available to constrain values of vertical hydraulic conductivity for the sandstone aquifer. The vertical hydraulic conductivity was based on the 1 to 1,000 range of vertical to horizontal conductivity ratios. Thus, the vertical hydraulic conductivity of the sandstone aquifer was set to 2 m/d, or one-tenth the horizontal hydraulic conductivity. Again, this may seem somewhat arbitrary, but model results are expected to be insensitive to the vertical hydraulic conductivity of the sandstone aquifer. Because the focus of this study is the lower Tamiami aquifer, flow into or out of the aquifer will be controlled more by the vertical hydraulic conductivity of the underlying upper Hawthorn confining unit than the vertical hydraulic conductivity of the sandstone aquifer.

Because the hydrogeologic units do not coincide with model layers, bulk values of horizontal hydraulic conductivity (fig. 20) were computed as the weighted arithmetic mean of the hydraulic conductivities (table 3) that lie within the model cell (fig. 21). The weighted arithmetic mean is expressed as:

$$Kxy_{i,\,j,\,k} = \sum_{u=1}^{n} W_u Kxy_u \quad , \tag{6}$$

where $Kxy_{i,j,k}$ is the bulk horizontal hydraulic conductivity of the model cell i,j,k [L/T], u is a counter ranging from 1 to n, in which n is the number of hydrogeologic units within the model cell [dimensionless], W_u is weight representing the fraction of the model cell's thickness occupied by the hydrogeologic unit (the sum of the weights for each model cell must equal 1 [dimensionless]), and Kxy_u is the horizontal hydraulic conductivity of the hydrogeologic unit [L/T].

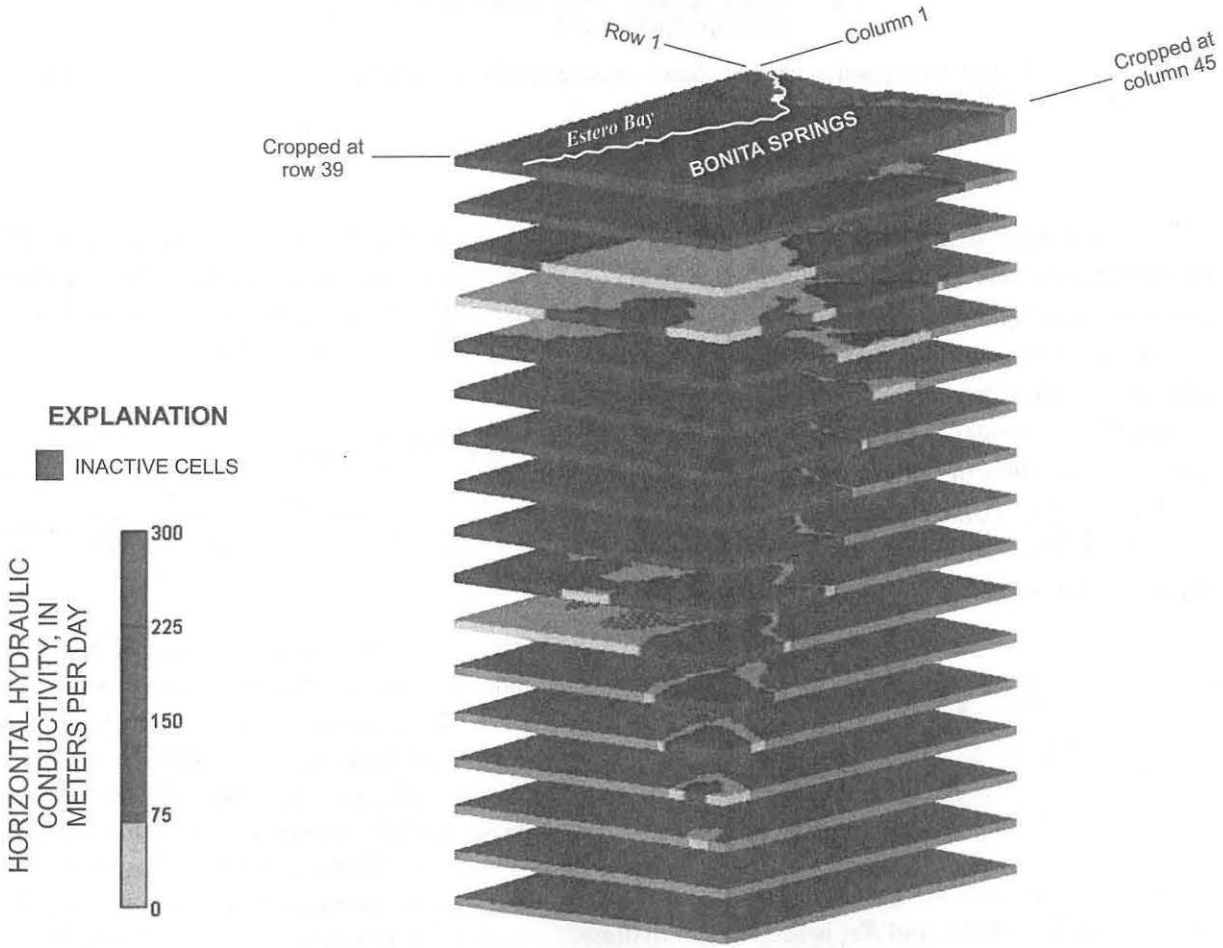


Figure 20. Distribution of bulk horizontal hydraulic conductivity in selected model cells.

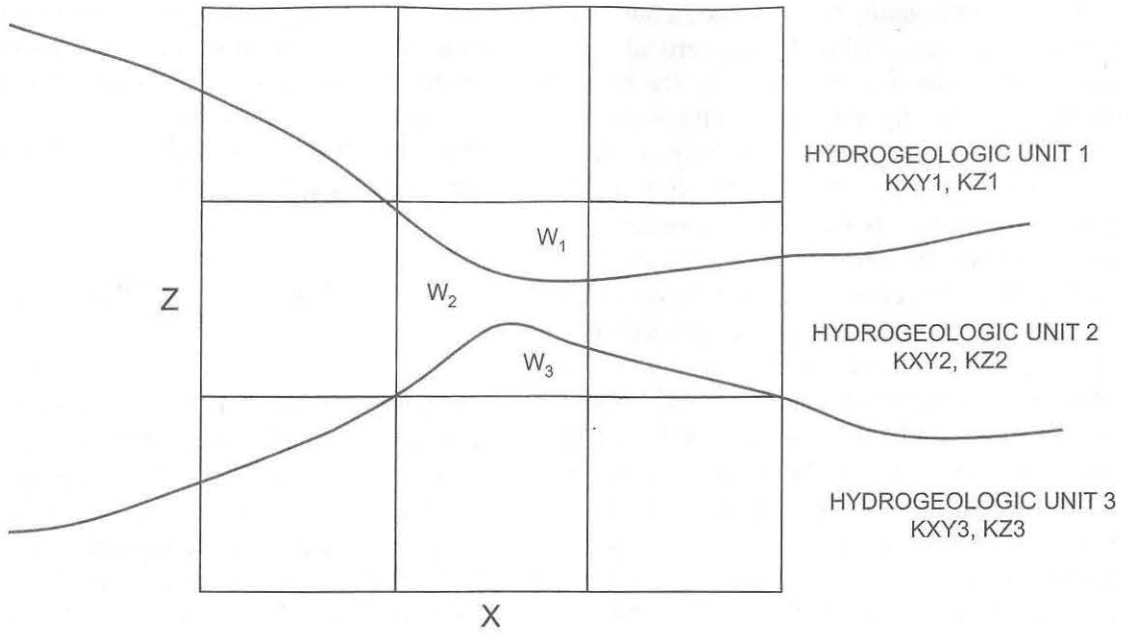


Figure 21. Approach used to compute bulk hydraulic conductivities for each model cell using weighted arithmetic and harmonic averaging.

Bulk values of vertical hydraulic conductivity for model cells were computed as the weighted harmonic mean of hydraulic conductivities (table 3) that lie within the model cell (fig. 21). A three-dimensional diagram of bulk values of vertical hydraulic conductivity would look similar to the three-dimensional diagram of bulk values of horizontal hydraulic conductivity (fig. 20), except values would range would from 15 to 0.003 m/d. The weighted harmonic mean is expressed as:

$$Kz_{i,\,j,\,k} = \frac{1}{\sum_{u=1}^{n} W_u \frac{1}{Kz_u}}, \qquad (7)$$

where $Kz_{i,j,k}$ is the bulk vertical hydraulic conductivity of the model cell [L/T], and Kz_u is the vertical hydraulic conductivity of the hydrogeologic unit [L/T].

Except for the bottom layer (layer 17), a VCONT term is required input for each model cell in a MODFLOW or SEAWAT simulation. Bulk values of VCONT were computed as:

$$VCONT_{i,\,j,\,k} = \frac{2(Kz_{i,\,j,\,k})(Kz_{i,\,j,\,k+1})}{\Delta b_{i,\,j,\,k}(Kz_{i,\,j,\,k}) + \Delta b_{i,\,j,\,k+1}(Kz_{i,\,j,\,k+1})}, \qquad (8)$$

where $VCONT_{i,j,k}$ is the required VCONT term [1/T], and $\Delta b_{i,j,k}$ is the thickness of the model cell [L].

Estimates of effective porosity were needed for variable-density ground-water flow simulations. Effective porosity, the percentage of interconnected pore space within geologic material, was uniformly set to 30 percent. This percentage is based on analysis of exploratory cores collected from the gray limestone and lower Tamiami aquifers in the study area (Reese and Cunningham, 2000).

Simulation of Predevelopment Conditions

In the first modeling task, the SEAWAT program was used to simulate the location of the interface prior to development. The year 1930 was selected to represent predevelopment conditions primarily because the network of canals had not yet been constructed (Ananta Nath, Big Cypress Basin, oral commun., 2001), and ground-water pumpage probably was negligible. A single steady-state stress period was used to represent conditions in 1930. The spatial discretization and aquifer properties previously described were used for the simulation. Results from the predevelopment model consist of three-dimensional distributions of head and salinity. These model results are used to help define a coastal boundary condition for model calibration (task 2). Results from the predevelopment simulation also are used as initial conditions for predictive simulations of saltwater movement (task 3).

Boundary Conditions

Boundary conditions for simulating the predevelopment distribution of saltwater include rainfall, evapotranspiration, rivers, lateral conditions of no flows, and constant heads with constant concentrations (pl. 1). Rainfall and evapotranspiration boundary conditions were used to allow the simulation to calculate the net recharge to the top of active model cells located inland from the coastline. Because rainfall and evapotranspiration are assigned to active cells in layer 1, these boundary conditions are not shaded nor labeled on plate 1. River boundary conditions were used to represent Spring Creek, and the Imperial, Cocohatchee and Estero Rivers. No-flow boundary conditions were used to represent predevelopment hydrologic divides that were assumed to exist along modern ground-water flow lines. Because each cell in layers 16 and 17 is a no-flow boundary condition, only layers 1 to 15 are plotted on plate 1. Layers 16 and 17 were kept in the model, however, in case they are needed to represent deeper hydrogeologic units in future investigations. Constant-head and constant-concentration boundary conditions were used to represent the Gulf of Mexico. The salinity of inflow from each source boundary condition was set to zero, with exception to the boundary conditions representing the Gulf of Mexico, which were assigned a salinity of seawater.

Recharge

Limited data were available that describe recharge in 1930; therefore, recharge was simulated using the approach described by Motz (1996) and Stewart and Langevin (1999). Using this approach, both rainfall and evapotranspiration are included in the model, with the maximum potential ground-water evapotranspiration rate set equal to the rainfall rate. This creates an aquifer system where water levels are controlled by land-surface topography (Motz, 1996). Using this method to simulate recharge is advantageous because spatial distributions of net recharge are generated rather than discrete zones. Disadvantages include the potential for additional uncertainty in model simulations due to the lack of data to support estimates of rainfall, maximum potential evapotranspiration rates, extinction depths, and the evapotranspiration surface.

Rainfall was entered using the Recharge package (McDonald and Harbaugh, 1988). The Recharge package requires input of an areal flux [L/T] to the top grid layer, a specified vertical distribution of layers, or the highest active cell in a vertical column of layers. The areal recharge flux was added to the highest active cell in a vertical column of layers. Average annual rainfall rates were computed from historical rainfall recorded at the Bonita Springs monitoring station from 1943 to 1999 (fig. 18). Years with no average annual rainfall rate indicate missing or insufficient data (1955-92). No trends of annual average rainfall rates are evident, thus an extrapolation relation to compute the average annual rainfall rate in 1930 was not necessary. The average of annual average rainfall rates was about 1.3 m/yr and was written as the areal flux in the Recharge package.

Evapotranspiration was entered using the Evapotranspiration package (McDonald and Harbaugh, 1988) where evapotranspiration is approximated as a linearly varying rate that is greatest at the evapotranspiration surface and decreases to zero at the extinction depth. As required by the coupled aquifer approach, the maximum evapotranspiration rate of the evapotranspiration surface was set equal to the rainfall rate. The evapotranspiration surface was set to land surface, and extinction depths were set to 5 m below land surface.

Extinction depths are uncertain in the study area. Extinction depths at about 0.3 to 2.1 m were used in previous modeling studies of southwestern Florida (Bower and others, 1990; Bennett, 1992). These depths were related to land use and based upon estimated root depths for various types of vegetation. In addition to vegetation root depth, evapotranspiration is

dependent upon other processes and properties, such as climate and soil type. For example, fine-grained soils will have deeper extinction depths than coarse-grained soils because more energy is required to lift ground water through coarse-grained soils.

A network of evapotranspiration stations maintained in southern Florida by the USGS suggests extinction depths of at least 1 m over many types of land cover (S.L. Kinnaman, U.S. Geological Survey, written commun., 2001). Tibbals (1990) estimated evapotranspiration rates of about 76 cm/yr in areas where the water table was about 4 m below land surface in east-central Florida. Merritt (1996) used extinction depths up to 6 m below land surface in a coastal ridge area of southeastern Florida. Setting extinction depths to 5 m below land surface seemed to be a reasonable compromise, given the current understanding of evapotranspiration in Florida.

Rivers

Predevelopment river boundary conditions (pl. 1) were entered using the River package (McDonald and Harbaugh, 1988). The conceptual model for the River package is based on the vertical leakage of water across river bottom sediments. The cross section of the river is conceptualized in the model code as rectangular with impermeable vertical sides. Leakage into or out of the model cell is dependent on the stage in the river (h_{riv}), the value of head in the model cell ($h_{i,j,k}$), and a conductance term. The conductance term of the river is mathematically defined as:

$$COND_{riv} = \frac{LwK_{seds}}{b_{seds}} , \qquad (9)$$

where $COND_{riv}$ is the conductance of the river bed [L^2/T],

L is the length of the river segment in the model cell [L],

w is the bottom width of the river [L],

K_{seds} is the vertical hydraulic conductivity of the river bottom sediments [L/T], and

b_{seds} is the thickness of the river bottom sediments [L].

The elevation of the base of the river bottom sediments is specified as *RBOT*, an input parameter for the River package. When $h_{i,j,k}$ is greater than *RBOT*, leakage from the aquifer to the river, Q_{riv}, is calculated as:

$$Q_{riv} = COND_{riv}(h_{riv} - h_{i,\,j,\,k}) . \qquad (10)$$

When $h_{i,j,k}$ is less than *RBOT*, the leakage rate from the river to the aquifer is calculated as:

$$Q_{riv} = COND_{riv}(h_{riv} - RBOT) . \qquad (11)$$

The Estero River, Imperial River, Cocohatchee River, and Spring Creek (fig. 1) were simulated with the River package. These surface-water features were digitized from a USGS 1:100,000-scale topographic-bathymetric map. For predevelopment conditions, an attempt was made to digitize only parts of the river and creek channels that appeared to be unaltered. Input for the River package includes the layer, row, column, h_{riv}, $COND_{riv}$, and *RBOT*. The layer, row, and column of river cells were determined by overlying the digitized river features with the model grid. The river stage, h_{riv}, was estimated at 0.5 m below the land-surface elevation of the model cell because this value seems reasonable, and no quantitative data describing river stages in 1930 exist. For each river cell, $COND_{riv}$ was computed by multiplying the area of the river or creek channel within the model cell by K_{seds}. The value of K_{seds} is assumed to be 15 m/d, which is the vertical hydraulic conductivity used for the water-table aquifer (table 3); the value of b_{seds} was set to 1 m for lack of a better value, and the value of *RBOT* was estimated at 2 m less than h_{riv}.

There may be some reason for concern about the lack of predevelopment data for assigning river parameter values. It is likely, however, that these parameters have little effect on the goal of this simulation, which is to simulate a predevelopment distribution of saltwater. River parameters control a relatively small component of the water budget in this simulation; namely, flow between the aquifer and surface-water features. Parameters that control small components of the water budget typically are less sensitive than parameters that control large components of the water budget.

No Flow

Ground-water divides observed in the water-table and lower Tamiami aquifers during March and September 1996 (fig. 22) were represented as no-flow boundary conditions in the predevelopment simulation (pl. 1). Representing a ground-water divide as a no-flow boundary is conceptually consistent with the actual behavior of the divide; ground water on each side of the divide moves away, and no flow crosses the divide (Reilly, 2001).

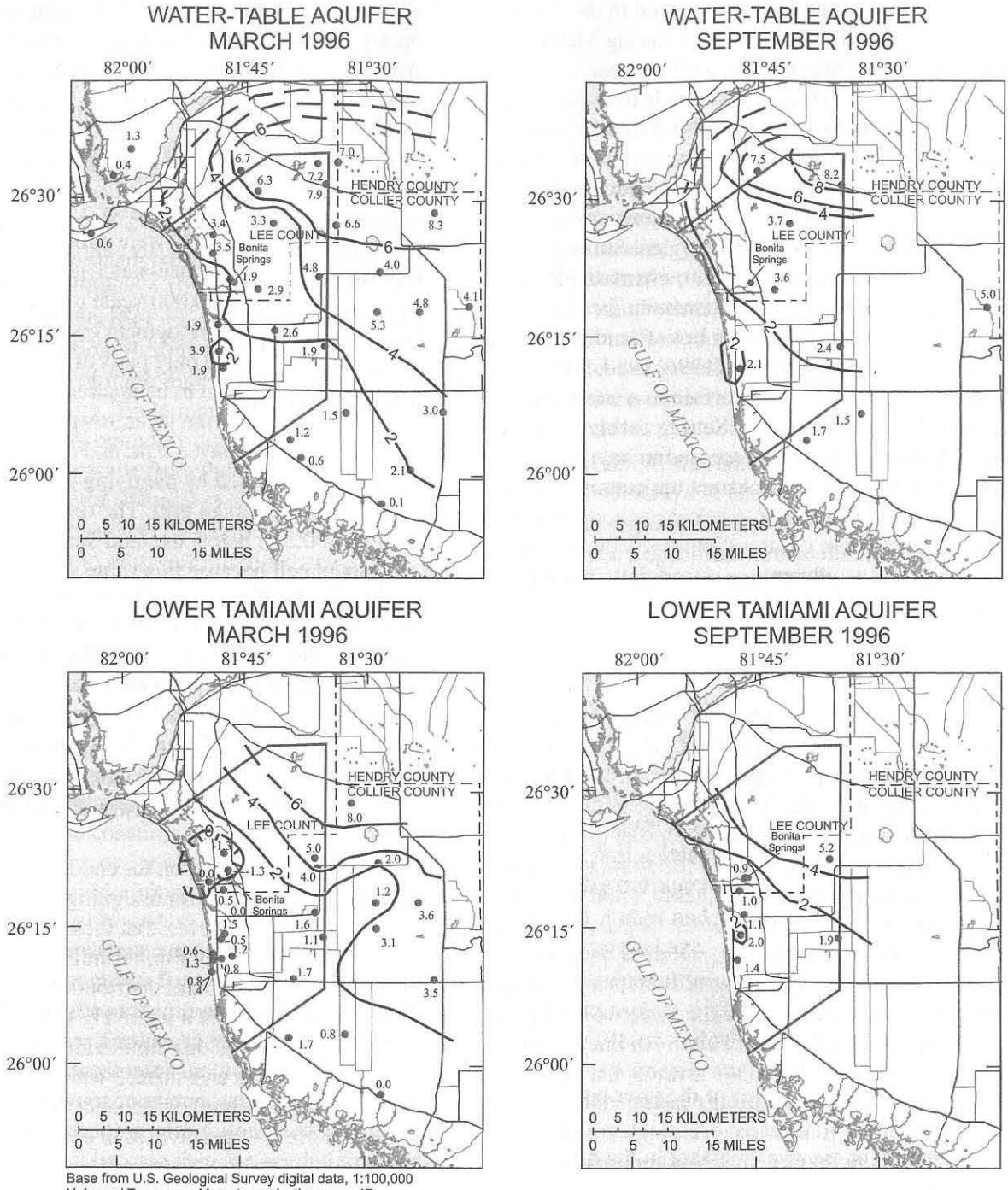


Figure 22. Average monthly water levels in the water-table and lower Tamiami aquifers during March and September 1996. NGVD 29 is National Geodetic Vertical Datum of 1929.

Ground-water divides observed in the water-table and lower Tamiami aquifers during March and September 1996 may or may not have been in the same location in 1930. It seems reasonable to expect that the northern and southern ground-water divides remain relatively stable. Recharge on the Florida Peninsula creates a mound of ground water in aquifers above sea level, resulting in flow from inland areas toward the coast. Additionally, contemporary ground-water withdrawal near these northern and southern divides is less prevalent, resulting in less opportunity for stress to move the location of these divides. The location of the eastern ground-water divide during 1930, however, is more uncertain; in fact, the divide may never have existed. This boundary condition probably is far enough away from the saltwater transition zone in the lower Tamiami aquifer to have little consequence on model results. Regardless, a better method for approximating the location of lateral predevelopment boundary conditions would reduce uncertainty in model results.

Constant Heads and Concentrations

Constant-head boundary conditions were entered into SEAWAT using the IBOUND and Shead arrays of the Basic package (McDonald and Harbaugh, 1988). An integer value less than zero in the IBOUND array of the Basic package indicates that the model cell has a constant-head throughout the simulation. The constant-head value will be equal to a real number entered in the same location of the Shead array of the Basic package. Constant-concentration boundary conditions were entered using the ICBUND array in the Basic Transport package and the Source Sink Mixing package (Zheng and Wang, 1998). An integer value less than zero in the ICBUND array of the Basic Transport package indicates the model cell has a constant concentration equal to a value specified for that model cell in the Source Sink Mixing package.

Constant-concentration boundary conditions were used for layer 1 and along the western boundary of the model in layers 2 to 15 to represent the Gulf of Mexico (pl. 1). The boundary conditions were assigned a constant salt concentration equal to 35 kg/m^3 (the salinity of seawater).

Constant-head boundary conditions were used in layer 1 and along the western boundary of the model in layers 2 to 15 to represent the Gulf of Mexico (pl. 1). Constant-head values representing the Gulf of Mexico in 1930 were assigned by: (1) computing the average value of sea level in 1996 using daily sea level measurements recorded at National Oceanic and Atmospheric Administration (NOAA) station 8725110 (not shown), (2) extrapolating sea level backward to 1930 using the average 1996 value and a 2-mm/yr rate of sea-level rise (National Research Council, 1987), and (3) converting the extrapolated 1930 sea level value to a hydrostatic freshwater equivalent sea level for input to the SEAWAT simulator. On average, sea level in 1996 was about 0.2 m above NGVD 1929. By extrapolating, sea level in 1930 was calculated to be about 0.07 m above NVGD 1929. Hydrostatic freshwater equivalent sea level (h_f) was computed using the following equation:

$$h_f = Z + \frac{\rho}{\rho_f}(h_s - Z) \quad . \tag{12}$$

Z was set to the elevation of the center of the model cell. Fluid density (ρ) was set to 1,025 kg/m^3 (density of saltwater). Extrapolated 1930 sea level (h_s) was computed as 0.07 m. Using the equation and data above, the freshwater equivalent sea level in 1930 was 0.12 m above NVGD 1929 for layer 1 and proportionately greater than 0.12 m at the western boundary of the model in layers 2 to 15 because the elevation of the center of these model cells, Z, is farther below NVGD 1929.

Simulation Results

The predevelopment simulation was run until heads and salinity reached steady state. An evaluation of simulated predevelopment heads (not shown) suggested that the model provides a reasonable representation of coastal ground-water flow. An estimate of the predevelopment distribution of saltwater is obtained by evaluating the solute concentrations simulated by the model.

A three-dimensional view of the predevelopment distribution of saltwater was prepared using Modelviewer, a visualization and animation program (Hsieh and Winston, 2002) (fig. 23). Although this view provides a more complete perspective of the predevelopment distribution of saltwater, it is difficult to visualize how ground-water salinity relates with other prominent features in the study area. Thus, a two-dimensional map showing the intersection of the predevelopment saltwater interface with the base of the lower Tamiami aquifer was prepared (fig. 24).

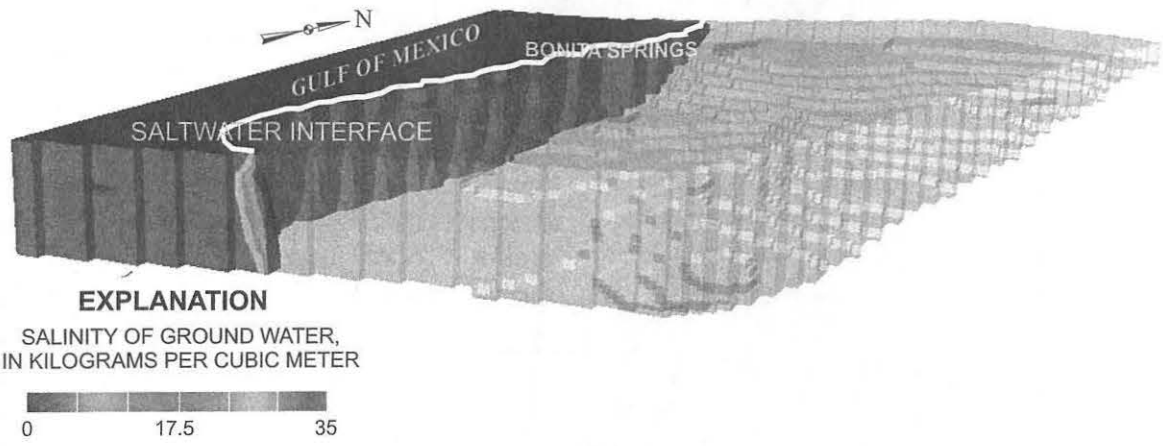


Figure 23. Three-dimensional view of the simulated predevelopment distribution of saltwater. All shaded areas represent active model cells. Blue and tan cells are equivalent in salinity; the tan shading is used to highlight the topography of the base of the lower Tamiami aquifer.

The predevelopment distribution of saltwater consists of a sharp, steep interface that roughly parallels the coast. Near Naples and central Estero Bay, the saltwater interface intersects with the base of the lower Tamiami aquifer directly beneath the coastline. In most other areas, the intersection is as much as 2 km offshore. Model results suggest the interface is directly beneath the coastline in locations where less ground water is discharging to the Gulf of Mexico. Conversely, the interface is farther from the coastline in locations where more ground water is discharging to the Gulf of Mexico. These results appear to be a reasonable estimate of salinity conditions in the water-table and lower Tamiami aquifers prior to modern stresses, such as ground-water development and canal drainage.

Model Calibration to Typical, Modern, and Seasonal Stresses

Model calibration was necessary to move the predevelopment distribution of saltwater to equilibrium with a reasonable representation of March and September 1996 conditions (table 2). The same spatial discretization and aquifer properties previously described were used for calibration. Two steady-state stress periods representing average March and September 1996 conditions were designed. The MODFLOW program was used to simulate ground-water flow.

The calibration objective of this study was to find the combination of model parameters or boundary conditions that best represent March and September 1996 conditions. Boundary conditions were assigned to closely resemble the time periods of interest. The parameter estimation routine, UCODE (Poeter and Hill, 1998), was used to "best fit" simulated heads and flows to their observed equivalents by solving for parameter estimates using a nonlinear least squares regression. The reliability or uncertainty in parameter estimates also was quantified with linear 95-percent confidence intervals.

Boundary Conditions

Boundary conditions for model calibration under March and September 1996 hydrologic conditions include no flow, constant heads, rivers, general heads, rainfall, evapotranspiration, and wells (pl. 2). No-flow boundary conditions were used to represent hydrologic divides and the saltwater interface. Layers 16 and 17 consist entirely of no-flow cells; therefore, these layers are not plotted on plate 2. Constant-head boundary conditions were used to represent the Gulf of Mexico. River boundary conditions were used to

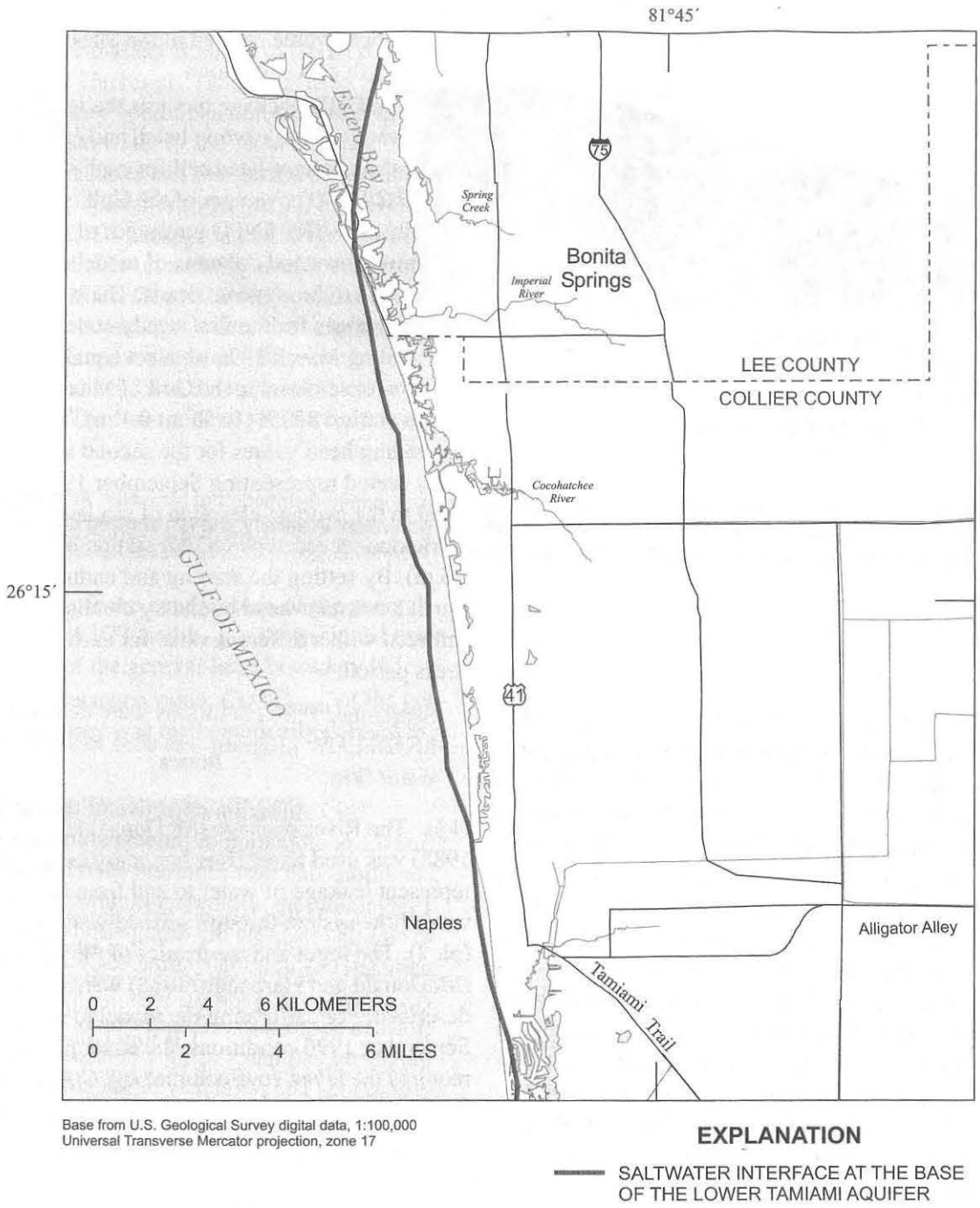


Figure 24. Approximate position of the simulated predevelopment saltwater interface at the base of the lower Tamiami aquifer.

represent local rivers and the system of canals in the southeastern part of the study area. General-head boundary conditions were used to represent deep leakage of ground water to and from the base of the lower Tamiami aquifer. Rainfall and evapotranspiration boundary conditions were used to represent net recharge; however, these boundary conditions are not plotted or labeled on plate 2 for the same reasons they are not plotted on plate 1 as previously mentioned. Well boundary conditions were used to represent ground-water pumpage from the water-table and lower Tamiami aquifers.

No Flow

The Basic package (McDonald and Harbaugh, 1988) was used to set no-flow boundary conditions that represent hydrologic divides and the saltwater interface (pl. 2). The input and mechanics of accomplishing this using the Basic package were previously described. No-flow boundary conditions representing hydrologic divides were assigned to model layers at the northern, eastern, and southern boundaries of the simulation for both steady-state stress periods. These boundary conditions were set using water-level contour maps of the water-table and lower Tamiami aquifers during March and September 1996 (fig. 22).

No-flow boundary conditions representing the saltwater interface in layers 2 to 15 beneath the Gulf of Mexico were set using the predevelopment distribution of saltwater. All model cells west of the 50-percent seawater zone in the predevelopment simulation were designated as no-flow cells in both steady-state stress periods. In systems where density changes abruptly between a freshwater zone and a more dense "salty" zone, the boundary between freshwater and saltwater can be conceptualized as a no-flow boundary condition when movement of the boundary is assumed to be of negligible importance to the problem (Reilly, 2001). Most water-level and flow observations for calibrating the model to March and September 1996 conditions are several kilometers inland with chloride concentrations less than 1,000 mg/L. This suggests the bulk of the saltwater interface has not moved through the vicinity of these observations, and the error in simulated heads and flows will more likely be attributable to uncertainty in rock properties and other boundary conditions, such as recharge, than from the position or movement of saltwater or brackish water with greater fluid density.

Constant Heads

The Constant Head Boundary (CHD) package (Leake and Prudic, 1991) was used to set constant-head boundary conditions that represent the average elevation of sea level in the Gulf of Mexico during March and September 1996. The IBOUND and Shead arrays in the Basic package could not be used because the average elevation of sea level in March 1996 (the first steady-state stress period) is different than the average elevation of sea level in September 1996 (the second steady-state stress period). The IBOUND and Shead arrays of the Basic package can apply only one constant head value entered in the Shead array for the entire length of a simulation.

The CHD package requires the input of the layer, row, column, starting head, and ending head values for the constant-head cell for each stress period. The ARC/INFO coverages of the Gulf of Mexico were overlain with ARC/INFO coverages of the model grid to identify rows and columns of model cells in layer 1 that needed to be constant heads. The starting and ending head values for the first steady-state stress period representing March 1996 were set equal to the average elevation of sea level in the Gulf of Mexico recorded at Naples station 8725110 (about 0.1 m). The starting and ending head values for the second steady-state stress period representing September 1996 were set equal to the average elevation of sea level in the Gulf of Mexico recorded by NOAA station 8725110 (about 0.3 m). By setting the starting and ending head values equal, a constant-head boundary condition was enforced with a different value for each steady-state stress period.

Rivers

The River package (McDonald and Harbaugh, 1988) was used to set river boundary conditions that represent leakage of water to and from the groundwater flow system through surface-water channels (pl. 2). The input and mechanics of the River package (McDonald and Harbaugh, 1988) were previously described. For calibrating the model to March and September 1996 conditions, the River package requires the layer, row, column, h_{riv}, $COND_{riv}$, and *RBOT* for both steady-state stress periods. The layer, row, and column of river cells were determined by overlying ARC/INFO coverages of contemporary surface-water features with the model grid. The USGS or SFWMD surface-water gaging stations, if available, were used to interpolate or extrapolate average March and September 1996 h_{riv} values for both steady-state stress periods. For each river cell, $COND_{riv}$ was computed using equation 9. The value of K_{seds} is assumed to be 15 m/d, which is the vertical hydraulic conductivity used for the water-table aquifer (table 3); the value of b_{seds} was given a reasonable value of 1 m, and the value of *RBOT* was about 2 m less than h_{riv}.

General Heads

The General-Head Boundary (GHB) package (McDonald and Harbaugh, 1988) was used to set general-head boundary conditions that represent the deep leakage of ground water to and from the base of the lower Tamiami aquifer and the sandstone aquifer during March and September 1996 (pl. 2). In MODFLOW-88, the GHB package is one of the most robust packages available for simulating a wide range of boundary conditions. General-head boundaries are head-dependent boundaries where the volumetric flux, Q_{GHB}, is proportional to the head difference between an assigned external head and the approximated head in the model cell. The form of Darcy's law used to characterize the flux is:

$$Q_{GHB} = COND_{GHB}(h_{GHB} - h_{i,\,j,\,k}) \quad , \qquad (13)$$

where $COND_{GHB}$ is the conductance of the general-head boundary [L^2/T], and h_{GHB} is the assigned external head value of the general-head boundary [L].

The conductance value, $COND_{GHB}$, of the general-head boundary was mathematically defined as:

$$COND_{GHB} = \frac{LwK_{GHB}}{b_{GHB}} \quad , \qquad (14)$$

where L is the length of the model cell [L], w is the width of the model cell [L], K_{GHB} is the vertical hydraulic conductivity of the upper Hawthorn confining unit [L/T], and b_{GHB} is the thickness of the upper Hawthorn confining unit [L].

Variables L and w of the model cells were assigned values of 600 m each, and a value of 0.003 m/d was used for K_{GHB} (Montgomery, 1988). A value of 9.14 m was used for b_{GHB}, the average thickness of the upper Hawthorn confining unit reported by Knapp and others (1986). The b_{GHB} could not be spatially variable because no published maps of the thickness of this unit could be found.

The h_{GHB} values were set using contour maps of the potentiometric surface of the sandstone aquifer. Sufficient water-level measurements were obtained for the March 1996 steady stress period, but not for the September 1996 period. To approximately define the potentiometric surface of the sandstone aquifer, water levels at 15 monitoring wells for March 1996 were averaged, plotted, contoured, and interpolated to the h_{GHB}. For the September 1996 period, average water levels at the same 15 monitoring wells were computed, plotted, and contoured to define the average potentiometric surface of the sandstone aquifer for the entire 1996 calendar year. This average surface then was interpolated to the h_{GHB} for the September 1996 steady-state stress period.

Recharge

The Recharge and Evapotranspiration packages (McDonald and Harbaugh, 1988) were used to represent net recharge, or the water applied to land surface through precipitation that exceeds evapotranspiration and runoff and infiltrates through the unsaturated zone to the water table. An areal flux [L/T] of rainfall minus runoff was applied to the highest active cell in a vertical column of layers using the Recharge package (McDonald and Harbaugh, 1988) for both steady-state stress periods. Average monthly rainfall rates were computed from daily rainfall totals collected in 1996 at a rainfall monitoring station near Bonita Springs. The average rainfall rate in March 1996 was about 0.3 cm/d, and the average rainfall rate in September 1996 was about 0.4 cm/d. Runoff was estimated using land-use coefficients developed during previous investigations of the study area (Bennett, 1992). These land-use coefficients suggest 10 to 30 percent of rainfall is converted to runoff during a storm event. The average of land-use coefficients (about 0.127) reported by Bennett (1992) was used to estimate the amount of rainfall lost to runoff during March and September 1996. A weighted average based on the individual area of each land-use type within the total area of the active model domain could not be computed because runoff coefficients for recent land-use maps were not available. As previously mentioned, runoff was subtracted from rainfall, and the resulting areal flux [L/T] was input for both steady-state stress periods in the Recharge package.

Evapotranspiration was simulated using the Evapotranspiration package (McDonald and Harbaugh, 1988), with the evapotranspiration surface set to land surface and an extinction depth set to 5 m at all active cells in the model domain. As previously defined, setting extinction depths to 5 m is a reasonable compromise given the current understanding of the evapotranspiration process in Florida. Maximum evapotranspiration rates were uniformly set across the model grid using free surface pan evaporation data (fig. 25) and a pan multiplier of 0.7 (Swancar and

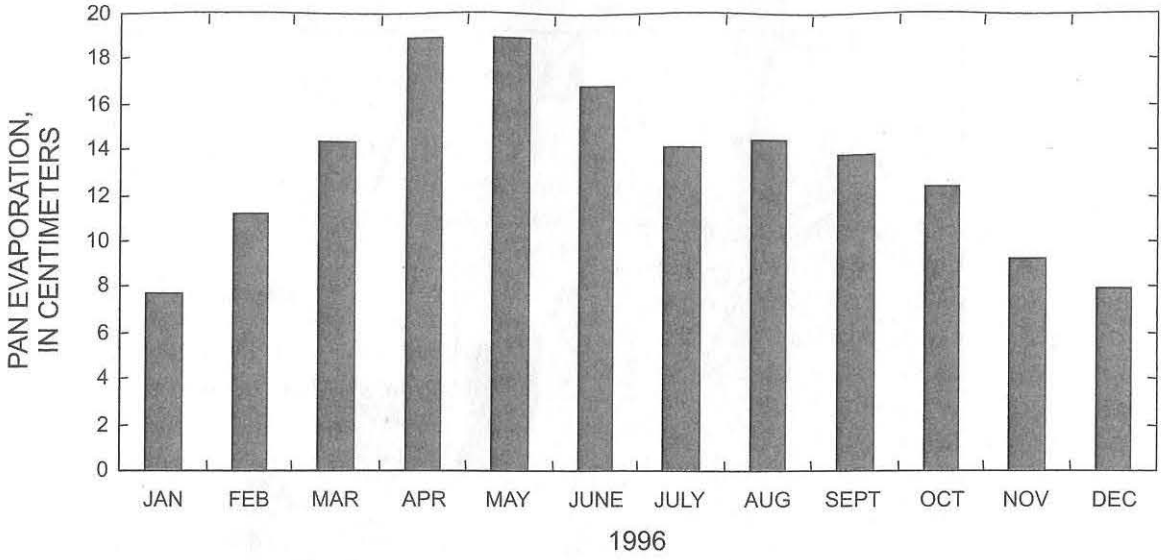


Figure 25. Total monthly pan evaporation from several monitoring stations near Bonita Springs.

others, 2000, p. 42). This means maximum ground-water evapotranspiration rates in the Evapotranspiration package were 70 percent of the average March 1996 pan evaporation rate for the first steady-state stress period and 70 percent of the average September 1996 pan evaporation rate for the second steady-state stress period.

Wells

The Well package (McDonald and Harbaugh, 1988) was used to represent the withdrawal of ground water from the water-table and lower Tamiami aquifers. Well boundaries may be used for injection or extraction wells. The layer, row, column, and injection or extraction volumetric rate are required input for the Well package. The location and volumetric rate of monitored ground-water pumpage were obtained from the SFWMD and translated to the appropriate layer, row, column, and stress period of the model simulation. Well construction information, such as depth to the top of casing and depth to the bottom of the open-hole interval, was used to determine the appropriate model layer in which to place the pumping well. Areas near Bonita Springs that are most likely to withdraw large quantities of unmonitored ground water from the lower Tamiami aquifer also were delineated (fig. 26) with the help of SFWMD personnel. Because this pumpage was unmonitored, volumetric rates and open-hole intervals were not known. The missing pumpage rates were set approximately equal to the monitored ground-water pumpage in March and September 1996. Although this may seem arbitrary, these missing pumpage rates were better estimated with UCODE during model calibration. The open-hole intervals of unmonitored pumping wells were assumed to be present at the center of the lower Tamiami aquifer (pl. 2).

Parameter Estimation

The model was calibrated with the UCODE parameter estimation routine (Poeter and Hill, 1998) to 41 average monthly head and 2 average monthly flow observations computed from USGS monitoring wells and gaging stations, respectively, in the study area (table 4). Each head observation is the average of all measurements made at the well during March or September 1996. Flow observations are the sum of the average of all flow measurements made at the northern and southern branches of the Estero River, Spring Creek, and Imperial River during March and September 1996.

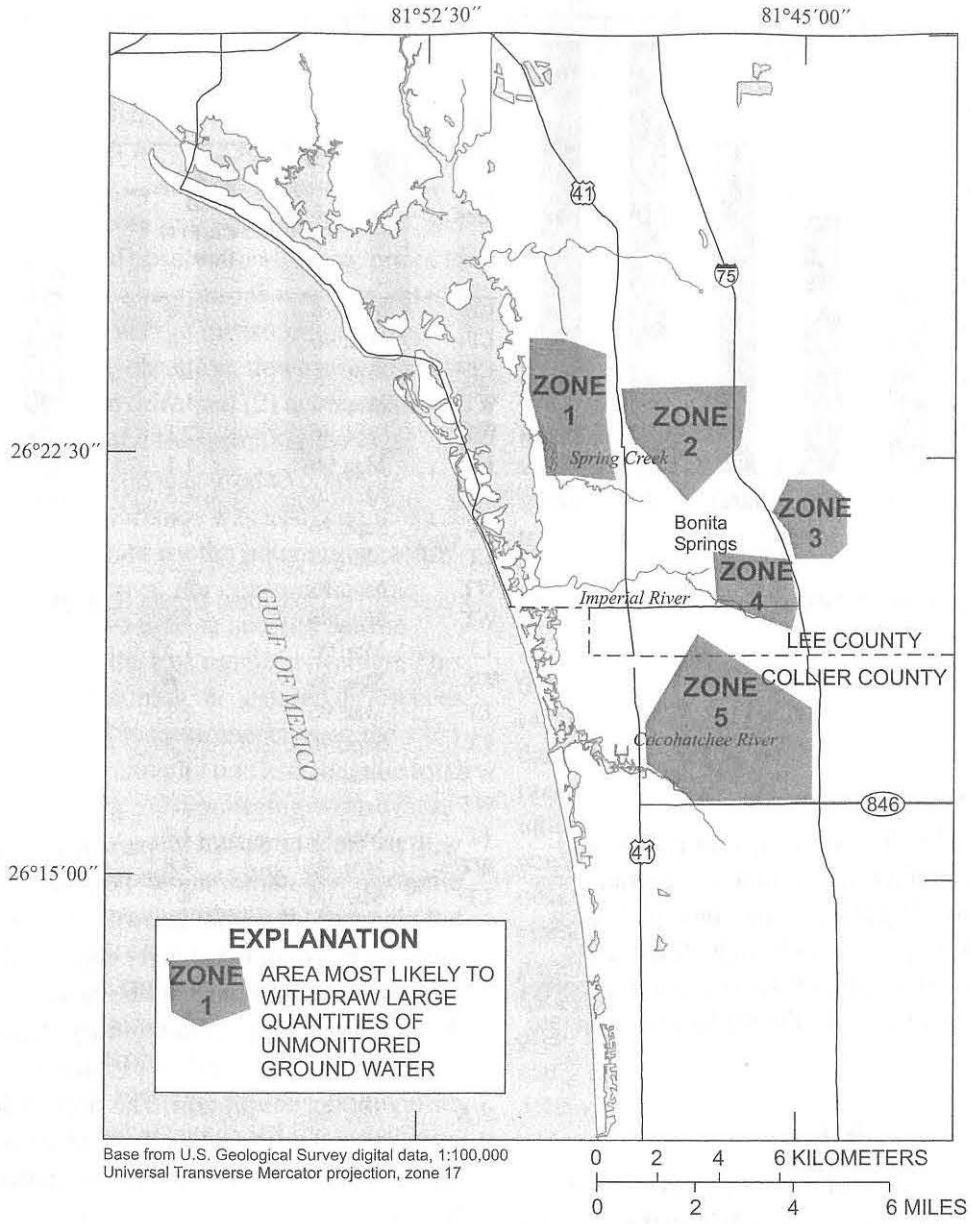


Figure 26. Areas with potentially large quantities of unmonitored ground-water pumpage.

With UCODE, head and flow observations were weighted and summed together with their simulated equivalents as the objective function, $S(b)$,

$$S(b) = \sum_{i=1}^{nh} w_i[h_i - h_i'(b)]^2 + \sum_{i=1}^{nq} w_i[q_i - q_i'(b)]^2, \quad (15)$$

where b is a vector containing values of each of the parameters being estimated, nh is the number of head observations, w_i is the weight for the ith observation, h_i is the ith observed water level, $h_i'(b)$ is the simulated equivalent of the ith observed water level (a function of b), nq is the number of flow observations, q_i is the ith observed flow, and $q_i'(b)$ is the simulated equivalent of the ith observed flow (a function of b). UCODE solved for parameter values, b, that minimize this objective function, $S(b)$, resulting in simulated heads and flows that most closely resemble their observed equivalents.

Table 4. Observations used during model calibration to March and September 1996 conditions

[Aquifer: LT, lower Tamiami aquifer; WT, water-table aquifer. USGS, U.S. Geological Survey; N/A, not applicable; QWDATA,Water Quality Database; ADAPS, Automated Data Processing System]

Site identification	Universal transverse mercator coordinates		Aquifer	Date	Average head (meters) or flow[1]	USGS data source
	x (meters)	y (meters)				
C-304	439677	2906341	LT	Mar. 96	1.6	QWDATA
C-391	420917	2897007	LT	Mar. 96	.8	ADAPS
C-391	420917	2897007	LT	Sept. 96	1.4	ADAPS
C-392	420945	2897038	WT	Mar. 96	1.9	ADAPS
C-392	420945	2897038	WT	Sept. 96	2.1	ADAPS
C-430	423141	2897516	LT	Mar. 96	1.2	QWDATA
C-460	421614	2902048	LT	Mar. 96	1.5	ADAPS
C-460	421614	2902048	LT	Sept. 96	2	ADAPS
C-489	420885	2900914	LT	Mar. 96	.5	QWDATA
C-492	439638	2917334	WT	Mar. 96	5	ADAPS
C-492	439638	2917334	WT	Sept. 96	5.3	ADAPS
C-516	419370	2896761	LT	Mar. 96	1.3	QWDATA
C-528	419240	2898054	LT	Mar. 96	.6	QWDATA
C-951	441394	2901359	LT	Mar. 96	1.1	ADAPS
C-951	441394	2901359	LT	Sept. 96	1.9	ADAPS
C-953	441394	2901359	WT	Mar. 96	1.9	ADAPS
C-953	441394	2901359	WT	Sept. 96	2.4	ADAPS
C-977	435395	2892948	LT	Mar. 96	1.7	QWDATA
C-978	440163	2915292	WT	Mar. 96	4.8	QWDATA
C-979	440163	2915292	LT	Mar. 96	4	QWDATA
C-997	431283	2904547	WT	Mar. 96	2.6	ADAPS
C-1004	422249	2906167	LT	Sept. 96	1.1	ADAPS
C-1059	419870	2905711	WT	Mar. 96	1.9	QWDATA
C-1061	420058	2900325	WT	Mar. 96	3.9	QWDATA
C-1083	421307	2910911	LT	Mar. 96	.5	ADAPS
C-1083	421307	2910911	LT	Sept. 96	1	ADAPS
FLOW1	N/A[2]	N/A[2]	N/A	Mar. 96	40,394	ADAPS
FLOW2	N/A[2]	N/A [2]	N/A	Sept. 96	271,820	ADAPS
L-738	422405	2913580	LT	Mar. 96	0	ADAPS
L-738	422405	2913580	LT	Sept. 96	.9	ADAPS
L-1964	439799	2938122	WT	Mar. 96	7.2	QWDATA
L-1999	427787	2932554	WT	Mar. 96	6.3	QWDATA
L-2195	427917	2912841	WT	Mar. 96	2.8	ADAPS
L-2195	427917	2912841	WT	Sept. 96	3.6	ADAPS
L-2308	418735	2923716	WT	Mar. 96	3.4	QWDATA
L-2550	430872	2926115	WT	Mar. 96	3.3	ADAPS
L-2550	430872	2926115	WT	Sept. 96	3.7	ADAPS
L-5722	422255	2914834	WT	Mar. 96	1.9	QWDATA
L-5723	422255	2914834	LT	Mar. 96	-1.3	QWDATA
L-5724	418350	2912528	WT	Mar. 96	2.6	QWDATA
L-5725	418332	2912489	LT	Mar. 96	0	QWDATA
L-5730	418739	2919993	WT	Mar. 96	3.4	QWDATA
L-5747	421417	2918346	LT	Mar. 96	-1.3	QWDATA

[1]Flow shown in meters per day.

[2]Flow observations are the sum of estimated flows at four different locations. These locations (northern and southern branches of the Estero River, Spring Creek, and Imperial River) are discussed in the text.

With UCODE, observations are weighted to: (1) maintain similar dimensions in the objective function so that head and flow residuals can be added together, and (2) emphasize observations that are more or less important to "best fit" with regression. For example, weights can be used to make an accurately measured observation more important to "best fit" and an inaccurately measured observation less important to "best fit." For this study, observations were weighted to: (1) account for the potential measurement error, such as the top-of-casing elevation, down-to-water distance, or instrumentation drift; and (2) account for the potential deviance from the true monthly average.

The variance statistic was used to compute observation weights. A variance was assigned to each observation well to account for the potential measurement errors described above. For convenience, the variance statistic was also used to account for the potential deviance from the true monthly average. This was accomplished by summing the squared differences of individual water-level measurements from the monthly average and dividing by one less than the total number of measurements. At monitoring wells where only one or two depth-to-water measurements were taken during March or September 1996, the average variance of water-level measurements at observation wells with continuous monitoring equipment was used. Using the variance statistic was convenient because variances are additive, and the final variance statistic used to calculate observation weights was the sum of the variance that accounts for measurement error and the variance that accounts for the potential deviance from the true monthly average.

A primary objective of this project was to accurately simulate saltwater movement in the lower Tamiami aquifer beneath Bonita Springs. To accomplish this objective, accurately simulated water levels in this area of the aquifer were necessary. Unmonitored ground-water pumpage created large cones of depression in the lower Tamiami aquifer beneath Bonita Springs. Large discrepancies between observed and simulated water levels initially were present in this area of the model because simulated water levels cannot be drawn down where pumpage data do not exist. For this reason, zones of unmonitored ground-water pumpage with "sufficient" sensitivity were estimated with UCODE, resulting in simulated water levels that closely match observed water levels in important areas near the coast.

Zones of unmonitored ground-water pumpage were determined to have "sufficient" sensitivity by examining composite-scaled sensitivities. Composite-scaled sensitivities (CSS) computed by UCODE are measures of the amount of information that all the observations provide for estimating a parameter (Poeter and Hill, 1998). If a parameter has large CSS, then the observations hold much information for estimating that parameter value. If a parameter has small CSS, then the observations hold little information for estimating that parameter value. Given this relation, the regression performed by UCODE can have difficulty converging on estimates of parameters with small CSS, because very little information is provided by the observations for estimating these parameter values. Thus, only parameters with large or "sufficient" CSS that are not correlated are successfully estimated with UCODE.

Parameter correlation is measured using correlation coefficients calculated as the covariance between two parameters divided by the product of their standard deviations (Hill, 1998). Correlation coefficients range from 1.0 to -1.0, with values close to 1.0 or -1.0 indicating parameters that are correlated or inversely correlated, but cannot be estimated uniquely with the observations used to calibrate a flow model. It is already well established that hydraulic conductivity parameters (K) and flow parameters (Q) representing, for example, recharge or ground-water pumpage are often highly correlated when calibrating a flow model using only hydraulic-head observations (Hill, 1998). Adding flow observations, such as streamflow gains and losses, can greatly reduce correlation of K and Q parameters and result in unique parameter estimates.

Unmonitored ground-water pumpage was correlated with the most sensitive model parameters (evapotranspiration extinction depth, canal conductance, and vertical hydraulic conductivities of the Tamiami confining beds and upper Hawthorn confining unit) as indicated by CSS (fig. 27) and correlation coefficients. This meant that while trying to estimate unmonitored ground-water pumpage with more sensitive model parameters, unique estimates could not be found. This is a disadvantage because: (1) a better regional model fit probably could be attained if the more sensitive model parameters could be estimated; and (2) some of the more sensitive model parameters, such as hydraulic conductivities and canal conductances, probably are more uncertain than the unmonitored ground-water pumpage. However, unique UCODE estimates of

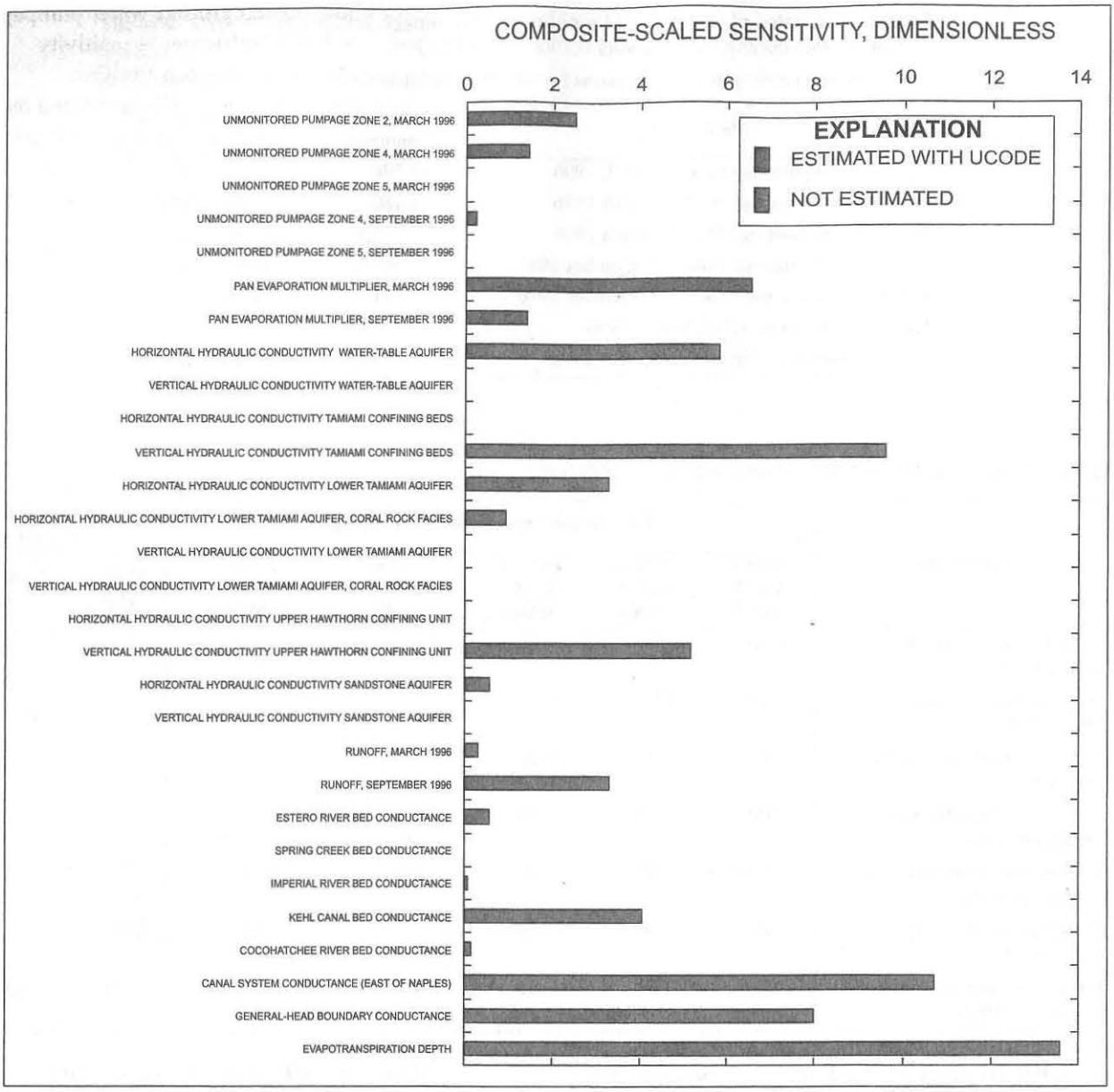


Figure 27. Composite-scaled sensitivities computed while calibrating the model to March and September 1996 conditions. Parameters with no visible bar have very small or zero sensitivity.

unmonitored ground-water pumpage zones with sufficient sensitivity and pan evaporation multipliers were found (table 5). The uniqueness is indicated by UCODE correlation coefficients (table 6) and the fact that final UCODE estimates of these parameters were not sensitive to the parameter starting values.

In the stress period representing September 1996, UCODE estimated a pan evaporation multiplier of 1.13, which means the maximum evapotranspiration rate is about 13 percent larger than the pan evaporation rate. This parameter estimate probably is unreasonable because maximum evapotranspiration rates likely are less than pan evaporation rates in most circumstances. Unreasonable parameter estimates are valuable because they suggest that either the model may not accurately represent some aspect of the physical system (most likely), or there may be an error in the observations used to calibrate the model (Poeter and Hill, 1997).

Table 5. Estimates of unmonitored ground-water pumpage and evapotranspiration multipliers with confidence intervals computed by UCODE

[Parameters are in cubic meters per day, except for evaporation multipliers, which are dimensionless]

Parameter	Parameter estimate	Linear 95-percent confidence interval
Unmonitored pumpage zone 1, March 1996	-1,080	275; -2,440
Unmonitored pumpage zone 4, March 1996	-1,180	1,650; -4,010
Unmonitored pumpage zone 5, March 1996	-6.1	4,450; -4,750
Unmonitored pumpage zone 4, September 1996	-352	4,610; -5,310
Unmonitored pumpage zone 5, September 1996	11	8.26; -30
Pan evaporation multiplier, March 1996	.64	0.78; 0.53
Pan evaporation multiplier, September 1996	1.13	1.46; 0.87

Table 6. UCODE estimated parameter correlation coefficients

Parameter	Unmonitored ground-water pumpage					Pan evaporation multiplier	
	Zone 1 (March 1996)	Zone 4, (March 1996)	Zone 5 (March 1996)	Zone 4, (September 1996)	Zone 5, (September 1996)	March 1996	September 1996
Unmonitored pumpage zone 1, March 1996	1.00						
Unmonitored pumpage zone 4, March 1996	-.15	1.00					
Unmonitored pumpage zone 5, March 1996	.03	-.38	1.00				
Unmonitored pumpage zone 4, September 1996	.00	.00	.00	1.00			
Unmonitored pumpage zone 5, September 1996	.00	.00	.00	.00	1.00		
Pan evaporation multiplier, March 1996	.06	.09	.26	.00	.00	1.00	
Pan evaporation multiplier September 1996	.00	.00	.01	.20	.00	.01	1.00

In this model, rainfall may be overestimated, runoff may be underestimated, hydraulic conductivity may be underestimated, or a combination of these and other errors may exist. It is also possible that a process such as interception that prevents rainfall from reaching the water table is not represented in the model. In any of these circumstances, UCODE would estimate a larger maximum evapotranspiration to compensate for the model error, or the missing process that affects "net recharge." Because maps of "net recharge" looked reasonable and were consistent with field observations by Krulikas and Giese (1995), the model error was not resolved. Although undesirable, the unresolved error was justified because compensating errors in a model representing the various processes that affect "net recharge" can produce "net recharge" rates that are accurate.

When estimating zones of unmonitored ground-water pumpage with sufficient sensitivity and pan evaporation multipliers, the nonlinear least-squares regression performed by UCODE converged by satisfying the sum of the squares residual criteria, which was set to zero difference between parameter estimation iterations. This means the difference in the weighted objective function changed by this amount over three parameter estimation or regression iterations (Poeter and Hill, 1998). A traditional statistic for reporting calibration results is the mean absolute error (MAE), which is calculated by taking the average of the absolute values of the differences between observed and simulated heads. The MAE of the calibration was 0.73 m for the 41 average monthly water-level observations in the water-table and lower Tamiami aquifers. Graphical representations of the model

calibration are made by comparing observed and simulated water levels (fig. 28) and comparing weighted residuals and weighted simulated values (fig. 29). The comparison of weighted residuals and weighted simulated values is presented because this plot may identify model bias or trends that are obscured by the traditional comparison of observed and simulated water levels (Mary Hill, U.S. Geological Survey, written commun., 1999). No bias or trends are obvious on the plot in figure 29. The calibration plots and MAE statistic suggest that the model adequately represents the ground-water flow system in the water-table and lower Tamiami aquifers near Bonita Springs.

A component of the water budget important to water managers is unmonitored ground-water pumpage. Estimates of unmonitored ground-water pumpage zone rates per cell with confidence intervals were computed by UCODE (table 5). By calibrating to March and September 1996 water-level and flow observations, the average 1996 rate of unmonitored ground-water pumpage is bracketed because the rate of unmonitored ground-water pumpage probably is greatest during March 1995 and lowest during September 1995, as evidenced by historical ground-water withdrawals. The average 1996 rate of unmonitored ground-water pumpage can be estimated by: (1) multiplying the UCODE-estimated unmonitored ground-water pumpage rate for each zone by the number of model cells in that zone, (2) summing the total rate of unmonitored ground-water pumpage in March 1996 and September 1996, and (3) computing a weighted average. The weight was based on a 7 to 5 ratio of dry- to wet-season months, a typical southwestern Florida water year (Virogroup, Inc., 1993). Using this method, the average estimated rate of unmonitored ground-water pumpage from the lower Tamiami aquifer was

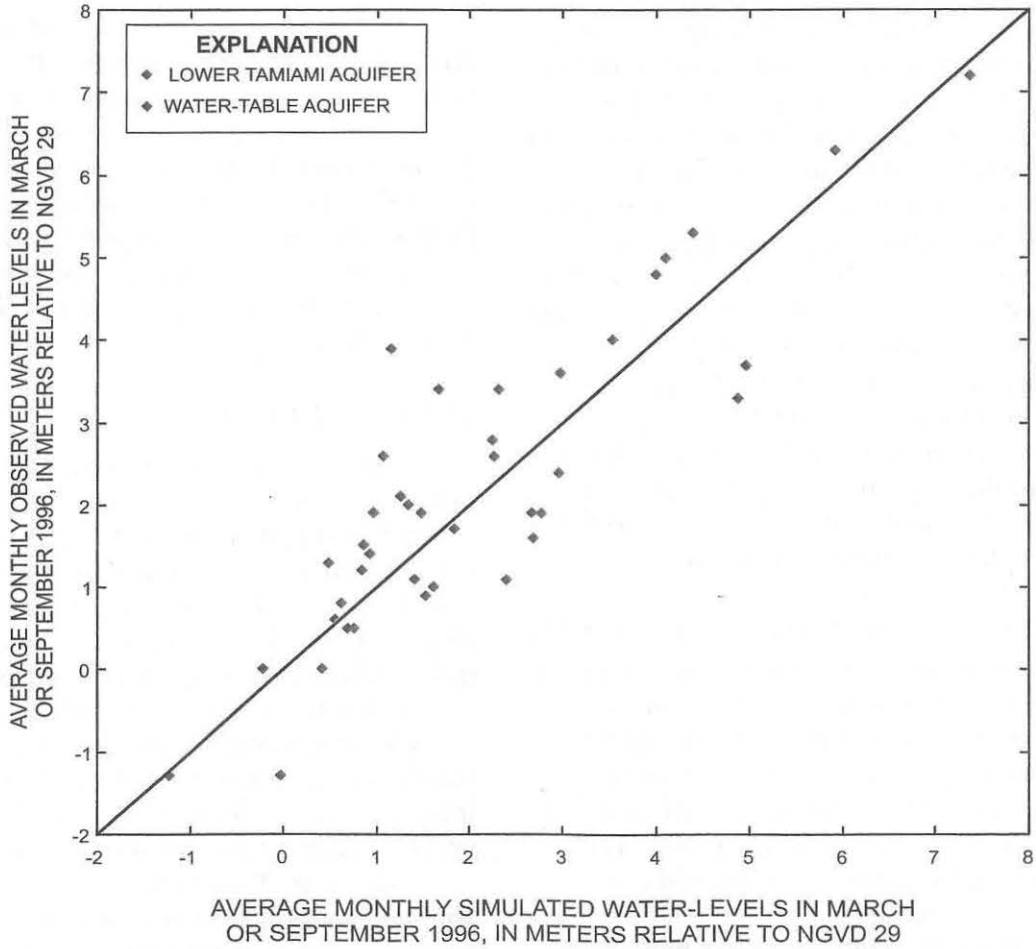


Figure 28. Comparison of observed and simulated water levels. NGVD 29 is National Geodetic Vertical Datum of 1929.

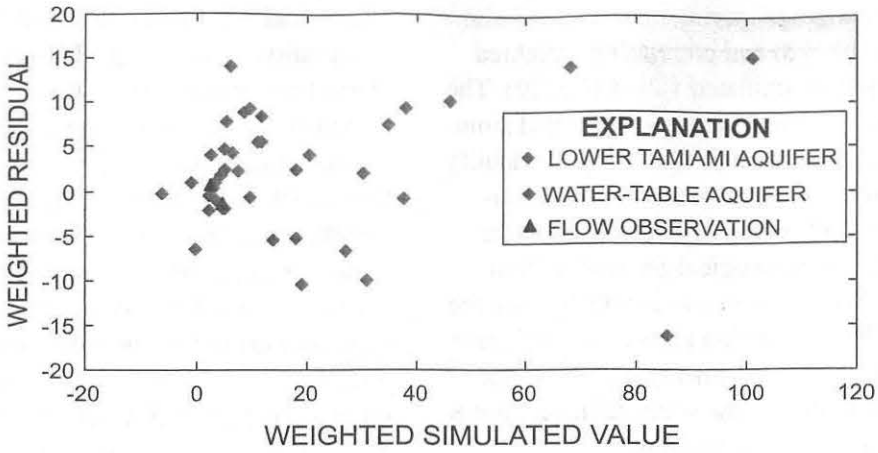


Figure 29. Comparison of weighted residuals and weighted simulated values.

about 52,000 m^3/d in 1996. The average estimated rate of monitored ground-water pumpage from the water-table and lower Tamiami aquifers in the active model domain (pl. 2) was about 59,000 m^3/d in 1996.

A good exercise to test a simulated water budget is to compare simulated net recharge with estimates of net recharge as computed by other methods. Krulikas and Giese (1995) used the chloride concentration ratio and flow-tube analysis methods to estimate net recharge, which ranged from 0 to 25 cm/yr in the study area in 1989. Net recharge maps were prepared for March and September 1996 using the cell-by-cell flow output from the MODFLOW simulations (figs. 30 and 31, respectively). Simulated values of net recharge generally ranged from 0 to 38 cm/yr. Net discharge occurred in small areas as indicated by the negative values shown in figures 30 and 31. One possible explanation for the difference in maximum net recharge rates (field-data computed compared to simulated) is that lowering the water table through pumping between 1989 and 1996 could have induced recharge rates in excess of 25 cm/yr (Krulikas and Giese, 1995).

Topography appears to influence the distribution of net recharge. In fact, simulation results suggest that there are localized areas in the water-table aquifer where net discharge occurs because of the close proximity of the water table to land surface and the effects of evapotranspiration (figs. 30 and 31). These net discharge areas constitute about 5 percent of the active model domain. Net recharge is greater in areas where land surface is relatively higher, such as Bonita Springs and areas south of the Caloosahatchee River along the Immokalee Rise (figs. 1 and 2), because the water table is deeper below land surface and the effects of evapotranspiration are less. The resulting net recharge maps (figs. 30 and 31) reflect the local topography.

Simulated water levels, streamflows, and net recharge rates adequately represent the empirical data describing these hydrologic processes in the study area. However, adequate representation of selected parameters does not ensure the accuracy of predictive simulations (Konikow and Bredehoft, 1992). Nevertheless, calibration or history matching is necessary to reduce errors in the conceptual model and to obtain more representative parameter values, given the scale of simulation.

Confidence Intervals

Linear 95-percent confidence intervals are one of the many useful statistics computed by UCODE during model calibration. Linear 95-percent confidence intervals were calculated for each UCODE estimated parameter, and represent a range that has a 95-percent probability of containing the true value if the model correctly represents the true ground-water flow system (Hill, 1998). The width of a confidence interval can be thought of as a measure of the likely precision of the parameter estimate. Wide intervals indicate less precision or more uncertainty, and narrow intervals indicate more precision or less uncertainty.

The linear 95-percent confidence intervals are wide for estimates of unmonitored ground-water pumpage and narrow for estimates of pan evapotranspiration multipliers (table 5). This suggests unmonitored ground-water pumpage rates are estimated with

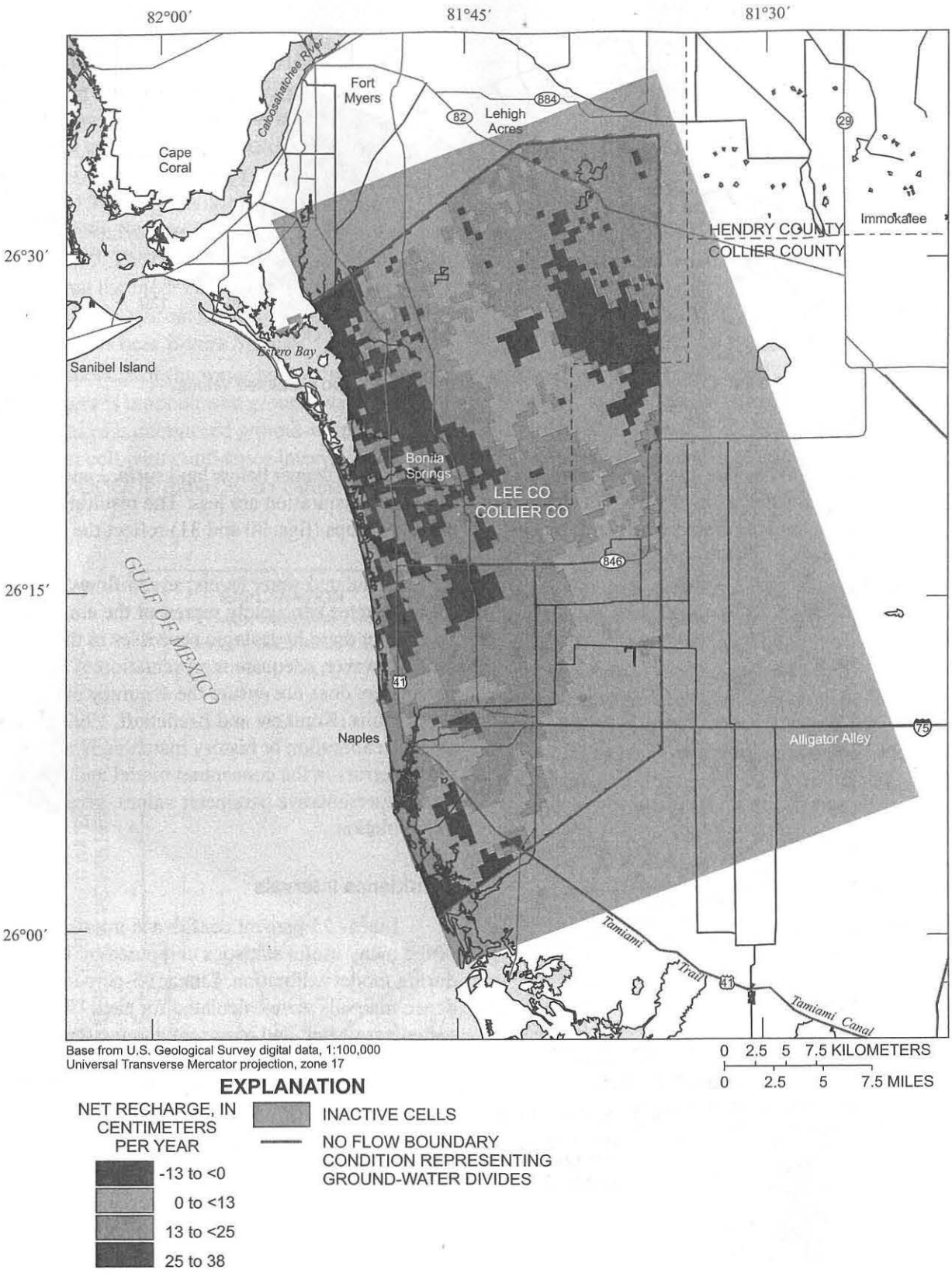


Figure 30. Simulated net recharge to the water-table aquifer during March 1996.

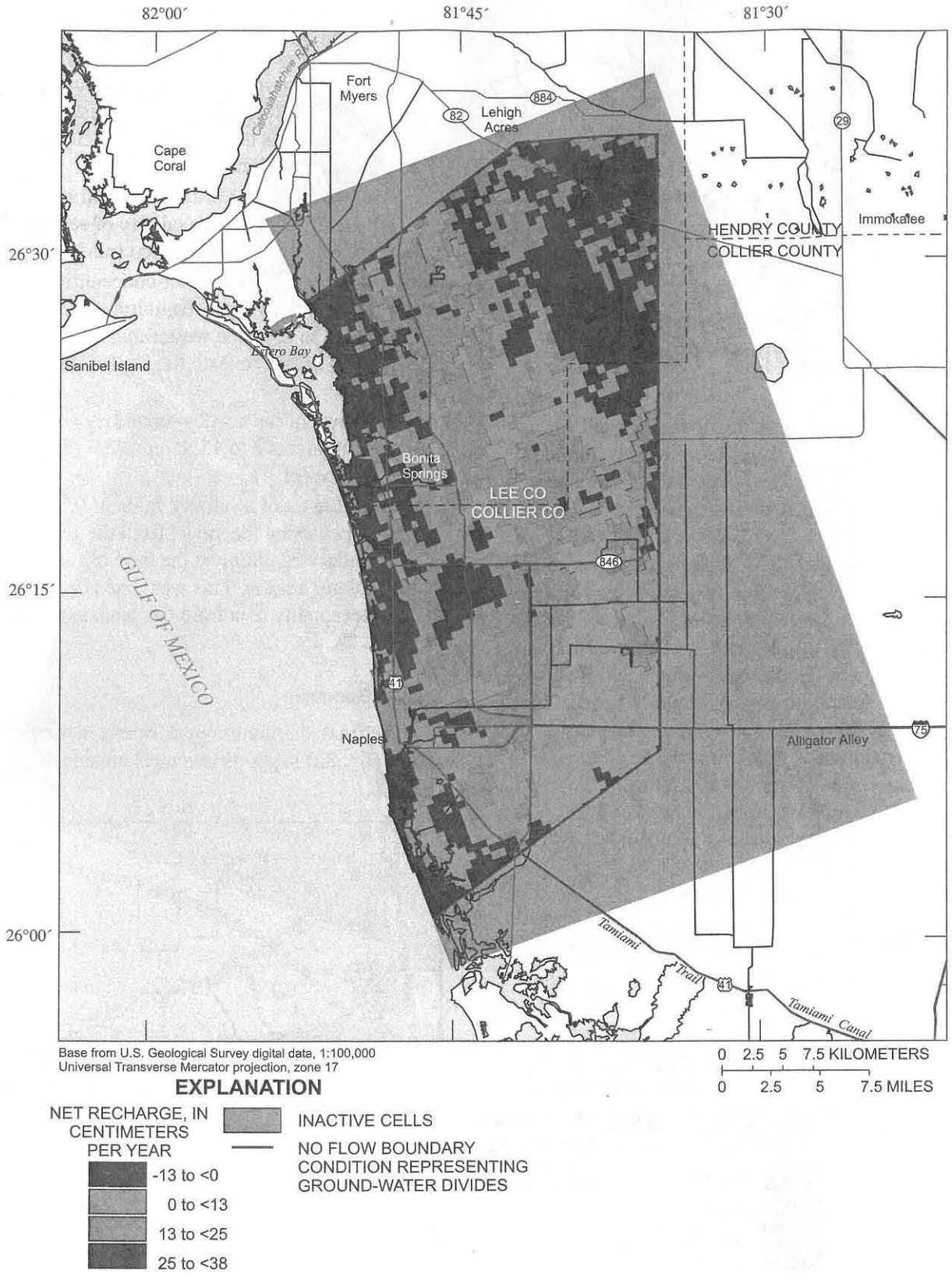


Figure 31. Simulated net recharge to the water-table aquifer during September 1996.

less precision or more uncertainty than pan evaporation multipliers. The design of the USGS network of monitoring wells and streamgaging stations in the study area apparently provides more information on estimating pan evaporation multipliers than estimating unmonitored ground-water pumpage rates. Conversely, one could also say that the pan evaporation parameters explain more of the water-level and discharge data monitored by the network than does the unmonitored ground-water pumpage.

Potential Movement of Saltwater to Equilibrium with Typical, Modern, and Seasonal Stresses

The predevelopment distribution of saltwater was moved to dynamic equilibrium with calibrated March and September 1996 steady-state stress periods (table 2). The same spatial discretization and aquifer properties previously described were used. Calibrated March and September 1996 steady-state stress periods were run successively until saltwater entering and leaving the simulation was about equal, which took about 600 years, or 1,200 steady-state stress periods. The SEAWAT program (Guo and Langevin, 2002) was used with initial conditions that consisted of the final distribution of freshwater equivalent head and salinity in the predevelopment simulation. The primary use of this simulation was to provide a baseline scenario to help identify potential mechanisms of saltwater intrusion and to estimate the potential extent of saltwater intrusion at dynamic equilibrium with modern stresses. Sensitivity analyses were performed for each of these primary objectives using the baseline scenario results.

In general, boundary conditions for this simulation are the same as boundary conditions used while calibrating the model to March and September 1996 conditions (pl. 2). The UCODE estimates of unmonitored ground-water pumpage and pan evaporation multipliers (table 5) were used. Some minor modifications to boundary conditions were necessary.

- Conversion of constant-head boundary conditions (pl. 2) to freshwater equivalent constant-head boundary conditions in the Gulf of Mexico, and conversion of the external heads of general-head boundary conditions (pl. 2) to freshwater equivalent external heads at the base of the lower Tamiami aquifer. These conversions were accomplished using chloride concentrations measured in the field, where data were available.
- Assignment of a constant concentration boundary equal to 35 kg/m^3 (salinity of seawater) in layer 1 at the Gulf of Mexico (pl. 2).
- Assignment of a constant-concentration boundary equal to 35 kg/m^3 (salinity of seawater) in layers 2 to 15 at the westernmost column (column 1) in and beneath the Gulf of Mexico (pl. 1).
- Removal of the no-flow boundary condition used in layers 2 to 15 to represent the saltwater interface (pl. 2).
- Assignment of a salinity value of 0.3 kg/m^3 to water entering the model from the general-head boundary condition at the base of the lower Tamiami aquifer. This was based on limited water-quality data from the sandstone aquifer (pl. 2).

Baseline Scenario

The final distribution of saltwater in the baseline scenario (fig. 32) supports two mechanisms of

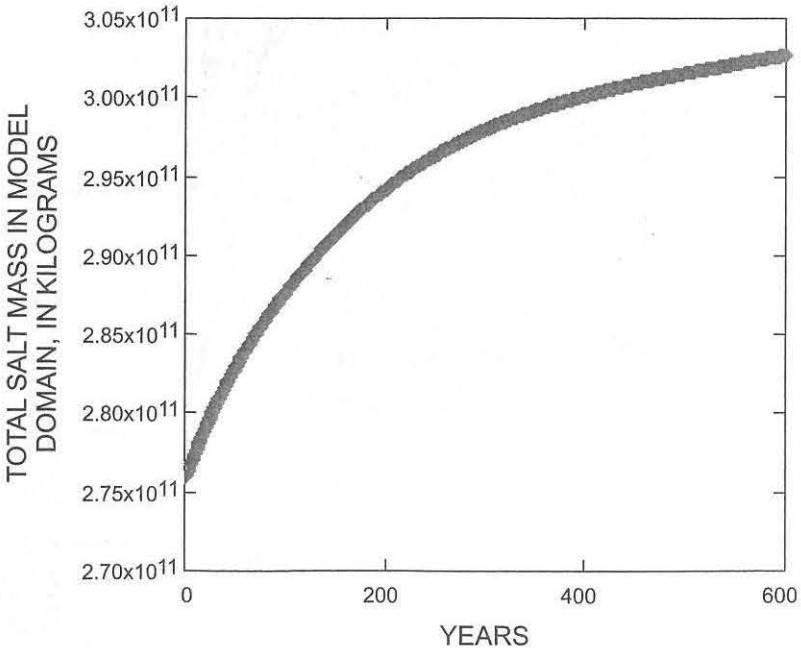


Figure 32. Total salt mass in the model while moving the simulated predevelopment distribution of saltwater to equilibrium with calibrated March and September 1996 conditions.

saltwater intrusion in the lower Tamiami aquifer near Bonita Springs—upconing and lateral saltwater intrusion. Results from the baseline scenario were used to estimate the potential extent of saltwater intrusion in the lower Tamiami aquifer beneath Bonita Springs.

Mechanisms of Saltwater Intrusion

The baseline scenario suggests that upconing of saltwater is the most predominant saltwater intrusion mechanism in the lower Tamiami aquifer beneath Bonita Springs (figs. 33 and 34). Predominance was

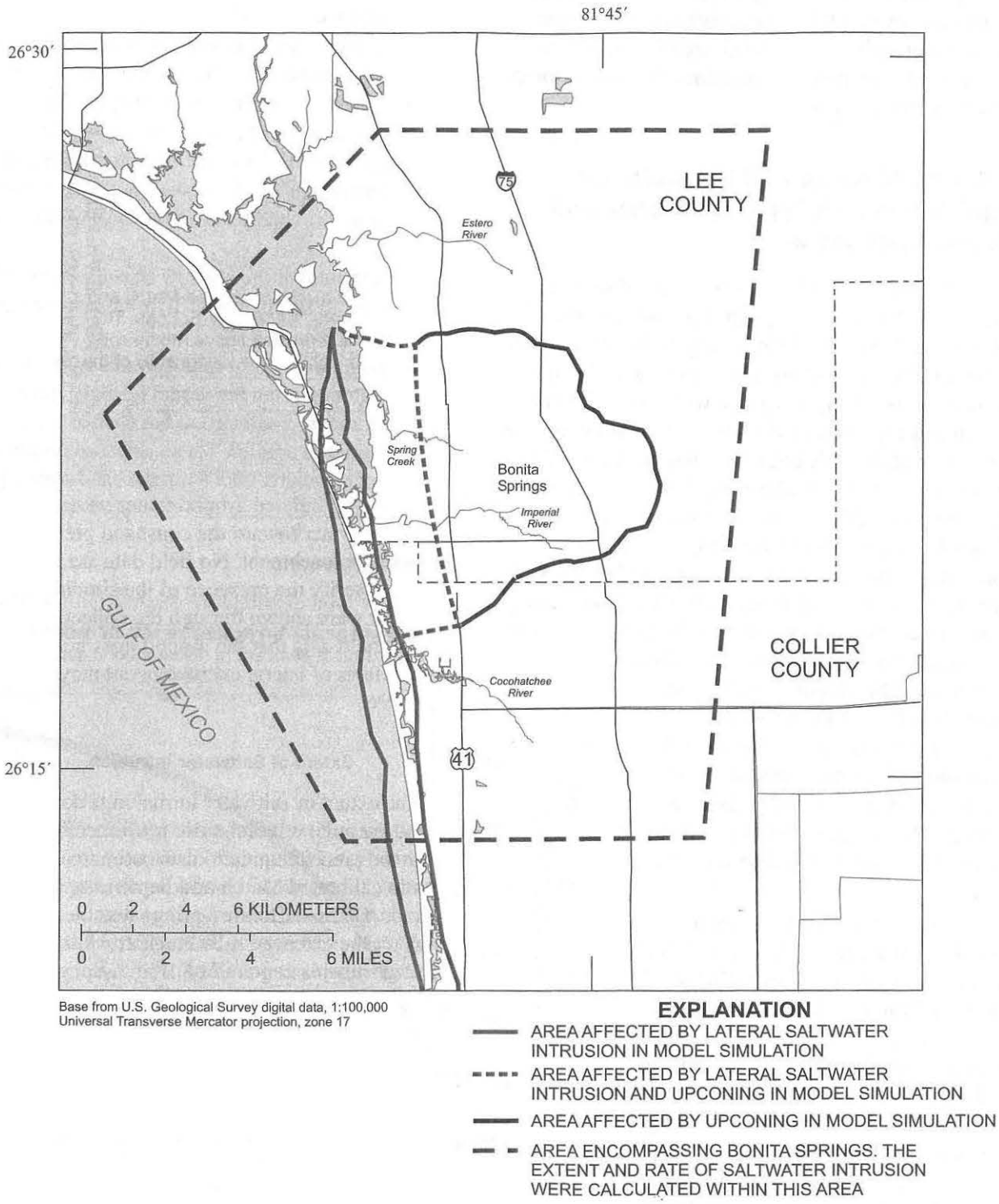


Figure 33. Simulated potential extent of saltwater intrusion in the lower Tamiami aquifer from the baseline scenario near Bonita Springs.

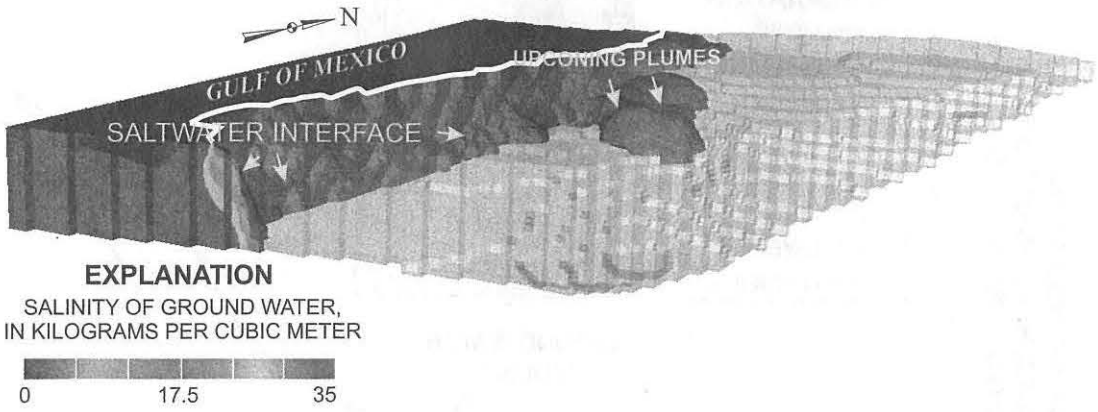


Figure 34. The saltwater interface and upconing plumes near equilibrium with calibrated March and September 1996 conditions in the water-table and lower Tamiami aquifers near Bonita Springs. The upconing plumes are directly beneath Bonita Springs. All shaded areas represent active model cells. Blue and tan cells are equivalent in salinity; the tan shading is used to highlight the topography of the base of the lower Tamiami aquifer.

established by identifying the saltwater intrusion mechanism that affected the largest inland area. A plume of higher salinity ground water (encompassing about 100 km^2 in area) developed in the lower Tamiami aquifer near Bonita Springs after 600 years of transport with calibrated March and September 1996 conditions. By animating model results, it was determined that this plume of higher salinity ground water developed from upconing of ground water in the underlying sandstone aquifer.

The baseline scenario suggests that lateral encroachment is the second most predominant mechanism of saltwater intrusion in the lower Tamiami aquifer near Bonita Springs (figs. 33 and 34). The saltwater interface in the lower Tamiami aquifer near Bonita Springs moved about 1.5 km inland from its predevelopment position after 600 years of transport with calibrated March and September 1996 conditions. As a result, the rate of lateral encroachment averaged about 2.5 m/yr, which is the total distance that the saltwater interface moved (1.5 km) divided by the time length of the baseline scenario (600 years). Additionally, the baseline scenario suggests that lateral encroachment into the potentiometric depression (fig. 22) of the lower Tamiami aquifer was hindered by the presence of a ground-water mound located between the saltwater interface and the potentiometric depression (fig. 35). This simulated ground-water mound seems to force freshwater toward the coast and prevents further lateral encroachment. No field data are available, however, to verify the presence of the simulated mound. If it were shown through the collection of additional field data that the mound does not exist, then the effects of lateral encroachment may be much more severe.

Extent of Saltwater Intrusion

The extent of saltwater intrusion is defined herein as the areal or volumetric movement of saltwater from the predevelopment distribution to equilibrium with calibrated March and September 1996 conditions. Because Bonita Springs was the main area of concern, the extent of saltwater intrusion was computed for a subarea centered on Bonita Springs (fig. 33). The baseline scenario suggests that the areal extent of saltwater intrusion at the base of the lower Tamiami aquifer is about 100 km^2, and the volumetric extent of saltwater intrusion is about 70,000 hectare-meters (fig. 34). The volumetric extent of saltwater intrusion was computed using the same subarea, vertically extended only through the active cells representing the lower Tamiami aquifer. Within this volume, the extent of saltwater intrusion was computed by: (1) summing the volume of cells in the lower Tamiami

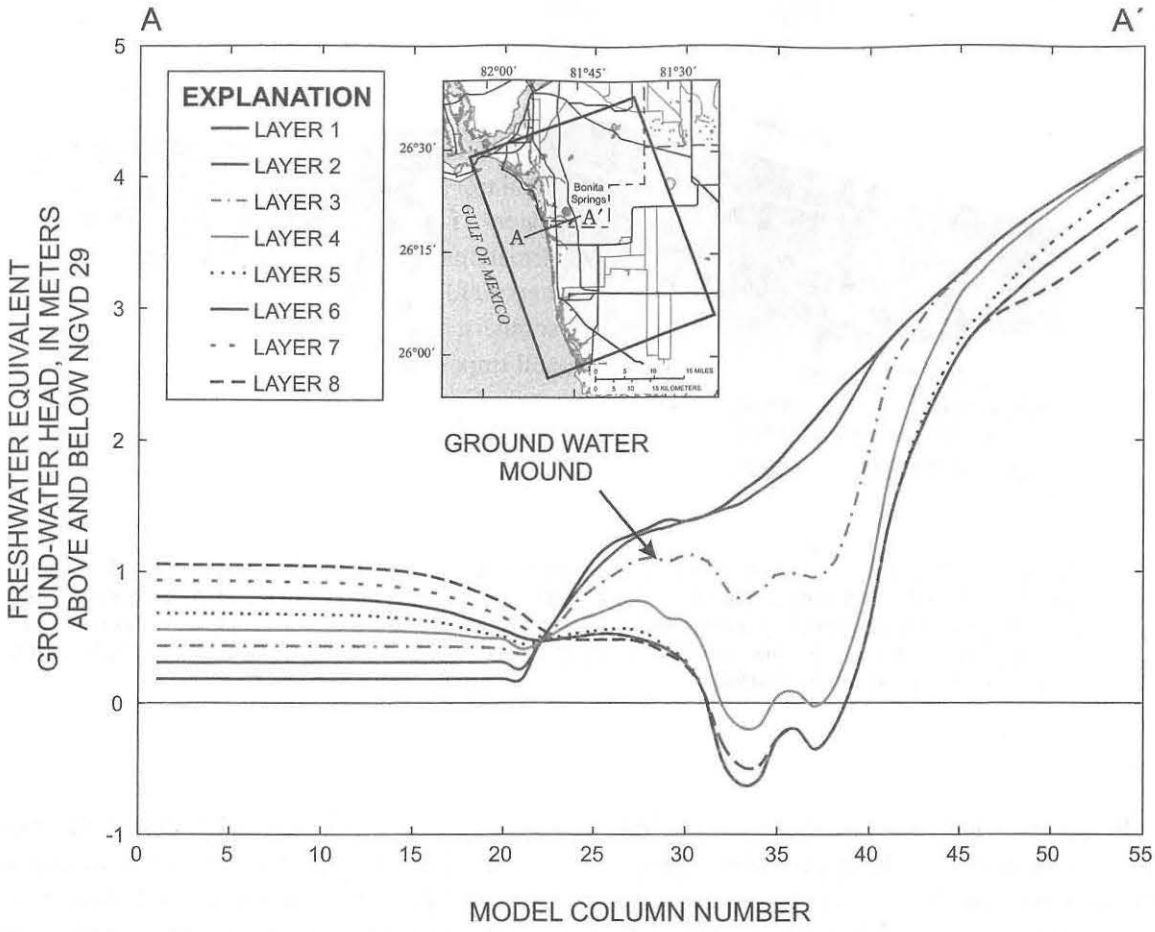


Figure 35. Cross section A-A' along row 40 of the model grid showing a mound of ground water between the cones of depression in the lower Tamiami aquifer and the saltwater interface.

aquifer with a salinity value less than the potable limit (a chloride concentration of about 250 mg/L) in the predevelopment distribution of saltwater, (2) summing the volume of cells in the lower Tamiami aquifer with salinity values less than the potable limit in the baseline scenario, and (3) subtracting the two volumes to isolate a volumetric extent of saltwater intrusion.

Areas affected by saltwater intrusion in the baseline scenario (fig. 33) coincide with areas that seem to be affected by saltwater intrusion as indicated in isochlor maps created by Schmerge (2001) and Knapp and others (1986) (fig. 16). There are discrepancies, however, between simulated salinities and salinities measured at the same location in the field. Possible causes of these discrepancies include that: (1) dispersive solute transport was not performed in the baseline scenario, and (2) the model was run for 600 years with 1996 conditions, so the results cannot be directly compared.

Sensitivity Analyses

The two goals of sensitivity analysis were to: (1) determine how uncertainty in the baseline scenario parameters and boundary conditions may affect solution results, and (2) determine which parameters and boundary conditions in the baseline scenario are most important to solution results. The phrase "important to solution results" is used rather than "influential on solution results" because *influence* has a specific statistical meaning related more to the occurrence and leverage characteristics of the observations used

during calibration. Solution results of primary interest for this study include mechanisms of saltwater intrusion and the potential extent of saltwater intrusion. Thus, sensitivity analyses were performed for both of these primary objectives. If the primary objective could be easily quantified, the two goals of sensitivity analyses (as stated above) were more completely accomplished. For example, the extent of saltwater intrusion was relatively easy to quantify in three dimensions; therefore, parameter values and parameter uncertainties most important to this primary objective were more easily determined.

Mechanisms of Saltwater Intrusion

The sensitivity analyses, described in this section, were used to help identify mechanisms of saltwater intrusion into the lower Tamiami aquifer near Bonita Springs. Identifying predominant mechanisms of saltwater intrusion was a difficult objective to quantify; therefore, sensitivity analysis scenarios were designed instead of using quantitative prediction-scaled sensitivities (PSS) as done by Poeter and Hill (1998). Two sensitivity analysis scenarios were designed to evaluate potential mechanisms of saltwater intrusion without changing simulated heads and flows from their calibrated values. It is important to maintain simulated heads and flows near observed values during sensitivity analyses so the model still resembles the system being studied (Poeter, 2001).

Sensitivity scenario 1 was designed to test the potential for downward leakage of saltwater from a tidal canal or river. This scenario was conducted by modifying the river boundary conditions in the baseline scenario. Unlike the baseline scenario, river cells (pl. 2) in sensitivity scenario 1 were assigned a salinity value of 35 kg/m^3 in an area about 8 to 16 km inland from the Gulf of Mexico along Spring Creek and the Estero, Imperial, and Cocohatchee Rivers (fig. 1). The MAE of water-level observations was 0.73 m using this modification to river-cell boundary conditions, which is the same as the MAE of water-level observations without this modification to river-cell boundary conditions. This suggests the modification did not substantially change heads from their calibrated values. Additionally, simulated baseflow was not substantially different from its calibrated value.

After 600 years of advective solute transport with the river modification noted above, the distribution of saltwater in the lower Tamiami aquifer is identical to the distribution of saltwater in the lower Tamiami aquifer in the baseline scenario (fig. 36). Ground-water flow vectors in sensitivity scenario 1 suggest baseflow from the aquifer to the river prevents salt in the river cells from leaking downward into the water-table aquifer and, subsequently, into the lower Tamiami aquifer. Field reconnaissance along the headwaters of the Imperial River during July 2000 confirmed the presence of baseflow from the aquifer to the Imperial River. Gaging stations on the northern and southern branches of the Estero River, Spring Creek, and Imperial River record flow during the dry season, suggesting ground water flows from the water-table aquifer to these rivers or creeks even in times of drought.

Sensitivity scenario 2 was designed to test a leaky artesian well as a mechanism of saltwater intrusion in the lower Tamiami aquifer near Bonita Springs. This scenario was conducted by modifying a general-head boundary condition at the base of the lower Tamiami aquifer in one model cell (layer 7, row 38, column 28). This single general-head boundary cell was modified to represent a hypothetical leaky artesian ground-water well with connection to the lower Hawthorn producing zone (fig. 3). The external head for the general-head boundary was set to the average of water levels measured in well L-2310 (fig. 36) (Prinos and others, 1996). This well has casing that is open to the lower Hawthorn producing zone. During March and September 1996, average water levels in well L-2310 were adjusted for freshwater equivalence using a salinity value of 1.3 kg/m^3, which is similar to salinity values measured in the lower Hawthorn producing zone by Reese (2000). The conductance term for the general-head boundary was computed using the area of a 0.1-m diameter well and a hydraulic conductivity of 1 x 10^6 m/d. The high value of hydraulic conductivity is considered large enough to transmit water (like a leaky well would transmit) from the lower Hawthorn producing zone to the base of the lower Tamiami aquifer. The salinity of the general-head boundary, representing the lower Hawthorn producing zone locally, was set to the salinity value used to adjust average measured water levels for freshwater equivalence (1.3 kg/m^3). The MAE of water-level observations was 0.71 m using this modification to represent a leaky well, which was slightly less than the MAE to water-level observations without this modification.

The distribution of saltwater at the base of the lower Tamiami aquifer, after 600 years of advective solute transport using the general-head boundary mod-

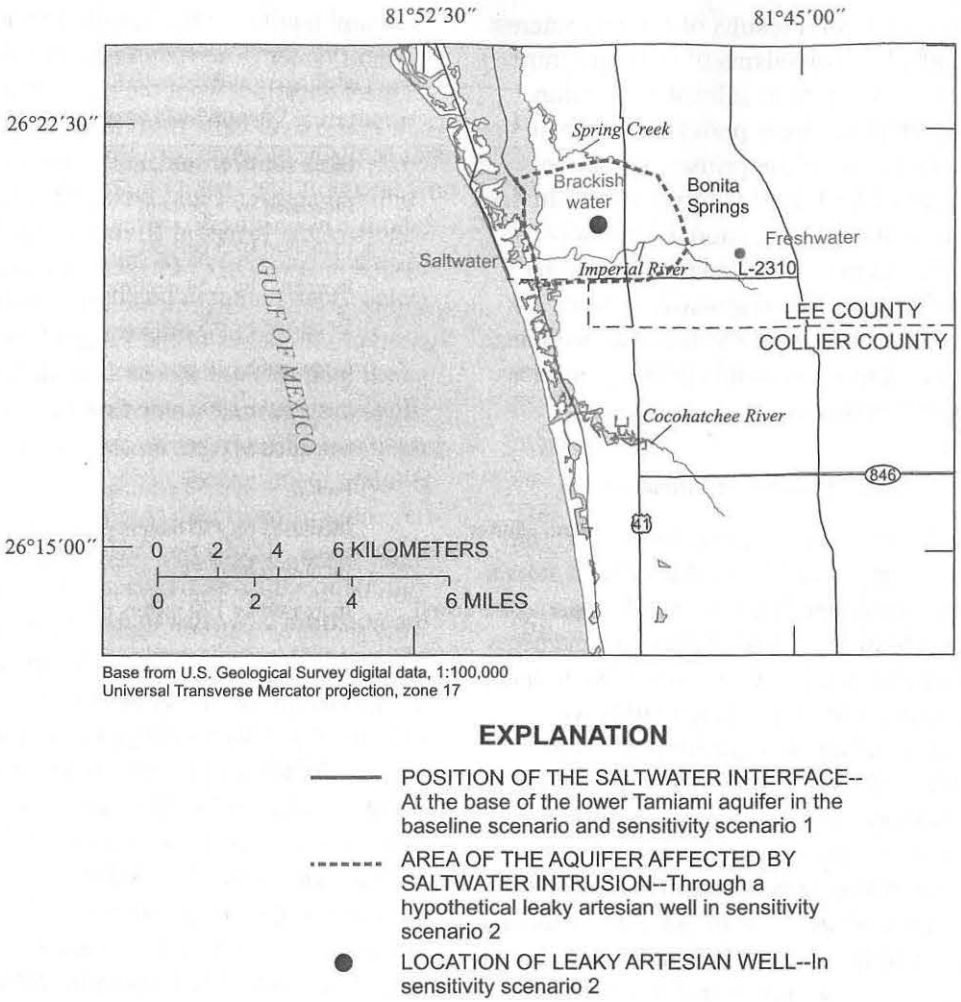


Figure 36. Distribution of saltwater at the base of the lower Tamiami aquifer at the end of the baseline scenario, and two sensitivity analysis scenarios.

ification noted above, is quite different than the distribution of saltwater at the base of the lower Tamiami producing zone in the baseline scenario (fig. 36). The different distribution of salinity suggests leaky wells with connection to the lower Hawthorn producing zone could transport large amounts of saltwater into areas of the lower Tamiami aquifer previously occupied by fresher ground water. These results probably have a physical basis because leaky artesian wells have often been identified as sources of saltwater intrusion in shallow aquifers in southwestern Florida (Burns, 1983; Schmerge, 2001).

Extent of Saltwater Intrusion

The sensitivity analyses, described in this section, were used to help identify the parameters and parameter uncertainties most important to estimating the extent of saltwater intrusion in the lower Tamiami aquifer near Bonita Springs (table 7). Estimating the extent of saltwater intrusion was an objective relatively easy to quantify; therefore, quantitative PSS (Hill, 1998) were computed instead of using sensitivity analysis scenarios. PSS allow parameters to be ranked by relative importance. Furthermore, the contribution of uncertainty in a given input parameter to the overall uncertainty in a model increases as sensitivity coefficients increase (Zheng and Bennett, 2002). As discussed, these sensitivity coefficients are analogous to the PSS that are computed and described herein. Thus, the main contributors of uncertainty to estimating the extent of saltwater intrusion in the lower Tamiami aquifer may be identified by the PSS presented herein.

Table 7. Changes made to baseline scenario parameters for a sensitivity analysis of the extent of saltwater intrusion in the lower Tamiami aquifer near Bonita Springs

Parameter	Change from baseline scenario
Sea level	Increased by 5 percent
Elevation of general-head boundary	Increased by 5 percent
River bottoms	Increased by 5 percent
Runoff for March 1996	Increased by 2.54 centimeters
Potentiometric surface of the sandstone aquifer	Increased by 0.5 meters
Ground-water pumpage	Increased by 10 percent
Horizontal hydraulic conductivity of water-table aquifer	Increased by 700 meters per day
Vertical hydraulic conductivity of Tamiami confining beds	Increased by 0.005 meter per day
Runoff September 1996	Increased by 2.54 centimeters
Horizontal hydraulic conductivity, zone 1, lower Tamiami aquifer	Increased by 130 meters per day
Salinity in sandstone aquifer	Increased by 0.3 kilogram per cubic meter
Horizontal hydraulic conductivity, zone 2, lower Tamiami aquifer (coral reef facies)	Increased by 170 meters per day
Vertical hydraulic conductivity of upper Hawthorn confining unit	Increased by 0.006 meter per day
Horizontal hydraulic conductivity of sandstone aquifer	Increased by 80 meters per day
River and canal stages	Increased both by 0.05 meter per day
River salinity	Increased by 0.3 kilogram per cubic meter
Pan evaporation multiplier for March 1996	Increased by 5 percent
Pan evaporation multiplier for September 1996	Increased by 5 percent
General-head boundary conductance	Increased by 100 percent
River conductance	Increased by 100 percent
Effective porosity	Decreased by 20 percent

The PSS were calculated using the volumetric estimate rather than the areal estimate of the extent of saltwater intrusion in the baseline scenario. The volumetric estimate is more representative of the extent of saltwater intrusion that would be observed in the real ground-water flow system near Bonita Springs (saltwater moves in three dimensions). The PSS were computed as:

$$PSS = (\Delta PD/\Delta B)(B/100)(100/PD), \qquad (16)$$

where ΔPD is the change in the volumetric extent of saltwater intrusion from the baseline scenario, ΔB is the perturbation of the parameter; B is the parameter value in the baseline scenario; and PD is the volumetric extent of saltwater intrusion in the baseline scenario. The resulting statistic is the ratio of the fractional change in the volumetric extent of saltwater intrusion after 600 years of transport to the fractional change in the parameter value.

Preliminary attempts to save time by shortening the time length of the baseline scenario (600 years) and, thus, the time length of PSS runs, resulted in zero sensitivity for many parameters because the change in the volumetric extent of saltwater intrusion (ΔPD) remained the same as the volumetric extent of saltwater intrusion in the baseline scenario (PD). Additionally, zero sensitivity was computed when parameter perturbations (ΔB) were too small. In theory, PSS should approach an exact value as the size of parameter perturbations (ΔB) decrease. However, Poeter and Hill (1998) explain that small parameter perturbations (ΔB) could result in zero sensitivity because, for instance, the volumetric extent of saltwater intrusion under small parameter perturbations (ΔB) could remain the same as the volumetric extent of saltwater

intrusion in the baseline scenario (*PD*) within the accuracy of the model output. Under this circumstance, ΔPD in equation 16 would be equal to zero, resulting in zero sensitivity. Conversely, parameter perturbations (ΔB) that are too large can result in inaccurate PSS because simulated heads and flows may no longer be near observed values, resulting in a model that no longer resembles the system being studied. Parameter perturbations listed in table 7 were determined based on this information.

Because the equations used to compute the extent of saltwater intrusion may be nonlinear with respect to some parameter values, the PSS can change with different perturbations in the parameter value (ΔB) (table 7). This change is described in more general terms by Zheng and Bennett (2002). Based on this description, it is also expected that if the equations used to estimate the extent of saltwater intrusion are linear with respect to a parameter value (B), then the different perturbations in the parameter value (ΔB) will result in the same PSS.

Apparently, runoff, pan evaporation multipliers, ground-water pumpage, sea level and salinity of the Gulf of Mexico, and the potentiometric surface of the sandstone aquifer (when ranked by PSS) are most important for estimating the extent of saltwater intrusion near Bonita Springs (fig. 37). Future efforts at estimating the extent of saltwater intrusion in this location would likely benefit from improved representation of these stresses and boundary conditions. For simplicity of reporting and communicating results, the sensitivity of evapotranspiration parameters and runoff can be grouped into net recharge, although it is notable that dry-season sensitivities for these two processes are higher than wet-season sensitivities (fig. 37). When trying to estimate the extent of saltwater intrusion in the lower Tamiami aquifer near Bonita Springs, determination of net recharge during the dry season apparently is more important than during the wet season. This may be because the dry season generally comprises more days of a total year than the wet season.

The CSS that were computed during calibration (fig. 27) were compared with the PSS that were computed during sensitivity analysis of the extent of saltwater intrusion at equilibrium in the lower Tamiami aquifer near Bonita Springs (fig. 37). The CSS of evapotranspiration parameters and runoff can be grouped together to emphasize that observed conditions near Bonita Springs provided the most information for estimating net recharge. Additionally,

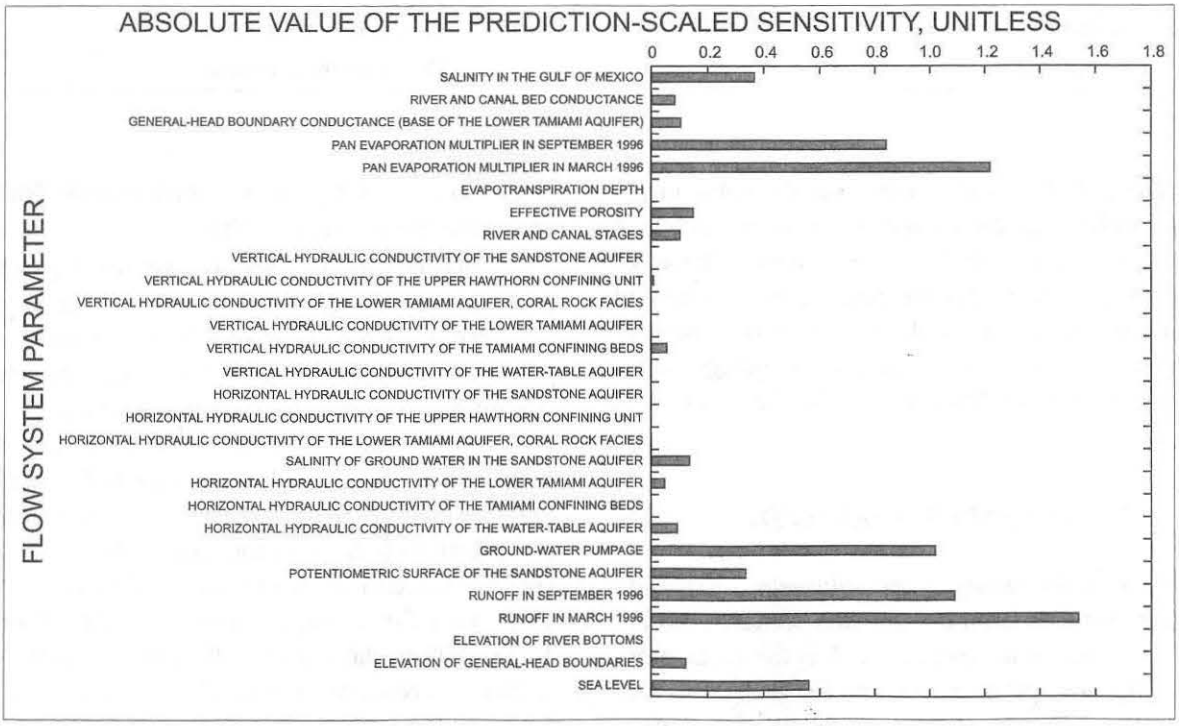


Figure 37. Sensitivity analysis of the extent of saltwater intrusion. Parameters with no visible bar have very small or zero sensitivity.

the PSS of evapotranspiration parameters and runoff (fig. 37) can be grouped together to emphasize net recharge as the most important parameter for estimating the extent of saltwater intrusion in the lower Tamiami aquifer near Bonita Springs. The fact that observed conditions provided the most information for estimating net recharge (the parameter most important for estimating the extent of saltwater intrusion in the lower Tamiami aquifer near Bonita Springs) is encouraging and supports the idea that calibrated ground-water flow models can adequately simulate saltwater movement.

The next most important parameter for estimating the extent of saltwater intrusion in the lower Tamiami aquifer near Bonita Springs is ground-water pumpage, as evidenced by the PSS (fig. 37). Water level and flow observations used while calibrating the model provided relatively little information for estimating unmonitored ground-water pumpage rates as evidenced by the CSS (fig. 27), and the width of the 95-percent confidence intervals on estimates of unmonitored ground-water pumpage rates (table 5). Future efforts to simulate saltwater movement would benefit by improving the representation and estimates of ground-water pumpage, because this parameter was second in relative importance to estimating the extent of saltwater intrusion, but was not precisely estimated with UCODE.

Model Limitations

The model results and interpretations described in this report are limited by: (1) assumptions inherent to MODFLOW-88 and SEAWAT that may or may not be satisfied; (2) difficulty in characterizing small-scale heterogeneity that may greatly influence regional ground-water flow and saltwater movement; (3) the modeling approach; and (4) the inability to quantitatively assess uncertainty in a rigorous fashion for the modeling objectives. The primary objectives were to identify the predominant mechanisms of saltwater intrusion and to estimate the extent of saltwater intrusion in the lower Tamiami aquifer near Bonita Springs.

The partial differential equations approximated by MODFLOW-88 and SEAWAT are based on many assumptions. Those assumptions relevant to simulating saltwater intrusion in the lower Tamiami aquifer near Bonita Springs are that: (1) ground water fully saturates the porous media in areas of ground-water flow, (2) ground-water flow is described by Darcy's law or a variable-density form of Darcy's law, (3) the fluid is incompressible, (4) the standard expression for specific storage in a confined aquifer is applicable, (5) isothermal conditions prevail, (7) fluid density is a linear function of ground-water salinity, and (8) the coordinate system is aligned with the principal axis of the permeability tensor so that this tensor is diagonal for anisotropic media. The natural system probably violates some of these assumptions, thus the relevance of model results and interpretations to the natural system are limited by the degree to which individual assumptions are violated.

The difficulty in characterizing small-scale heterogeneity limits model results, because this heterogeneity may greatly influence regional ground-water flow and saltwater movement in the study area. Complete and accurate characterization of heterogeneity in the lower Tamiami aquifer, including subsurface structural complexity, variations in hydraulic properties, and variations in stresses at multiple scales, was not attainable even with the numerous studies documented over the years. Thus, heterogeneity at multiple scales was averaged, interpolated, or zoned into finite-difference approximations that neglect small-scale particularities, which may be important in the true ground-water flow system in the lower Tamiami aquifer near Bonita Springs.

Clearly, the influence of heterogeneity in porosity at any one particular scale on movement of saltwater is not understood. Effective porosity was assigned a uniform value of 30 percent (Reese and Cunningham, 2000) in the baseline scenario. However, ground-water tracer tests suggest fractures and/or high permeability zones can give effective porosities of 2 to 4 percent (Langevin and others, 1998). Furthermore, some researchers have suggested decimeter-scale heterogeneities and preferential flow paths have the dominant effect on solute transport at the plume scale, with 15 percent of the aquifer involved in advective transport while 85 percent of the aquifer serves as a reservoir for essentially immobile solute (Zheng and Gorelick, 2001). Collectively, these investigations highlight the difficulty in characterizing small-scale heterogeneity and suggest the likelihood of a "dual porosity" system. Further research into this limitation would be useful.

Several assumptions and estimations were employed in the modeling approach that could limit the reliability of results. These include, but are not limited to: (1) the steady-state assumption, (2) estimating

stresses rather than hydraulic conductivities during model calibration, (3) the 7 to 5 ratio of dry- to wet-season months in a typical southwestern Florida water year, (4) neglecting the effects of dispersion on simulations of saltwater movement, and (5) initial conditions for simulating the movement of saltwater at equilibrium.

Steady-state flow occurs when at any point in the flow field, the magnitude and direction of the flow velocity are constant with time (Freeze and Cherry, 1979). Because longer term average values are being computed, a steady-state assumption was employed while computing the predevelopment distribution of saltwater, calibrating to March and September 1996 conditions, and moving saltwater at equilibrium. The steady-state assumption is limiting because transient particularities that could be important to saltwater movement in the lower Tamiami aquifer near Bonita Springs may not be considered. Additionally, using the steady-state assumption to calibrate to March and September 1996 conditions is limiting because it is possible the regional ground-water flow system is never at true steady state as defined by Freeze and Cherry (1979).

Most ground-water models are calibrated by adjusting hydraulic conductivity parameters until simulated results match observed field conditions. The model documented here was calibrated by estimating unmonitored ground-water pumpage and pan evaporation multipliers with UCODE. Unmonitored ground-water pumpage was estimated because accurately simulated water levels in the lower Tamiami aquifer beneath Bonita Springs was most important for accurately simulating saltwater movement—a primary objective of this study. Hydraulic conductivity was correlated with unmonitored ground-water pumpage and, therefore, could not be uniquely estimated together with UCODE. This was unfortunate because the model was more sensitive to hydraulic conductivity parameters, such as canal conductances and the vertical hydraulic conductivity of the Tamiami confining beds, than to pan evaporation multipliers. A better model fit may have resulted by estimating hydraulic conductivity parameters. Additional observations, particularly flow observations, could help obliterate the correlation between unknown pumpage and hydraulic conductivity parameters. Future modeling efforts would likely benefit from using additional flow observations while calibrating.

Previous studies have used a 7 to 5 ratio to represent the number of dry-season months to the number of wet-season months during a typical water year in southwestern Florida. The 7 to 5 ratio is potentially limiting because a plot of average monthly rainfall from 69 rainfall stations in southwestern Florida suggests the possibility that an 8 to 4 ratio may be more appropriate (fig. 38). The 7 to 5 ratio was used in this study to estimate annual average unmonitored ground-water pumpage rates, and also was used in the baseline scenario and during sensitivity of the baseline

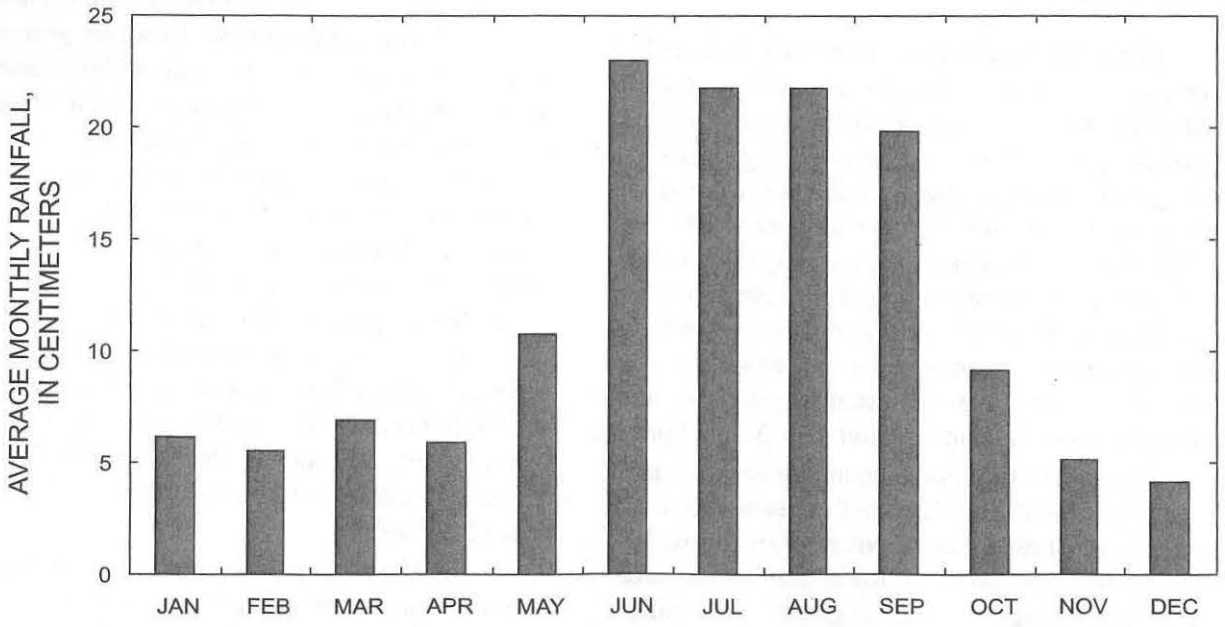


Figure 38. Average monthly rainfall from selected rainfall stations in southwestern Florida, 1909-99.

scenario. Using an 8 to 4 ratio would likely have little effect on identifying predominant mechanisms of saltwater intrusion and have little effect on sensitivity analysis of the baseline scenario. It is probable, however, that using an 8 to 4 ratio would increase estimates of unmonitored ground-water pumpage and increase estimates of the extent of saltwater intrusion.

Neglecting the effects of dispersion on simulations of saltwater movement limits the relevance of model results to the real nature of ground-water flow and saltwater movement in the study area. This is a limitation because: (1) the real nature of saltwater movement involves mixing, and (2) a dispersive solute-transport simulation suggests dispersion will reduce the extent of saltwater intrusion in the lower Tamiami aquifer near Bonita Springs.

In a hypothetical dispersive solute-transport simulation, dispersivity in three dimensions was estimated using the relation defined in Gelhar and others (1992) and Zheng and Bennett (1995). Longitudinal dispersivity was set to 60 m, or one-tenth the horizontal model cell dimension (Gelhar and others, 1992). Transverse and vertical dispersivities were set to 6 m, or one-tenth the longitudinal dispersivity (Zheng and Bennett, 1995). Six hundred years of dispersive and advective solute transport was simulated using the same modeling approach employed in the baseline scenario. In general, dispersion reduced the extent of saltwater intrusion. These results are consistent with historical studies (Cooper, 1964; Glover, 1964; Henry, 1964; Kohout, 1964) of the effects of dispersion on the saltwater interface, which suggest that including the effects of dispersion moves the interface seaward.

Dispersion was not simulated while solving for the predevelopment distribution of saltwater, during the baseline scenario, and during sensitivity analysis of the baseline scenario due to the length of computer run times and uncertainty in estimates of dispersivity. Field estimates of dispersivity in the lower Tamiami aquifer near Bonita Springs could be useful to constrain the potential effects of dispersion on saltwater movement. If computer run times are substantially diminished, and if field data can be obtained to set reasonable values of dispersivity at the scale of the model grid, then detailed three-dimensional studies of the position and behavior of the "toe" of the saltwater interface in the lower Tamiami aquifer could be more conclusively accomplished.

The lack of initial conditions is a well documented limitation for studies of solute transport in ground water. Although maps of salinity distribution are available (Knapp and others, 1986; Schmerge, 2001), these maps are based on field data collected over time. Only sparse amounts of salinity data are available to instantaneously capture the distribution of saltwater at any given time. If salinity is known only at a few points within the region to be modeled, and assumed initial values are assigned in between, the unrealistic flows probably will be calculated by the variable-density ground-water flow simulator (Voss, 1999). A practical solution to this problem was found by attempting to solve for initial conditions using predevelopment stresses and boundary conditions assumed or extrapolated from contemporary data. This approach has several advantages, as outlined in the modeling approach section of the report, but still is limiting because more accurate solutions to the primary objectives of this study could be obtained if the true distribution of freshwater equivalent head and ground-water salinity were known. Airborne electromagnetic survey techniques (Fitterman and Deszcz-Pan, 1998), if successfully applied to the water-table and lower Tamiami aquifers in southwestern Florida, could represent another useful solution to the lack of data on initial conditions for saltwater intrusion simulations near Bonita Springs.

Parameter and conceptual uncertainty limit the applicability of the modeling results presented here. When parameters are changed within reasonable ranges, or combinations of parameters are changed within reasonable ranges, mechanisms of saltwater intrusion become more or less predominant, saltwater moves to different extents, and saltwater moves at different rates. This problem is exacerbated by conceptual uncertainty because the ground-water flow system could be represented equally well by many different boundary conditions, regional distributions of aquifer properties, and initial conditions. The effects of this uncertainty on the primary study objectives were indirectly addressed through sensitivity analyses. Linear 95-percent confidence intervals, computed for each primary modeling objective, would probably be a practical and useful type of analysis to directly address parameter uncertainty. The effects of parameter and conceptual uncertainty could be directly addressed using a composite range of confidence intervals for a reasonable set of conceptual models (Poeter, 2001). However, these analyses were considered beyond the scope of this investigation.

SUMMARY

Saltwater intrusion is a concern near Bonita Springs in southwestern Florida where the average annual potentiometric surface in some areas of the lower Tamiami aquifer is below sea level. Field data were analyzed, and model simulations were performed to: (1) spatially quantify modern and seasonal stresses, (2) help identify potential mechanisms of saltwater intrusion, (3) and estimate the potential extent of saltwater intrusion in the lower Tamiami aquifer near Bonita Springs.

MODFLOW and the inverse modeling routine UCODE were used to spatially quantify modern and seasonal stresses in 1996 by calibrating a constant-density ground-water flow model. The model was calibrated by assuming hydraulic conductivity parameters were accurate and by estimating unmonitored ground-water pumpage and pan-evaporation multipliers with UCODE. Additionally, uncertainty in estimates of these parameters was quantified through 95-percent confidence intervals. These confidence intervals indicate more uncertainty or less reliability in the estimates of unmonitored ground-water pumpage than estimates of pan-evaporation multipliers due to the nature and distribution of observations used during calibration. Comparison of simulated water levels, streamflows, and net recharge with field data demonstrate the adequacy of the simulated water budget.

Net recharge and unmonitored ground-water pumpage are two components of the water budget of interest to water managers. Using modeling results for 1996, average net recharge to the water-table aquifer was estimated to range between 0 and 38 cm/yr, and unmonitored ground-water pumpage from the lower Tamiami aquifer was estimated to be 52,000 m^3/d. Net recharge less than zero occurred over less than 5 percent of the active model domain due to the close proximity of the water table to land surface. The average estimated rate of unmonitored ground-water pumpage in 1996 from the lower Tamiami aquifer (52,000 m^3/d) was almost as much as the monitored ground-water pumpage in 1996 from the water-table and lower Tamiami aquifers (59,000 m^3/d) in the active model domain.

Potential mechanisms of saltwater intrusion into the lower Tamiami aquifer near Bonita Springs include: (1) lateral inland movement of the freshwater-saltwater interface from the southwestern coast of Florida; (2) upward leakage from deeper, saline water-bearing zones through natural upwelling and upconing, both of which could occur as diffuse upward flow through semiconfining layers, conduit flow through karst features, or pipe flow through leaky artesian wells; (3) downward leakage of saltwater from surface-water channels; and (4) movement of unflushed pockets of relict seawater. Of the many potential mechanisms, field data and variable-density ground-water flow simulations suggest upconing is probably of utmost concern, and lateral encroachment is probably of second most concern in the lower Tamiami aquifer beneath Bonita Springs. This interpretation is uncertain, however, because the predominance of leaky wells with connection to deeper, more saline, and more pressurized aquifers was difficult to establish.

The potential extent of saltwater intrusion was estimated using a variable-density ground-water flow simulator and 1996 seasonal stresses. The potential extent of saltwater intrusion in the lower Tamiami aquifer beneath Bonita Springs is about 100 km^2 and 70,000 hectare-meters. The volumetric extent of saltwater intrusion was most sensitive to changes in recharge, ground-water pumpage, sea level, salinity of the Gulf of Mexico, and the potentiometric surface of the sandstone aquifer, respectively, as indicated by prediction-scaled sensitivities. Future efforts at estimating the extent of saltwater intrusion in this area would likely benefit from improved representation of these hydrologic stresses and boundary conditions.

Composite-scaled sensitivities that were computed while calibrating the model were compared with prediction-scaled sensitivities computed for the potential extent of saltwater intrusion predicted by the model. Composite-scaled sensitivities suggested observed conditions provided the most information for estimating net recharge. Prediction-scaled sensitivities suggested net recharge is the most important parameter for estimating the extent of saltwater intrusion in the lower Tamiami aquifer beneath Bonita Springs. This consistency was encouraging and supports the idea that calibrated ground-water flow models can be used to adequately simulate saltwater movement.

SELECTED REFERENCES

Albury, Carl, Langevin, C.D., and Stewart, M.T., 1998, Determining the feasibility for wetland rehydration: Simulation of application rates and transport of reclaimed water: Hydrogeology Laboratory, University of South Florida, Tampa, 11 p.

Anderson, M.P., and Woessner, W.W., 1992, Applied groundwater modeling: London, Academic Press, 381 p.

Badon-Ghyben, W., 1888, Nota in verband met de voorgenomen putboring nabij Amsterdam (Notes on the probable results of well drilling near Amsterdam): The Hague, Tijdschrift van het Koninklijk Instituut van Ingenieurs, p. 8-22.

Bear, Jacob, and others 1999, Seawater intrusion in coastal aquifers – concepts, methods, and practices: The Netherlands, Kluwer Academic Publishers, 625 p.

Bennett, W., 1992, Three dimensional finite difference ground-water flow model of western Collier County, Florida: West Palm Beach, South Florida Water Management District Technical Publication 92-04, 358 p.

Boggess, D.H., Missimer, T.M., and O'Donnell, T.H., 1981, Hydrogeologic sections through Lee County and adjacent areas of Hendry and Collier Counties, Florida: U.S. Geological Survey Open-File Report 81-638, 1 sheet.

Bower, R.F., Adams, K.M., and Restrepo, J.I., 1990, Three dimensional finite difference ground-water flow model of Lee County, Florida: West Palm Beach, South Florida Water Management District Technical Publication 90-01, 283 p.

Burns, W.S., 1983, Well plugging applications to the inter-aquifer migration of saline groundwater in Lee County, Florida: West Palm Beach, South Florida Water Management District Technical Publication 83-8, 77 p.

Clark, I.D., and Fritz, Peter, 1997, Environmental isotopes in hydrogeology: Boca Raton, Fla., Lewis Publishers, 328 p.

Cooper, H.H., 1964, Sea water in coastal aquifers: U.S. Geological Survey Water-Supply Paper 1613-C, 84 p.

Edwards, L.E., Weedman, S.D., Simmons, K.B., and others, 1998, Lithostratigraphy, petrostratigraphy, biostratigraphy, and strontium isotope stratigraphy of the surficial aquifer system of western Collier County, Florida: U.S. Geological Survey Open-File Report 98-205, 79 p.

Fernald, E.A., and Purdum, E.D., eds., 1998, Water resources atlas of Florida: Gainesville, University Press of Florida, 312 p.

Fitterman D.V., and Deszcz-Pan, M., 1998, Helicopter EM mapping of saltwater intrusion in Everglades National Park: Florida Exploration Geophysics, v. 29, p. 240-243.

Freeze, A.R., and Cherry, J.A., 1979, Groundwater: Englewood Cliffs, N.J., Prentice Hall, 604 p.

Gee and Jenson, Inc., 1980, Regional water resources study in the Big Cypress Basin: 106 p.

Gelhar L.W., Welty, C., and Rehfeldt, K.R., 1992, A critical review of data on field-scale dispersion in aquifers: Water Resources Research, v. 28, no. 7, p. 1955-1974.

Glover, R.E., 1964, The pattern of freshwater flow in a coastal aquifer in sea water in coastal aquifers: U.S. Geological Survey Water-Supply Paper 1613-C, 84 p.

Guo, Weixing, and Bennett, G.D., 1998, SEAWAT –A computer program for simulations of ground-water flow of variable density: Fort Myers, Fla., Report prepared by Missimer International, Inc., 51 p.

Guo, Weixing, and Langevin, C.D., 2002, User's guide to SEAWAT: A computer program for simulation of three-dimensional variable-density ground-water flow: U.S. Geological Survey Techniques of Water-Resources Investigations, book 6, chap. A7, 77 p.

Henry, H.R., 1964, Interfaces between salt water and fresh water in coastal aquifers in sea water in coastal aquifers: U.S. Geological Survey Water-Supply Paper 1613–C, 84 p.

Herzberg, A., 1901, DieWasserversorgung einiger Nordseeber (The water supply of parts of the North Sea coast in Germany): Z. Gasbeleucht Wasserversorg, 844 p.

Hill, M.C., 1998, Methods and guidelines for effective model calibration: U.S. Geological Survey Water-Resources Investigations Report 98-4005, 90 p.

Hite, L.R., 1997, Aquifer delineation in southwest Florida using time-domain electromagnetics: Dayton, Ohio, MS Thesis, Wright State University, 77 p.

Hsieh, P., and Winston, R.B., 2002, User's guide to model viewer: A program for three dimensional visualization of ground-water model results: U.S. Geological Survey Open-File Report 02-106, 18 p.

Hull, J.E., and Meyer, F.W., 1973, Salinity studies in East Glades agricultural area, southeastern Dade County, Florida: Tallahassee Florida Bureau of Geology Report of Investigations 66, 39 p.

Johnson Engineering, Inc.; Agnoli, Barber and Brundage, Inc.; and Boylan Environmental Consultants, Inc., 1999, South Lee County watershed plan: Report Prepared for the South Florida Water Management District, West Palm Beach,12 chapters and appendix.

Jones, B.F., Vengosh, A., Rosenthal, E., and Yechiele, Y., 1999, Geochemical investigations; *in* Bear, Jacob, and others, eds., Seawater intrusion in coastal aquifers–Concepts, methods, and practices: The Netherlands, Kluwer Academic Publishers, p. 51-71.

Klein, Howard, 1954, Ground-water resources of the Naples area, Collier County, Florida: Tallahassee Florida Geological Survey Report of Investigations 11, 63 p.

Klein, Howard, and Ratzlaff, K.W., 1989, Changes in saltwater intrusion in the Biscayne aquifer, Hialeah-Miami Springs area, Dade County, Florida: U.S. Geological Survey Water-Resources Investigations Report 87-4249, 1 sheet.

Klein, Howard, and Waller, B.G., 1985, Synopsis of saltwater intrusion in Dade County, Florida, through 1984: U.S. Geological Survey Water-Resources Investigations Report 85-4101, 1 sheet.

Knapp, M.S., Burns, W.S., and Sharp, T.S., 1986, Preliminary assessment of the ground-water resources of western Collier County, Florida: West Palm Beach, South Florida Water Management District Technical Publication 86-1, 142 p.

Kohout, F.A., 1964, The flow of fresh water and salt water in the Biscayne aquifer of the Miami area, Florida; *in* Cooper, H.H., and others, eds., Sea water in coastal aquifers: U.S. Geological Survey Water–Supply Paper 1613-C, p. C-12-C-32.

——— 1979, Satellite observations of a geothermal submarine spring off the Florida west coast: Satellite Hydrology: American Water Resources Association, June, p. 570-577.

Konikow, L.F., and Bredehoft, J.D., 1992, Ground-water models cannot be validated: Advances in Water Resources, v. 15, p. 75-83.

Konikow, L.F., and Reilly, T.E., 1999, Seawater intrusion in the United States; *in* Bear, Jacob, and others, eds., Seawater intrusion in coastal aquifers-Concepts, methods and practices: The Netherlands, Kluwer Academic Publishers, p. 463-506.

Krulikas, R.K., and Giese, G.L., 1995, Recharge to the surficial aquifer system in Lee and Hendry Counties, Florida: U.S. Geological Survey Water-Resources Investigations Report 95-0003, 21 p.

Langevin, C.D., 2001, Simulation of ground-water discharge to Biscayne Bay, southeastern Florida: U.S. Geological Survey Water-Resources Investigations Report 00-4251, 127 p.

Langevin, C.D., and Guo, Weixing, 1999, Improvements to SEAWAT, a variable-density modeling code: EOS Transactions, v. 80, no. 46, p. F-373.

Langevin, C.D., Thompson, D., LaRoche, J., and others,1998, Development of a conceptual hydrogeologic model from field and laboratory data, phase II results, North Lakes wetland Hillsborough County, Florida: Hydrogeology Laboratory, Geology Department, University of South Florida, Tampa, 63 p.

Leake, S.A., and Prudic, D.E., 1991, Documentation of a computer program to simulate aquifer-system compaction using the finite-difference ground-water flow model: U.S. Geological Survey Techniques of Water Resources Investigations, book 6, chap. A2, 68 p.

McCoy, H.J., 1962, Ground-water resources of Collier County, Florida: Tallahassee Florida Geological Survey Report of Investigations 31, 79 p.

McDonald, M.G., and Harbaugh, A.W., 1988, A modular three-dimensional finite-difference ground-water flow model: U.S. Geological Survey Techniques of Water Resources Investigations, book 6, chap. A1, 586 p.

Meeder, J.F., 1979, The Pliocene fossil reef of southwest Florida: Miami Geological Society 1979 Field Trip Guidebook, 18 p.

Merritt, M.L., 1996, Assessment of saltwater intrusion in southern coastal Broward County, Florida: U.S. Geological Survey Water-Resources Investigations Report 96-4221, 133 p.

Meyer, F.W., 1989, Hydrogeology, ground-water movement, and subsurface storage in the Floridan aquifer system in southern Florida: U.S. Geological Survey Professional Paper 1403-G, 59 p.

Montgomery, James, M., Consulting Engineers Inc., 1988, Lee County Water Resources Management Project.

Motz, L.H., 1996, Nonsteady-state drawdowns in two coupled aquifers: Journal of Irrigation and Drainage Engineering, v. 122, no. 1, p. 19-23.

National Research Council, 1987, Responding to changes in sea level change: Engineering implications: Washington D.C., National Academy Press, 148 p.

Parker, G.G., Ferguson, G.E., Love, S.K., and others, 1955, Water resources of southeastern Florida: U.S. Geological Survey Water-Supply Paper 1255, 965 p.

Poeter, E.P., 2001, Initial conditions, sensitivities and other reflections on the modeling odyssey; *in* Proceedings of MODFLOW 2001 and other Modeling Odysseys, September 11-14, 2001: Golden, Colo., International Ground-Water Modeling Center (IGWMC), Colorado School of Mines, v. 1, p. 14.

Poeter, E.P., and Hill, M.C., 1997, Inverse models: A necessary next step in ground-water modeling: Ground Water, v. 35, no. 2, p. 250-260.

——— 1998, Documentation of UCODE, a computer code for universal inverse modeling: U.S. Geological Survey Water-Resources Investigations Report 98-4080, 116 p.

Prinos, S.T., Lietz, A.C., and Irvin, Bruce, 2002, Design of a real-time ground-water level monitoring network and portrayal of hydrologic conditions in southern Florida: U.S. Geological Survey Water-Resources Investigations Report 01-4275.

Prinos, S.T., Richards, Tom, and Krulikas, Richard, 1996, Water-resources data – south Florida, Volume 2B, ground water: U.S. Geological Survey Water-Data Report FL-96-2B, 610 p.

Reese, R.S., 2000, Hydrogeology and distribution of salinity in the Floridan aquifer system, southwestern Florida: U.S. Geological Survey Water-Resources Investigations Report 98-4253, 86 p.

Reese, R.S., and Cunningham, K.J., 2000, Hydrogeology of the gray limestone aquifer in southern Florida: U.S. Geological Survey Water-Resources Investigations Report 99-4213, 244 p.

Reilly, T.E., 2001, System and boundary conceptualization in ground-water flow simulation: U.S. Geological Survey Techniques of Water Resources Investigations, book 3, chap. B8, 30 p.

Sacks, L.A., and Tihansky, A.B., 1996, Geochemical and isotopic composition of ground water with emphasis on sources of sulfate in the Upper Floridan aquifer and intermediate aquifer system in southwest Florida: U.S. Geological Survey Water-Resources Investigations Report 96-4146, 55 p.

Sanford, W.E., and others, 1998, Numerical analysis of seawater circulation in carbonate platforms: Part I. Geothermal convection: American Journal of Science, v. 298, no. 12, p. 801-828.

Schmerge, D.L., 2001, Distribution and origin of saline water in the surficial and intermediate aquifer systems in southwestern Florida: U.S Geological Survey Water-Resources Investigations Report 01-4159, 41 p.

Sherwood, C.B., and Klein, Howard, 1963, Saline groundwater in southern Florida: Ground Water, v. 1, no. 2, 6 p.

Shoemaker, W.B., 1998, Geophysical delineation of hydrostratigraphy in the Big Cypress National Preserve, Florida: Tampa MS Thesis, University of South Florida, 119 p.

Sonenshein, R.S., 1997, Delineation and extent of saltwater intrusion in the Biscayne aquifer, eastern Dade County, Florida, 1995: U.S. Geological Survey Water Resources Investigations Report 96-4285, 1 sheet.

Sonenshein, R.S., and Koszalka, E.J., 1996, Trends in water-table altitude (1984-93) and saltwater intrusion (1974-93) in the Biscayne aquifer, Dade County, Florida: U.S. Geological Survey Open-File Report 95-705, 2 sheets.

South Florida Water Management District, 1989, ARC information coverage of south Florida watershed basins: West Palm Beach, originally created by Jim Lane.

——— 1994, The lower west coast water supply plan, appendices: West Palm Beach, South Florida Water Management District Publication, 12 sections.

Stewart, M.T., 1999, Geophysical investigations; *in* Bear, Jacob, and others, eds., Seawater intrusion in coastal aquifers-Concepts, methods and practices: The Netherlands, Kluwer Academic Publishers, p. 9-50.

Stewart, M.T., and Langevin, C.D., 1999, Post audit of a numerical prediction of wellfield drawdown in a semiconfined aquifer system: Ground Water, v. 37, no. 2, p. 245-250.

Stewart, M.T., Lizanec, T., and Layton, M., 1982, Application of DC resistivity surveys to regional hydrogeologic investigation, Collier County, Florida: West Palm Beach, South Florida Water Management District Technical Publication 82-6, 95 p.

Swancar, A., Lee, T.M., and O'Hare, T.M., 2000, Hydrogeologic setting, water budget, and preliminary analysis of ground-water exchange at Lake Starr, a seepage lake in Polk County, Florida: U.S. Geological Survey Water-Resources Investigations Report 00-4030, 72 p.

Tibbals, C.H., 1990, Hydrology of the Floridan aquifer system in east-central Florida: U.S. Geological Survey Professional Paper 1403-E, 98 p.

Virogroup, Inc., 1993, Lee County regional water supply master plan, ground-water hydrology and computer impact modeling of potential future withdrawals: Report prepared for the South Florida Water Management District, West Palm Beach, 174 p.

Voss, C.I., 1999, USGS SUTRA code –History, practical use, and application in Hawaii, *in* Bear, Jacob, and others, eds., Seawater intrusion in coastal aquifers–Concepts, methods and practices: The Netherlands, Kluwer Academic Publishers, p. 249-313.

Wedderburn, L.A., Knapp, M.S., Waltz, D.P., and Burns, W.S., 1982, Hydrogeologic reconnaissance of Lee County, Florida, West Palm Beach, South Florida Water Management District Technical Publication 82-1, 192 p.

Weedman, S.D., 1999, Lithostratigraphy, geophysics, biostratigraphy, and strontium isotope stratigraphy of the surficial aquifer system of eastern Collier County and northern Monroe County, Florida: U.S. Geological Survey Open-File Report 99-432, 125 p.

Weedman, S.D., Paillet, F.L., Means, G.H., and Scott, T.M., 1997, Lithology and geophysics of the surficial aquifer system in western Collier County, Florida: U.S. Geological Survey Open-File Report 97-436, 167 p.

Zheng, Chunmiao, and Bennett, G.D., 1995, Applied contaminant transport modeling: New York, N.Y., Van Nostrand Reinhold, A Division of International Thomson Publishing, Inc., 440 p.

——— 2002, Applied contaminant transport modeling (2d ed.): New York, John Wiley and Sons, Inc., 621 p.

Zheng, Chunmiao, and Gorelick, S.M., 2001, Analysis of solute transport and remediation in flow fields influenced by decimeter-scale preferential flow path, *in* Proceedings of MODFLOW 2001 and other Modeling Odysseys, September 11-14, 2001, Golden, Colo., International Ground-water Modeling Center (IGWMC), Colorado School of Mines, v. 1, p. 11.

Zheng, Chunmiao, and Wang, P.P., 1998, MT3Dms-A modular three-dimensional multispecies transport model for simulation of advection, dispersion and chemical reactions of contaminants in ground-water systems: Tuscaloosa, University of Alabama Department of Geology and Mathematics, 7 chapters.

Appendix

Monitoring Stations Used for this Study

[Station type: C, chloride; E, pan-evapotranspiration; R, rainfall; WL, water level. Data source: DBHYDRO, South Florida Water Management District hydrometorologic database; NWIS, U.S. Geological Survey National Water Information System]

Appendix. Monitoring stations used in this study

Station identification	Station type	Latitude	Longitude	Data source
951EXT_R	R	261809	814118	DBHYDRO
ALVA FAR_R	R	264245	813747	DBHYDRO
ASGROW	R	261616	814229	DBHYDRO
BARRON_R	R	255801	812059	DBHYDRO
BAY WEST_R	R	261630	814208	DBHYDRO
BCBNAPLE_R	R	261331	814829	DBHYDRO
BONITA S_R	R	262001	814459	DBHYDRO
C-39	C	254859	812315	NWIS
C-54	WL	261019	805301	NWIS
C-54	C	261019	805301	NWIS
C-54_R	R	261019	805301	DBHYDRO
C-123	C	261004	814757	NWIS
C-130	C	260903	814803	NWIS
C-131	WL	262522	811618	NWIS
C-131	C	262522	811618	NWIS
C-161	C	261024	814706	NWIS
C-175	C	260913	814345	NWIS
C-258	C	262505	812458	NWIS
C-269	C	255701	812744	NWIS
C-296	C	260641	812042	NWIS
C-296_R	R	260641	812042	DBHYDRO
C-298	C	262508	812351	NWIS
C-303	C	261622	814122	NWIS
C-304	C	261636	813612	NWIS
C-308	C	260920	811558	NWIS
C-311	C	255431	812209	NWIS
C-321	C	261436	814724	NWIS
C-363	C	262556	812424	NWIS
C-384	C	261621	814506	NWIS
C-391	WL	261125	814702	NWIS
C-392	WL	261125	814700	NWIS
C-392	C	261125	814700	NWIS
C-409	C	261025	814800	NWIS
C-409A	WL	261025	814800	NWIS
C-409A	C	261025	814800	NWIS
C-424	C	261525	814803	NWIS
C-430	C	261147	814606	NWIS
C-445	C	255135	812305	NWIS
C-446	C	260449	814115	NWIS
C-458	C	261402	814613	NWIS
C-459	C	261404	814706	NWIS
C-460	WL	261406	814654	NWIS
C-460	C	261406	814654	NWIS
C-462	WL	262725	812606	NWIS
C-462	C	262725	812606	NWIS
C-472A	C	260926	814751	NWIS
C-474	C	261115	814822	NWIS
C-474A	C	261115	814822	NWIS
C-489	C	261303	814738	NWIS
C-490	C	261244	814802	NWIS
C-491	C	261118	814800	NWIS
C-492	WL	262229	813618	NWIS
C-492	C	262229	813618	NWIS
C-495	C	255749	811817	NWIS
C-496	WL	260112	812438	NWIS
C-496	C	260112	812438	NWIS
C-503	C	261742	812353	NWIS
C-506A	WL	261234	814801	NWIS
C-506A	C	261234	814801	NWIS
C-515	C	261347	814801	NWIS
C-516	C	261157	814757	NWIS
C-524	C	260949	814832	NWIS
C-525	C	261003	814836	NWIS
C-526	C	261019	814840	NWIS
C-527	C	261049	814847	NWIS
C-528	C	261201	814829	NWIS
C-531	WL	262900	812729	NWIS
C-531	C	262900	812729	NWIS
C-532	C	262900	812729	NWIS
C-575	C	261318	814804	NWIS
C-598	WL	261418	813053	NWIS
C-598	C	261418	813053	NWIS
C-599	C	260631	814113	NWIS
C-600	WL	260550	814418	NWIS
C-600	C	260550	814418	NWIS
C-684	C	261741	812353	NWIS
C-687	C	262555	812837	NWIS
C-688	C	261803	813547	NWIS
C-689	C	261741	812353	NWIS
C-690	WL	260630	813234	NWIS
C-690	C	260630	813234	NWIS
C-948	C	261348	813516	NWIS
C-951	WL	261348	813511	NWIS
C-951	C	261348	813511	NWIS
C-953	WL	261348	813511	NWIS
C-953	C	261348	813511	NWIS
C-955	C	261722	813512	NWIS
C-956	C	261344	813847	NWIS
C-963	C	262122	813554	NWIS
C-965	C	262137	812041	NWIS
C-966	C	262137	812041	NWIS
C-967	C	260541	814305	NWIS
C-968	WL	260335	813915	NWIS
C-968	C	260335	813915	NWIS
C-969	WL	260231	814013	NWIS
C-969	C	260238	814014	NWIS
C-970	C	261722	813512	NWIS
C-971	C	261722	813512	NWIS
C-972	C	260844	813241	NWIS
C-973	C	260844	813241	NWIS
C-974	C	260942	813241	NWIS
C-975	C	260305	813913	NWIS
C-976	C	260916	813858	NWIS
C-977	C	260916	813858	NWIS
C-978	C	262122	813554	NWIS
C-979	C	262122	813554	NWIS
C-980	C	261344	813847	NWIS
C-981	C	262159	812833	NWIS

Appendix. Monitoring stations used in this study (Continued)

Station identification	Station type	Latitude	Longitude	Data source
C-982	C	262159	812833	NWIS
C-983	C	262159	812833	NWIS
C-984	C	261734	812854	NWIS
C-985	C	261734	812854	NWIS
C-986	C	261201	812048	NWIS
C-987	C	260310	812725	NWIS
C-988	WL	261445	812848	NWIS
C-988	C	261445	812848	NWIS
C-989	WL	261734	812854	NWIS
C-989	C	261734	812854	NWIS
C-995	C	255704	812137	NWIS
C-996	C	260909	814111	NWIS
C-997	WL	252751	802833	NWIS
C-997	C	261530	814120	NWIS
C-998	C	261621	814501	NWIS
C-999	C	261509	814848	NWIS
C-1000	C	261104	814748	NWIS
C-1001	C	261117	814802	NWIS
C-1002	C	261242	814653	NWIS
C-1003	C	261437	814802	NWIS
C-1004	WL	261621	814643	NWIS
C-1004	C	261621	814643	NWIS
C-1026	C	261234	814801	NWIS
C-1051	C	261025	814637	NWIS
C-1052	C	260920	814604	NWIS
C-1053	C	260920	814604	NWIS
C-1054	C	261128	814609	NWIS
C-1055	C	261212	814412	NWIS
C-1056	C	261458	814608	NWIS
C-1057	C	261538	814611	NWIS
C-1058	C	261538	814611	NWIS
C-1059	C	261605	814808	NWIS
C-1060	C	261500	814803	NWIS
C-1061	C	261312	814800	NWIS
C-1062	C	260926	814750	NWIS
C-1063	C	260138	813758	NWIS
C-1064	WL	260138	813758	NWIS
C-1064	C	260138	813758	NWIS
C-1065	C	255638	812813	NWIS
C-1066	C	255638	812813	NWIS
C-1067	C	260315	813230	NWIS
C-1068	C	260315	813230	NWIS
C-1069	C	260814	812142	NWIS
C-1070	C	260814	812142	NWIS
C-1071	WL	261824	811718	NWIS
C-1071	C	261824	811718	NWIS
C-1072	WL	261824	811718	NWIS
C-1072	C	261824	811718	NWIS
C-1073	C	261741	812353	NWIS
C-1074	WL	262520	811620	NWIS
C-1074	C	262520	811620	NWIS
C-1075	C	262823	812131	NWIS
C-1076	C	262823	812131	NWIS
C-1077	C	262823	812131	NWIS
C-1078	C	262559	812704	NWIS
C-1079	C	262159	812823	NWIS
C-1080	C	262229	813618	NWIS
C-1081	C	260248	814121	NWIS
C-1082	C	261805	814733	NWIS
C-1083	WL	261856	814719	NWIS
CAPECOR1_R	R	263524	820054	DBHYDRO
CAPECOR2_R	R	263445	815748	DBHYDRO
CAPTIVA_R	R	263201	821059	DBHYDRO
CARIBBEA_E	E	261001	814659	DBHYDRO
CCWTP_R	R	261601	814659	DBHYDRO
CCWWTP_R	R	261606	814712	DBHYDRO
CCWWTP2_R	R	261431	814029	DBHYDRO
COCO1_R	R	261622	814647	DBHYDRO
COCOH.WB_R	R	261622	814550	DBHYDRO
COLGOV_R	R	260747	814545	DBHYDRO
COLLICTY	R	261011	814116	DBHYDRO
COLLIER_R	R	260924	813929	DBHYDRO
COLLISEM	R	255926	813529	DBHYDRO
COPELAND_R	R	255701	812136	DBHYDRO
CORK.CP_R	R	262427	813658	DBHYDRO
CORK.HQ_E	R	262301	813459	DBHYDRO
CORK.HQ_R	R	262301	813459	DBHYDRO
CORK.LCI_R	R	262431	813417	DBHYDRO
CORK.SD_R	R	262147	813826	DBHYDRO
CORK.TOW_R	R	263123	813459	DBHYDRO
CORK_R	R	262520	813443	DBHYDRO
CORKISL	R	262152	813531	DBHYDRO
DANHP_R	R	255843	812851	DBHYDRO
DUDA.NAP_R	R	260151	813911	DBHYDRO
EAGLECRK	R	260307	814224	DBHYDRO
ESTERO T_R	R	262826	815017	DBHYDRO
EVERGL 2_R	R	255043	812313	DBHYDRO
FAKA_R	R	255738	813034	DBHYDRO
FAKAHAT_R	R	255845	812429	DBHYDRO
FAKAHATC_R	R	261002	812140	DBHYDRO
FORT MEY_R	R	263501	815159	DBHYDRO
FPWX	R	262557	814324	DBHYDRO
FT MEYER_R	R	263451	815151	DBHYDRO
GOLD.FS_R	R	261058	814216	DBHYDRO
GOLD.W1_R	R	261004	814604	DBHYDRO
GOLD.WP_R	R	261101	814159	DBHYDRO
GOLD.WP2_R	R	261001	814214	DBHYDRO
GOLD.WP3_E	E	261001	814159	DBHYDRO
GOLD75	R	260929	813114	DBHYDRO
GOLDFS2	R	261342	813755	DBHYDRO
GORDON_R	R	261022	814705	DBHYDRO
HENDER_R	R	260559	814112	DBHYDRO
IMMOKA 2_R	R	262426	812459	DBHYDRO
IMMOKA 3_R	R	262741	812614	DBHYDRO
IMMOKALE_R	R	262335	812425	DBHYDRO
JUNGLE L_R	R	261005	814723	DBHYDRO
KANTORS_R	R	261129	814141	DBHYDRO
L TRAFFO_R	R	262601	812859	DBHYDRO
L.B.MINO_R	R	264436	813557	DBHYDRO
L-246	C	263803	814934	NWIS

Appendix. Monitoring stations used in this study (Continued)

Station identification	Station type	Latitude	Longi-tude	Data source
L-331	C	263126	815117	NWIS
L-345	C	262035	814647	NWIS
L-346	C	262035	814646	NWIS
L-351	C	262911	820035	NWIS
L-352	C	262909	820037	NWIS
L-357	C	263059	815607	NWIS
L-581	WL	263533	815921	NWIS
L-581	C	263533	815921	NWIS
L-585	C	262709	820053	NWIS
L-588	C	262539	820456	NWIS
L-590	C	262549	820509	NWIS
L-652	C	264102	814429	NWIS
L-721	C	264154	820222	NWIS
L-726	C	264426	814539	NWIS
L-727	WL	263851	813653	NWIS
L-727	C	263851	813653	NWIS
L-728	C	263713	814611	NWIS
L-729	WL	263336	813942	NWIS
L-729	C	263336	813942	NWIS
L-730	C	263138	815458	NWIS
L-730	WL	263138	815458	NWIS
L-731	WL	262704	813401	NWIS
L-731	C	262704	813401	NWIS
L-735	C	262840	815030	NWIS
L-738	C	262023	814641	NWIS
L-739	C	262658	814434	NWIS
L-741	C	262553	814856	NWIS
L-742	WL	263324	815223	NWIS
L-742	C	263324	815223	NWIS
L-781	WL	263835	820052	NWIS
L-781	C	263835	820052	NWIS
L-954	WL	263904	815503	NWIS
L-954	C	263904	815503	NWIS
L-1058	C	263815	820206	NWIS
L-1059	C	264518	820220	NWIS
L-1089	C	263125	815213	NWIS
L-1099	C	264054	815631	NWIS
L-1106	C	264055	815925	NWIS
L-1107	C	264147	815922	NWIS
L-1108	C	264145	815825	NWIS
L-1109	C	264056	815830	NWIS
L-1110	C	264242	815823	NWIS
L-1111	C	264148	815626	NWIS
L-1113	C	264121	820220	NWIS
L-1114	C	263721	815730	NWIS
L-1115	C	263906	815727	NWIS
L-1116	C	263634	820026	NWIS
L-1117	C	263439	815631	NWIS
L-1121	C	263328	815119	NWIS
L-1124	C	263247	815314	NWIS
L-1129	C	263324	815352	NWIS
L-1136	C	263533	815921	NWIS
L-1137	WL	263951	813553	NWIS
L-1137	C	263951	813553	NWIS
L-1138	C	262704	813401	NWIS
L-1156	C	263316	815241	NWIS
L-1403	WL	262550	820352	NWIS
L-1403	C	262550	820352	NWIS
L-1418	WL	263631	813752	NWIS
L-1418	C	263631	813752	NWIS
L-1456	C	262623	820219	NWIS
L-1457	C	262623	820219	NWIS
L-1598	C	263234	815502	NWIS
L-1625	C	263330	813942	NWIS
L-1634	C	262436	815350	NWIS
L-1635	C	262436	815349	NWIS
L-1691	WL	262043	814549	NWIS
L-1691	C	262043	814549	NWIS
L-1853	C	262707	814353	NWIS
L-1907	C	264309	814059	NWIS
L-1963	C	263345	813616	NWIS
L-1964	C	263345	813616	NWIS
L-1965	C	263354	813357	NWIS
L-1968	C	263808	814302	NWIS
L-1973	C	263719	814849	NWIS
L-1974	C	263719	814849	NWIS
L-1975	C	264400	814246	NWIS
L-1976	C	264400	814246	NWIS
L-1977	C	264321	813656	NWIS
L-1978	C	264321	813656	NWIS
L-1983	C	263042	814330	NWIS
L-1984	C	262714	814145	NWIS
L-1985	C	262714	814146	NWIS
L-1992	C	263354	813357	NWIS
L-1993	WL	263252	814527	NWIS
L-1993	C	263252	814527	NWIS
L-1994	WL	263252	814527	NWIS
L-1994	C	263252	814527	NWIS
L-1995	WL	263252	814527	NWIS
L-1995	C	263252	814527	NWIS
L-1996	WL	261955	814100	NWIS
L-1996	C	261955	814100	NWIS
L-1997	WL	261955	814100	NWIS
L-1997	C	261955	814100	NWIS
L-1998	WL	263042	814330	NWIS
L-1998	C	263042	814330	NWIS
L-1999	C	263042	814330	NWIS
L-2186	WL	263345	813616	NWIS
L-2186	C	263345	813616	NWIS
L-2187	C	263951	813553	NWIS
L-2190	C	264145	815202	NWIS
L-2191	C	264145	815202	NWIS
L-2192	C	262700	813824	NWIS
L-2194	WL	261958	814321	NWIS
L-2194	C	261958	814321	NWIS
L-2195	WL	261958	814321	NWIS
L-2195	C	261958	814321	NWIS
L-2198	C	261955	814321	NWIS
L-2200	C	264330	813403	NWIS
L-2202	C	264330	813403	NWIS

Appendix. Monitoring stations used in this study (Continued)

Station identification	Station type	Latitude	Longitude	Data source
L-2204	C	263330	813942	NWIS
L-2212	C	262832	815758	NWIS
L-2215	C	263128	813515	NWIS
L-2216	C	264609	814540	NWIS
L-2217	C	264609	814540	NWIS
L-2244	C	263243	815720	NWIS
L-2292	C	263719	814849	NWIS
L-2295	C	262553	814856	NWIS
L-2308	C	262553	814856	NWIS
L-2310	C	262023	814641	NWIS
L-2311	C	263345	813616	NWIS
L-2313	C	262704	813401	NWIS
L-2315	C	263005	821116	NWIS
L-2328	C	264609	814540	NWIS
L-2341	C	264518	815131	NWIS
L-2434	WL	263527	820101	NWIS
L-2434	C	263527	820101	NWIS
L-2435	C	263407	815559	NWIS
L-2524	C	262623	820743	NWIS
L-2525	C	263118	820509	NWIS
L-2526	C	264518	820220	NWIS
L-2527	C	263956	820830	NWIS
L-2528	C	263908	815926	NWIS
L-2529	C	262914	815624	NWIS
L-2530	C	264309	814053	NWIS
L-2531	C	264428	813625	NWIS
L-2549	C	263956	820830	NWIS
L-2550	WL	262712	814137	NWIS
L-2640	C	263814	815527	NWIS
L-2641	C	263534	815733	NWIS
L-2642	C	263258	815856	NWIS
L-2643	C	263254	820141	NWIS
L-2644	WL	263441	820219	NWIS
L-2644	C	263441	820219	NWIS
L-2645	C	263744	820411	NWIS
L-2646	C	264538	815521	NWIS
L-2700	C	264003	820127	NWIS
L-2701	WL	263820	815857	NWIS
L-2701	C	263820	815857	NWIS
L-2702	WL	263622	815636	NWIS
L-2702	C	263622	815636	NWIS
L-2703	WL	263358	815755	NWIS
L-2703	C	263358	815755	NWIS
L-2820	C	263956	820830	NWIS
L-2821	C	263118	820509	NWIS
L-3203	C	263814	815527	NWIS
L-3204	C	263534	815733	NWIS
L-3205	C	263258	815856	NWIS
L-3206	C	263254	820141	NWIS
L-3207	C	263441	820219	NWIS
L-3208	C	263744	820411	NWIS
L-3209	C	264538	815521	NWIS
L-3210	C	264003	820127	NWIS
L-3211	C	263820	815857	NWIS
L-3212	C	263622	815636	NWIS
L-3213	C	263358	815755	NWIS
L-3214	C	263956	820830	NWIS
L-3215	C	263118	820509	NWIS
L-4820	C	264054	815724	NWIS
L-5648	C	263250	814743	NWIS
L-5649	WL	262935	814957	NWIS
L-5649	C	262935	814957	NWIS
L-5664	C	262515	813933	NWIS
L-5665	C	262515	813933	NWIS
L-5666	C	262514	814328	NWIS
L-5667	C	262514	814325	NWIS
L-5668	C	262514	814717	NWIS
L-5669	C	262512	814717	NWIS
L-5672	C	262332	813831	NWIS
L-5673	C	262332	813831	NWIS
L-5707	C	263853	815147	NWIS
L-5720	C	263250	814743	NWIS
L-5721	C	262935	814957	NWIS
L-5722	C	262103	814643	NWIS
L-5723	C	262103	814643	NWIS
L-5724	C	261947	814902	NWIS
L-5725	C	261947	814902	NWIS
L-5726	C	261900	814818	NWIS
L-5727	C	261900	814818	NWIS
LEHIGH 1_R	R	263625	813859	DBHYDRO
LEHIGH 2_R	R	263907	813935	DBHYDRO
LEHIGH 3_R	R	263726	813403	DBHYDRO
LEHIGH 4_R	R	263325	813623	DBHYDRO
LEHIGH 5_R	R	263616	814218	DBHYDRO
LEHIGH 6_R	R	263701	814359	DBHYDRO
LEHIGH E_R	R	263301	814259	DBHYDRO
LEHIGH W_R	R	263626	813859	DBHYDRO
LEHIGH_R	R	263625	813859	DBHYDRO
MARCO FI_R	R	255548	814201	DBHYDRO
MARCO TO_R	R	260001	813459	DBHYDRO
MILES 2_R	R	261145	812045	DBHYDRO
MILES 3_E	E	261100	812600	DBHYDRO
MILES CI_R	R	261104	812047	DBHYDRO
MONROE T_R	R	255131	810624	DBHYDRO
NAPLES C_R	R	260738	814459	DBHYDRO
NAPLES T_R	R	260914	814532	DBHYDRO
NAPLES_R	R	261005	814723	DBHYDRO
NNAPFS42	R	261620	814332	DBHYDRO
NP-EVC	R	255112	812249	DBHYDRO
NP-OAS	R	255127	810205	DBHYDRO
OASIS	R	255101	810159	DBHYDRO
RACOON PT	R	255801	811859	DBHYDRO
ROYAL HA_R	R	255926	813529	DBHYDRO
S79_R	R	264326	814154	DBHYDRO
SDS_R	R	261630	814208	DBHYDRO
SILVER S_R	R	261749	812618	DBHYDRO
SITE #1_R	R	260900	814100	DBHYDRO
SITE #2_R	R	255300	811800	DBHYDRO
SITE1_R	R	261643	813341	DBHYDRO
SITE2_R	R	261149	814016	DBHYDRO

Appendix. Monitoring stations used in this study (Continued)

Station identification	Station type	Latitude	Longi-tude	Data source	Station identification	Station type	Latitude	Longi-tude	Data source
SITE3_R	R	260343	813124	DBHYDRO	SR_R	R	263501	815159	DBHYDRO
SITE4 2_R	R	261616	813144	DBHYDRO	STEPHAN	R	261011	814116	DBHYDRO
SIX L.7_R	R	260114	813723	DBHYDRO	TAMIAMI_R	R	255311	811529	DBHYDRO
SLEE_R	R	264145	814637	DBHYDRO	USDA IMM_R	R	262741	812614	DBHYDRO
					VICTORIA_R	R	261541	814614	DBHYDRO